Thesis

PhD in Mechanical Engineering, Fluids and Aeronautics

Title:

Study and characterization of mechanical properties of wood-PLA composite (Timberfill) material parts built through fused filament fabrication

Author:

Mohammad Damous Zandi

Supervisors:

Dr. J. Antonio Travieso Rodríguez

Dr. Ramón Jerez Mesa

Barcelona, 5th of June, 2020

UNIVERSITAT POLITÈCNICA DE CATALUNYA
BARCELONATECH

Title: Study and characterization of mechanical properties of wood-PLA composite (Timberfill) material parts built through fused filament fabrication

Author: Mohammad Damous Zandi

Advisors: J. Antonio Travieso Rodríguez

Ramón Jerez Mesa

Abstract: This dissertation is an experimental study on the influence of manufacturing parameters on the mechanical behavior of wood-PLA (Timberfill) parts built through Fused Filament Fabrication (FFF). Tensile, bending and fatigue tests are performed on different specimens following different ASTM and ISO Standards describing the processes. To avoid the production of a large number of specimens, a design of experiments (DoE) through Taguchi orthogonal arrays is designed and the influence of the factors are evaluated using analysis of variance (ANOVA). Ultimately, this work allowed the determination of the most effective combination of parameters that can obtain the best mechanical properties of parts built of Timberfill material. Furthermore, interesting conclusions about how filaments are welded during the FFF process, and how this impacts the final resistance of the material, are taken into consideration. Also, a comparison FFF specimens have been compared to other ones manufactured through injection molding to investigate how the processing conditions affects the mechanical properties of the material. Finally, the main conclusion of this research is the validation of the experimental results through a finite element model (FEM) simulation of the mechanical behavior of the material through ANSYS software.

Keywords: Additive Manufacturing, Fused Filament Fabrication, Timberfill, Mechanical Behavior, wood-PLA, FEM

Dissertation presented by Mohammad Damous Zandi in partial fulfillment of the requirements for the degrees of

Doctor per la Universitat Politècnica de Catalunya

Acknowledgement

Foremost, I would like to express my sincere gratitude to my supervisors Prof. José Antonio Travieso Rodríguez and Prof. Ramón Jerez Mesa for their continuous support of my PhD study and research, for their patience, motivation, enthusiasm, and immense knowledge. Their guidance helped me in all the time of research and writing of this thesis. I could not have imagined having a better advisor and mentor for my PhD study.

Besides my advisors, I would like to sincerely thank the rest of my thesis committee: Prof. Jordi Lluma, Prof. Jordi Jorba, Prof. Giovanni Gomez, for more technical-scientific support and of course for their encouragements, insightful comments, and hard questions.

My thanks go out to my labmates and department students, Cyrus Amini, Julen Durlan for their support for the finite element model and Marc Mimbrero Gallardo, Bàrbara Adrover Monserrat, Ismael Fernandez who so kindly and generously participated in this research. Also I thank my friends Farzam Nosrati, Ali Bagheri, Mezgeen Rasol, Kourosh Nasr Esfahani, Rasol Aghazadeh and all concerned persons who co-operated with me in this regard.

Last but not the least, I owe quite a lot to my family who allowed me to travel to Spain and support me all throughout my studies. I would like to dedicate this study to them as an indication of their significance in this study, as well as in my life.

Summary

This research is based on how an additive manufacturing (AM) technology affects the mechanical properties of an innovative commercial wood-PLA composite material (Timberfill). Specifically fatigue, tensile, and flexural tests are performed and the results are evaluated. To manufacture the experimental samples one of the most common AM techniques, namely fused filament fabrication (FFF), is applied. For this reason, some of the most influential printing parameters in different levels are selected and have been combined together to manufacture the samples in a wide range of building conditions. To avoid manufacturing a large number of specimens, a design of experiments (DoE) through Taguchi orthogonal arrays is designed and the influence of the factors have been analyzed performing an analysis of variance (ANOVA). As a conclusion the optimal combination of the parameters and levels have been obtained for each one of the applied mechanical tests and higher values of responses have been derived from these set of parameters. Since the above mentioned material is composite of wood fibers with PLA, all of the obtained results are compared to the pure PLA to find how this composition modifies the behavior of the pure material.

On the other hand, tensile and flexural tests have been carried out on solid Timberfill specimens manufactured through injection molding to assess how the processing technology affects the macroscopic mechanical properties of the workpieces, based on how the material is composed as a consequence of the process. Finally, the flexural strength of the material has been simulated and compared to the experimental results. The achieved deformation behavior curves validate the experimental test and that would be one of the main conclusions of this research.

Resumen

Esta investigación se basa en la tecnología de fabricación aditiva (AM) y tiene como objetivo estudiar las propiedades mecánicas y caracterizar el comportamiento de un material comercial innovador, compuesto de PLA con fibras de madera (Timberfill). Específicamente, se realizan pruebas de fatiga, tracción y flexión y se evalúan los resultados para concluir sobre los mismos. Para fabricar las muestras experimentales se aplica una de las técnicas más comunes llamadas fabricación de filamentos fundidos (FFF), y se ha considerado la influencia de los parámetros de fabricación en las propiedades mecánicas de las mismas. Por esta razón, se han seleccionado algunos de los parámetros de impresión más influyentes en diferentes niveles y se han combinado para fabricar las muestras en una amplia gama de condiciones de construcción. Para evitar la fabricación de una gran cantidad de muestras, se ha utilizado un diseño de experimentos (DoE) a través de matrices ortogonales de Taguchi y se ha analizado la influencia de los factores realizando un análisis de varianza (ANOVA). Como conclusión, se ha obtenido la combinación óptima de los parámetros y niveles para cada una de las pruebas mecánicas realizadas y se han detectado los valores más altos de respuestas de éstos. Dado que el material mencionado anteriormente es un compuesto de PLA con fibras de madera, todos los resultados obtenidos se comparan con el PLA puro para encontrar la efectividad de esta composición.

Por otro lado, se han realizado también pruebas de tracción y flexión a muestras sólidas de Timberfill fabricadas mediante moldeo por inyección para investigar las diferencias entre esta tecnología y la fabricación aditiva. Los resultados muestran que la resistencia mecánica de las muestras impresas es más bajas que las inyectadas, por lo que el porcentaje de solidez podría ser la razón principal de este efecto.

Además, la resistencia a la flexión del material se ha simulado y comparado con los resultados experimentales. Las curvas de comportamiento de deformación logradas validan la prueba experimental lo cual es una de las principales conclusiones de esta investigación.

Resum

Aquesta investigació es basa en la tecnologia de fabricació additiva (AM) i té com a objectiu estudiar les propietats mecàniques i caracteritzar el comportament d'un material comercial innovador, format de PLA amb fibres de fusta (Timberfill). Específicament, es realitzen proves de fatiga, tracció i flexió i s'avaluen els resultats per concloure sobre els mateixos. Per fabricar les mostres experimentals s'aplica una de les tècniques més comunes anomenada fabricació de filaments fosos (FFF), i s'ha considerat la influència dels paràmetres de fabricació en les propietats mecàniques de les mateixes. Per aquesta raó, s'han seleccionat alguns dels paràmetres d'impressió més influents en diferents nivells i s'han combinat per fabricar les mostres en una àmplia gamma de condicions de construcció. Per evitar la fabricació d'una gran quantitat de mostres, s'ha utilitzat un disseny d'experiments (DoE) a través de matrius ortogonals de Taguchi i s'ha analitzat la influència dels factors realitzant una anàlisi de variància (ANOVA). Com a conclusió, s'ha obtingut la combinació òptima dels paràmetres i nivells per a cadascuna de les proves mecàniques realitzades i s'han detectat els valors més alts de respostes d'aquests. Atès que el material esmentat anteriorment és un compost de PLA amb fibres de fusta, tots els resultats obtinguts es comparen amb el PLA pur per trobar l'efectivitat d'aquesta composició.

D'altra banda, s'han realitzat també proves de tracció i flexió a mostres sòlides de Timberfill fabricades mitjançant el procediment d'injecció per investigar les diferències entre aquesta tecnologia i la fabricació additiva. Els resultats mostren que la resistència mecànica de les mostres impreses és més baixes que les injectades, de manera que el percentatge de solidesa podria ser la raó principal d'aquest efecte.

A més, la resistència a la flexió del material s'ha simulat i comparat amb els resultats experimentals. Les corbes de comportament de deformació assolides validen la prova experimental la qual cosa és una de les principals conclusions d'aquesta investigació.

Contents

List of Figures

List of Tables

List of Symbols

General parameters

$\boldsymbol{E}$	Young's Module
$\boldsymbol{R_{P0.2}}$	Yield Strength
$\boldsymbol{\sigma_{max}}$	Maximum Stress
$\boldsymbol{\varepsilon}$	Maximum Deformation
$\boldsymbol{\nu}$	Poisson's Ratio
$\boldsymbol{G}$	Shear Module
$\boldsymbol{\rho}$	Density
$\boldsymbol{S_a}$	Maximum stress
$\boldsymbol{N_f}$	Cycle to failure
$\boldsymbol{S_\infty}$	Endurance limit

Abbreviations

AM	Additive Manufacturing
RP	Rapid Prototyping
3D	Three Dimensional
CAD	Computer-Aided Design
CAM	Computer-Aided Manufacturing
ANOVA	Analysis of Variance
DoE	Design of Experiment
UTS	Ultimate Tensile Strength
SN	Signal-Noise
FFF	Fused Filament Fabrication

FDM	Fused Deposition Modeling
IM	Injection Molding
PBF	Power Bed Fusion
CLT	Classical Laminate Theory
PLA	Polylactic Acid
ABS	Acrylonitrile Butadiene Styrene
WFRPCs	Wood Fiber-Reinforced PLA Composites
PC	Polycarbonate
PA	Polyamide
PVA	Polyvinyl alcohol
PMC	Polymer Matrix Composites
PEEK	Poly-Ether-Ether-Ketone
PB	Polybutadiene
SAN	Styrene-Acrylonitrile
WPC	Wood-Plastic Composite
PHA	Polyhydroxyalkanoates
HDPE	High-Density Polyethylene
XRD	X-ray Diffraction
ASTM	American Society of Testing Materials International
ISO	International Standards Organization
FEA	Finite Element Analysis
FEM	Finite Element Method
ADPL	ANSYS Parametric Design Language
SEM	Scanning Electron Microscopy
L/D	Length-to-Diameter ratio

Chapter 1

Introduction

Additive manufacturing (AM) is a group of techniques used to create 3D objects from a CAD/CAM model by depositing a material layer on top of previous layers [1]. Nowadays, additive manufacturing is rising up as an advanced manufacturing group of techniques due to its ability to make efficient use of different raw materials, as well as its potential to be implemented in innovative manufacturing environments based on the 4.0 Industry. One of the most common processes included in the family of AM methods relies on the thermal extrusion of a filament through a suitable extruder nozzle. This method is often referred to as Fused Filament Fabrication (FFF), or Fused Deposition Modelling (FDM). Through this technology the raw material presented as a filament, usually of PLA or ABS, which is progressively taken into a heated extruder. FFF printer prints a 3D object by extruding a stream of heated or semi-melted thermoplastic material, which is carefully positioned into layer upon layer, working from the bottom up as shown in Figure 1.1.

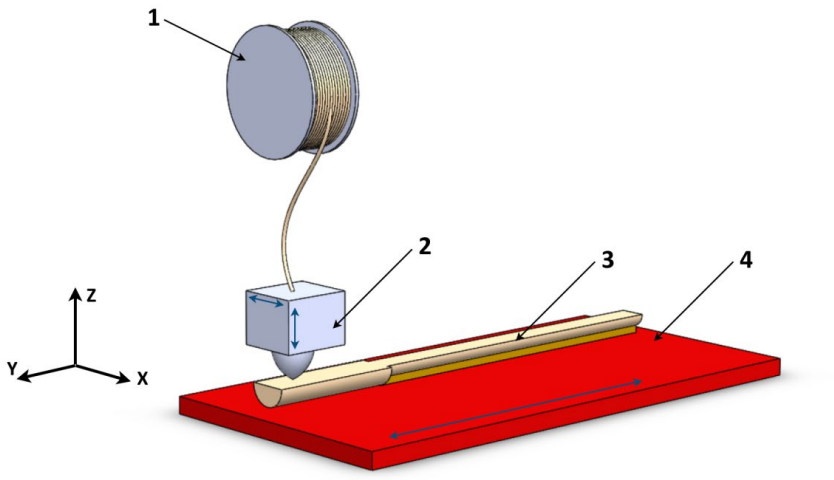

Figure 1.1. Scheme of FFF process: 1) Filament spool, 2) Extruder, 3) specimen, 4) hot bed.

Its low cost and simplicity has seen it emerge as the dominant AM method in the small-scale productive contexts. Despite its low cost, FFF covers a wide range of available feedstock materials and flexibility to fabricate complex shapes. It has also recently demonstrated its ability to manufacture multi-material

components containing discreet regions of different materials nature. Multi material FFF components have begun to demonstrate added multi-functionality in manufactured parts that are desirable for a range of applications.

1.1 Motivations

The characterization of new materials has been one of the major historical facilitators for the enhancement of industrial products. For instance, there are a big number of polymeric materials available to create the applicable objects depend on the manufacturing technology. These materials are mainly employed for prototyping designs and the creation of low performance parts, but the demand for new higher performance polymer materials and composites is growing [2]. While the manufacturers provide basic technical information about chemical and mechanical properties of raw materials, the date include in these datasheets are usually not standardized, and could lack applicability for industrial usages.

On the other hand, the performance characteristics of the materials could vary depending on the used manufacturing technology and the operating conditions which this phenomenon could occur by combining different manufacture parameters and levels through FFF technology as shall be presented in the state of the art chapter. So, it is highly motivating to introduce a new commercial applicable material and optimize its mechanical properties using a specific manufacturing technology.

Timberfill is a relatively innovative material, which is a composite of wood fibers with PLA. Characteristics of this material also could vary according to numerous manufacturing conditions that needs major work to determine its mechanical properties and find the effectiveness of the manufacturing conditions comparing the other technique. Since Timberfill is basically PLA reinforced by wood particles, it is the main point of this dissertation is finding out how and why the fibers change the material properties with compare to pure PLA. The following subsection presents the contributions expected to be delivered by this dissertation.

1.2 Research contributions

The present dissertation has concentrated on studying and characterize a relatively new material available as a commodity for manufacturers. The mechanical behavior of Timberfill pieces built through FFF considering tensile, flexural, and fatigue testing results are examined with the aim of finding the relations which in fact characterize the influence of the manufacturing parameters on the mechanical properties.

The measurement challenges for AM, whether it is metal or polymer, are similar. Parallels between the material systems include: characterization of raw materials, development of design allowable, in-situ

process and feedback control, workflow optimization, and modeling final properties [3]. With the exposed aim, the current work must tackle with various scientific issues that are to be answered.

1.2.1. Previous questions

1. Is it possible to improve the performance of innovative materials used for FFF by changing the process parameters to which they are subjected, so that better mechanical performance are achieved?
2. Can an optimal set of parameters be found, so that the productivity of innovative 3D printing materials can be maximized?
3. Could the performances of this kind of material be comparable to other applicable materials?
4. Is it possible to assess experimentally what is the actual effect of adding wood into a PLA matrix to enhance its overall performance? If so, what are the mechanisms that act to achieve this behavioral modification of the material?
5. Does processing the PLA-wood composite through FFF improves its performance and changes the properties of the material in comparison to when it is processed through traditional methods such as injection?
6. Is it possible obtain a model to characterize the mechanical properties of the PLA-wood material, considered that it has a double composite nature: (1) wood combined with PLA and (2) skin-deposited combined with infill-deposited material?

From these questions, a series of starting hypotheses for this work will be defined.

1.2.2. Hypothesis raised

1. To succeed in characterizing the PLA-wood composite for FFF, it is enough to combine the results obtained from tensile, fatigue and bending tests.
2. There is an optimal set of parameters to obtain the best mechanical properties in pieces manufactured in PLA-wood material by FFF.
3. By adding wood to the PLA matrix, the resistance and flexibility positively modified, because it increases the internal friction of the polymer filaments.
4. The mechanical properties of Timberfill processed through FFF are not only consequence of the raw material mechanical properties, but also of the combined effect of the material deposited in the infill and the skin of the workpiece. A model can be found to represent this coupled effect.

Considering the abovementioned issues, the main objectives of this dissertation can be defined.

1.3 Objectives

1.3.1. General objectives

1. Study and characterization of the mechanical properties of Timberfill parts built through the FFF technology, by relating them to the process parameters through which they are obtained.
2. Obtain the best combination of the influential parameters to achieve the better mechanical behavior of pieces.
3. Obtain a model to characterize the tensile mechanical properties of Timberfill, modelling the workpiece as a result of the coupled functioning of the infill material and the skin materials, both manufactured with the same raw material.

1.3.2. Specific objectives

1. Study and perform the experiments of mechanical properties of commercial Timberfill® material to characterize its specifications.
2. Obtain the best combination of influential parameters and levels through FFF manufacturing process to achieve better mechanical comportment.
3. Plan the experimental design using the Taguchi method to organize the manufacturing strategies.
4. Design and manufacture the specimens appropriately to carry out the desired mechanical tests according to the specifications stated in the procedure.
5. Analyze the tests results to find the best values through analyze of the variance (ANOVA) and obtain the most effective parameters.
6. Evaluate the results to compare the mechanical behaviors of Timberfill material with pure PLA material using the same manufacturing technique.
7. Develop a model to predict the behavior of tensile mechanical properties, applying a FEM method.

1.4 Thesis dissertation in brief

This thesis is organized in 7 chapters. In **Chapter 2** a review of bibliographical references that tackle with the issues considered in this dissertation as the state of the art is presented. Two main different parts are differentiated. The first section presents a definition of FFF process and different parameters which could be effective on the mechanical properties through this technology. The second section focuses on reviewing,

based on a bibliographical review, the mechanical properties of different materials which have been studied by other researchers.

The chapters that follow focus on three main case studies, each of them related to a different mechanical property of Timberfill. First, the tensile properties of the Timberfill material and the most influential parameters on this response are resulted in the **Chapter 3**. For this aim four various manufacturing parameters are selected to examine their effectiveness on the tensile properties of Timberfill. **Chapter 4** includes the manufacturing process of the specimens and the results of the flexural test executed on the Timberfill. For this reason, some of the effective parameters are selected for the design of experimental phase considering three different levels for each one them. All of the characteristic results achieved for Timberfill material are compared with pure PLA to find the influences of the manufacturing parameters and wood fibers composed with this material. Finally, fatigue lifespan is analyzed through bending rotative tests in **Chapter 5**. To manufacture the specimens, four printing parameters in three different levels are considered and the experiment is designed based on Taguchi orthogonal array. The results are analyzed and compared to PLA material achieved in previous work of research group applying the same process.

Chapter 6 explains a mechanical behavior model of Timberfill developed through a finite element model (FEM) technique. The objective of this model is to predict the tensile properties of a FFF workpiece, considering that is composed of two different materials: Timberfill deposited with an infill pattern, and Timberfill deposited around it as skin material. Ultimately, the contribution of each of them to the overall tensile properties of the workpieces shall be explored.

Finally, results are summarized in **Chapter 7** and scientific contributions achieved in this work are explained to clarify the final conclusions.

1.5 Publications

Publications in JCR indexed journals

1. Travieso-Rodriguez, j, a., **Zandi, M, D.**, Jerez-Mesa, R., Lluma-Fuentes, J., Gomez-Gras, G. (20). Fatigue behavior of PLA-wood composite manufactured by fused filament fabrication. *Journal of Materials Research and Technology*. (accepted 03/06/2020). JCR Impact Factor: 3.327. Q1, T1 (10/476), Metallurgy, Metallurgical Engineering. Citing by: 1
2. **Zandi, M, D.**, Jerez-Mesa, R., Lluma-Fuentes, J., Roa, J., Travieso-Rodriguez, J, A. (2020). Experimental analysis of manufacturing parameters' effect on the flexural properties of wood-PLA composite parts built through FFF. *The International journal of Advance Manufacturing*

Technology, 1-14. JCR Impact Factor: 2.496. Q2 (23/49), Engineering, Manufacturing. Citing by: 2

3. **Zandi, M, D.**, Jerez-Mesa, R., Lluma-Fuentes, J., Jorba-Peiro, J., Travieso-Rodriguez, J, A. (2020). Study of the manufacturing process effects of fused filament fabrication and injection-molding on tensile properties of composite PLA-wood parts. *The International journal of Advance Manufacturing Technology*, 1-11. DOI: 10.1007/s00170-020-05522-4. JCR Impact Factor: 2.496. Q2 (23/49), Engineering, Manufacturing. Citing by: 1
4. Nasr Esfahani K., **Zandi M.D.**, Travieso-Rodriguez J.A., Graells M., Pérez-Moya M. Manufacturing and application of 3D printed photo fenton reactors for wastewater treatment.

Contributions in international congresses

1. **Zandi, M, D.,** Jerez-Mesa, R., Lluma-Fuentes, J., Travieso-Rodriguez, J, A. Effects of building on condition on the tensile property of FFF Timberfill parts. *21th International Research/Expert Conference "Trends in the Development of Machinery and Associated Technology" TMT 2018*, Karlovy Vary (Czech Republic). September 2018.
2. **Zandi, M, D.,** Lluma-Fuentes, J., Jerez-Mesa, R., Travieso-Rodriguez, J, A. Effects of manufacturing parameters on fatigue performance of Timberfill parts through FFF. *8th Manufacturing Engineering Society International Conference*. Madrid (Spain), June 2019.
3. Nasr Esfahani K., **Zandi M.D.**, Travieso-Rodriguez J.A., Graells M., Pérez-Moya M. 3D printed lab-scale raceway ponds reactors applied to photo-Fenton processes. *16th International Conference on Environmental Science and Technology.* Rhodes (Greece), September, 2019.
4. Nasr Esfahani K., **Zandi M.D.**, Travieso-Rodriguez J.A., Graells M., Pérez-Moya M. Manufacturing and application of raceway pound for wastewater treatment. *6th European Conference on environmental applications of advanced oxidation processes.* Portorož-Portorose (Slovenia), June 2019.

Contributions in national congresses

1. **Mohammad Damous Zandi**, Ramon Jerez-Mesa, Jordi Lluma-Fuentes, J. Antonio Travieso-Rodriguez. Tensile and flexural test procedure and result analyzing performance. (2020). EEBE 3DDay, abstract book. ISBN: 978-84-09-19907-5
2. Bàrbara Adrover Monserrat, **M. Damous Zandi**, Jordi-Adalbert Marqués Salvador, Ramón Jerez-Mesa, Jordi Llumà, J. Antonio Travieso-Rodríguez. Selección de los parámetros de impresión en

piezas de un elastómero fabricado por filamento fundido. *XXIII Congreso Nacional de Ingeniería Mecánica. Jaén, 21-23 de octubre de 2020. Artículo aceptado para la presentación.*

3. **M. Damous Zandi**, Bàrbara Adrover Monserrat, Ramón Jerez-Mesa, Jordi Llumà, J. Antonio Travieso-Rodríguez. Influencia de los parámetros de impresión en la resistencia a la flexión de piezas de PLA – madera, fabricadas por filamento fundido. *XXIII Congreso Nacional de Ingeniería Mecánica. Jaén, 21-23 de octubre de 2020. Artículo aceptado para la presentación.*

Chapter 2

State of the art

This chapter contains the most relevant results gathered from an extensive bibliographical research which considers references regarding FFF. This is a generic process that could be adaptable and customized regarding specific needs through an extensive number of variable manufacturing parameters affecting the final mechanical properties of the different usable materials. This technology, which is in fact a type of AM, has gained significant academic as well as industry interest due to its ability to create complex geometries in short times, and has become a commodity in small scale manufacturing environments. AM has also inspired the development of the maker movement by democratizing design and manufacturing [2].

Recent advances in this technology have seen its use become far more widespread and it offers exciting possibilities for future development. However, due to the fast proliferation of a wide variety of technologies associated with AM, there is a lack of a comprehensive set of design principles, manufacturing guidelines, and standardization of best practices. These challenges are compounded by the fact that advancements in multiple technologies (for example materials processing, topology optimization) generate a positive feedback loop effect in advancing AM [4]. The first section of this chapter presents a definition of the FFF technology by specification of variable manufacturing parameters contributing to the process. The second section refers to the mechanical properties that are object of study in this dissertation, and that include the vast majority of the reviewed bibliography. Finally, the last section includes the results found on different materials processed through FFF.

2.1 Relevant customizable parameters of FFF

3D printing utilizing the extrusion of thermoplastic and elastomeric materials is easily the most common and recognizable FFF process. In order to build functional end-use parts using this technology it is needed to know how different parameters effect on the mentioned properties [5], which are quite varied and can affect in different ways on the final characteristics of the samples, whether part quality, mechanical behavior, geometrical details, surface texture, and cost. Therefore, it is important to know which of these parameters are relevant, so that a careful selection of their values is done, especially those which are most

common observed in the literature reviewed. The next subsections describe the most relevant parameters considered in this dissertation

2.1.1. Orientation

One of the most influential parameters which can effects the load transfer between filaments and interfaces is the manufacturing direction, also known as build orientation. Different building orientations of specimens according to the origin in the FFF machine is shown in Figure 2.1. The effectiveness of this parameter respect to laying direction of the extruded filaments could be varying according to different mechanical test and the application of the load subsequently. One of the mechanical test which could sense this effectiveness is tensile test while the traction force tries to break the filaments in 0°X orientation or separate the layers in 0°Y direction. Orientation can also have a significant impact on the finished surface and print time.

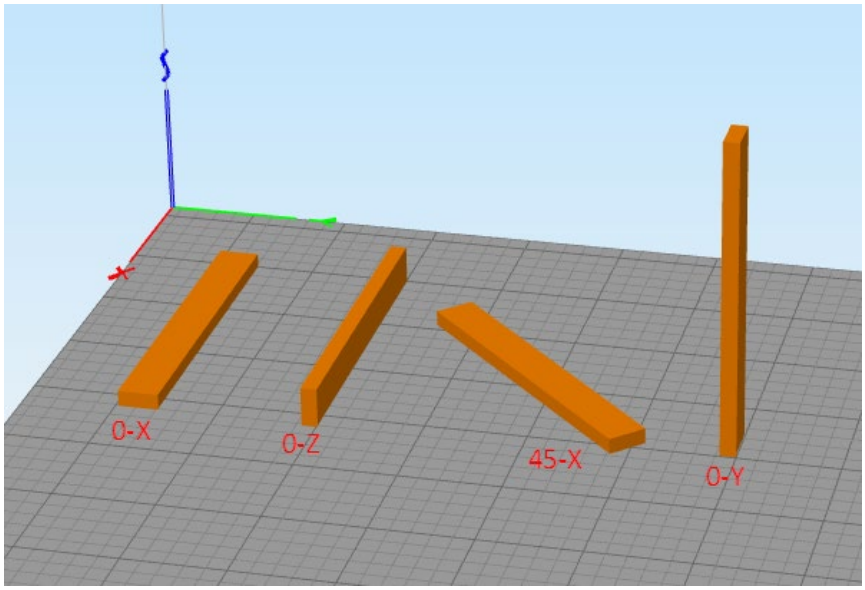

Figure 2.1. Different building orientation.

Very recently, several studies have been conducted with the aim of studying the influence of this parameter on the strength of parts fabricated with the most important additive manufacturing technologies. According to the literature [6], specimens built in the X-axis direction (the long axis of the specimens is directed towards the tray`s X direction, 0º relative to the X-Y plane) exhibited higher strength (maximum load and stress) values, compared to the strength measured on three-point bending specimens built in the Z direction.

Other authors [7], considered the results of fatigue behavior of PLA parts built in (X, Y and -45) different build orientations. This work observed that the ultimate tensile stress of PLA samples built in X-direction (PLA-X) was found to be the highest ranged from 60 to 64 % of raw PLA material. Also, it was observed that under cyclic loading application the PLA specimens built in -45 orientations achieved highest fatigue

life compared to those PLA specimens built in X and Y orientations. In [8] the process parameters that influence the tensile and shear properties are examined. The specimens are printed in four rasters ([+45/-45], [+30/-60], [+15/-75], and [0/90]) and three build orientations (0°-X, 0°-Z, 0°-Y) to determine directional properties of the Polycarbonate and acrylonitrile butadiene styrene materials. The largest degree of anisotropy was found when comparing the strain energy densities as the [+45/-45] in X orientation had a density that was 91% higher than the [+45/-45] in Y orientation. Raster orientation did not seem to affect the tensile and shear properties of the ABS specimens; however, build orientation did appear to affect both the 0°–Z and 0°-Y specimens. When evaluating the ABS shear specimens for anisotropy, differences of up to 25% were found when comparing shear modulus with similar dissimilarities in the shear strengths reported. The performance of the ABS specimens in tension was a poor indicator of performance in shear as properties varied significantly across the same orientation combinations. Stephen Oluwashola Akande et al. [9], fabricated tensile, flexural, notched, and un-notched impact tests specimens in PLA using FFF with different layer thicknesses, fill densities, orientation and printing velocities to determine the influence of process parameters on the quality of parts. This study resulted that notched impact testing of parts built in the Z-orientation offers a test method which, within the constraints of this study, is independent of process parameters. This then offers a convenient test with which to track machine performance over time, as, in principle, the same test and control limits can be applied across builds with different layer thicknesses and speeds. Additionally, a number of works have been considered this parameter on various properties of the different materials [10-14]. Accordingly rely on the selected mechanical properties for this work, it was interesting to consider the influence of orientation on the results of the innovative material.

2.1.2. Layer height

The height of the extruded filaments or layer height controls the height along vertical axis taken before extruding a new layer top of the previous one according to Figure 2.2. Some of the references that investigated the effectiveness of this parameter are mentioned following.

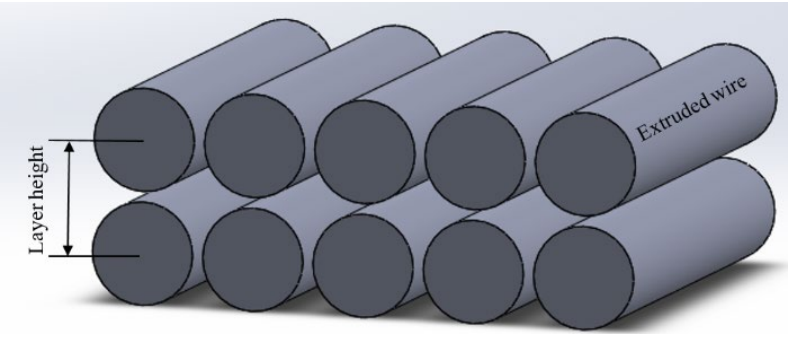

Figure 2.2. Deposited filaments.

The study [15], have examined the influence of deposition layer thickness on the mechanical properties of printed ABS material when manufacturing using FFF. Samples were printed at four independent layer thicknesses comprising 0.2, 0.4, 0.6 and 0.8 mm using a single printer nozzle with a diameter of 1 mm. Results found material strength and stiffness was greatest using smaller layer thicknesses, compared with larger layer thicknesses e.g. $\sigma y_{(0.2mm)}$ = 31.5 MPa, $UTS_{(0.2mm)}$ = 38.2MPa, compared with $\sigma y_{(0.8mm)}$ = 23.0 MPa, $UTS_{(0.8mm)}$ = 31.0 MPa. B.M. Tymrak et al. [16], concluded the result for layer heights, tensile strength averages varied by 11.9 MPa, or 22%, between 0.3 mm and 0.2 mm layer heights while elastic modulus varied by 194 MPa, or 6%, between 0.4 mm and 0.2 mm layer height on PLA. On the other hand Jerez-Mesa et al. [17], shown that the layer height has the most significant impact on fatigue life for PLA so that increasing the layer height, better results of number of cycles have been obtained until failure. As the connection between the extruded wires could be effected by the height of the layers and influence on the mechanical properties and there are still lack of present literature to determine the effects of this parameter on the different specifications of the end-user functional parts, it has been taken into a part of the present work to deeper investigation.

2.1.3. Nozzle diameter

The diameter of the nozzle determines the diameter of the extruded wire which its effectiveness on the mechanical properties, and surface roughness is investigated in major works. In order to reduce the size of voids, the layer height can be varied as a key printing parameter; the lower the layer height, the smaller the void size. The compromise is that by reducing the layer height, the printing time increases. When the layer height is less than the nozzle diameter, the cross section of the raster deforms to a rectangular shape with round corners [18]. The influence of this parameter also can vary regarding to printing velocity. In [19], Gomez-Gras et al. have studied the influence of five manufacturing parameters on fatigue life of PLA specimens. The results of this study indicates that fill density, nozzle diameter, and layer height are the most influential factors on fatigue lifespan. Accordingly, S. Bakrani et al. [20], have considered the FFF process based on reliable properties, such as printing parameters and physical properties of PLA polymers to optimize the printing conditions. The results indicated the variation in the shear rate according to the diameter of the nozzle and the inlet velocity. The shear rate attained its maximum value near the internal wall at high inlet velocities and smaller diameters. Finally, the distribution of the viscosity along the radius of the nozzle was obtained.

2.1.4. Fill density

This parameter defines the distance between the lines of the interior filling and consequently, solidity percentage of inside the piece as shown in Figure 2.3.

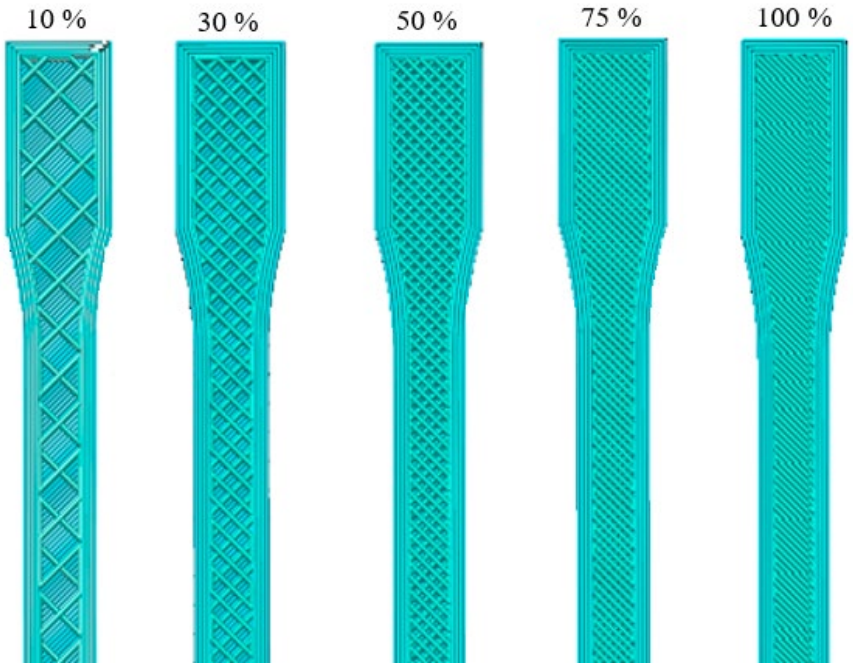

Figure 2.3. Graphical illustration of some filling percentages.

The percentages of this parameter can affect the mechanical properties significantly depend on the inside fullness of the parts while the amount of this percentage is critical in increasing/decreasing total material usage and costs. Carlos M.S. et al. [21], have evaluated the influence of interlayer cooling time (ILCT), nozzle diameter, fill density, raster angle and layer thickness on the ultimate tensile strength, yield strength, and elastic modulus of produced ABS parts through a design of experiments (DoE) approach. The result shown that nozzle diameter and fill density are the parameters that most influence the mechanical properties of ABS. The authors in [22] aims to investigate the properties of $\pm 45^{\circ}$ filling configuration with different filling degree for nylon, as well as calculating the effect of infill on the strength characteristics. It can be noted that after increasing the volume fraction of the infill structure above 60%, a significant increase in strength occurs. The ultimate strength of the fabricated samples is determined not only by the amount of material but also by the contact between the parallel tracks. Observation of the manufacturing process showed that when setting a theoretical volume fraction of filling in the range of 20–40%, neighboring tracks of the same layer do not touch each other. When the parameter is increased to 60% (which corresponds to the actual value of 54%), the parallel tracks contact, which leads to the formation of a continuous layer and increases the strength of the entire sample. The objective of another study [23] was to investigate the effect of variable infill density on the tensile and impact strength of polylactic acid (PLA) specimens printed by an open-source 3D printer. The results demonstrate that the specimens with varying infill density exhibit better tensile strength than the specimens with single infill density. The varying infill density specimens weigh lighter as compared to single infill density, which saves the raw material. The impact test

experimental data establishes that impact strength is directly proportional to the infill density. Thus, by varying the infill density, there is a reduction in the impact strength of the printed specimens. Since the optimum results of the properties are not achieved from the highest fill percentages [24, 25], it was motivating to consider this parameter to find individual specifications and probably its interaction with other strategies.

2.1.5. Infill pattern

Infill pattern allows to select different geometrical shapes such as (rectilinear, honeycomb, Hilbert curve, triangular, etc.) to fulfill inside of the samples as indicated in Figure 2.4. The influence of the various infill pattern by affecting on the raster angle and load direction could be considerable, therefore it has been taken into account in the present work widely. The study by A. Tsouknidas et al. [26], have examined the effect of layer heights, infill patterns and density on the energy dissipation properties of the printed PLA cylinders. This study shows rectilinear filling pattern compared favorably as it dissipated high kinetic energy values at lower force rates thus acting protectively towards the supporting structure. The experimental study [27], examined the effect of concentric, Hilbert curve, rectilinear, and honeycomb filling patterns at filling percentages of 20, 50 and 100% on the tensile and flexural strength of PLA material. The results indicate that concentric pattern yields the most desirable tensile and flexural tensile properties, at all filling percentages, apparently due to the alignment of deposited raster with the loading direction.

In another study [28], tensile testing of nylon-fiberglass composites is conducted on a DoE matrix based on Taguchi method. Process parameters such as fill density, fiber volume fraction, fill pattern and fiber-layering technique are varied and the samples are tested for their dimensions, productivity, yield strength, elastic modulus, ultimate tensile strength and elongation. This study resulted that the fill pattern and fiber orientation play the most important role in the mechanical properties.

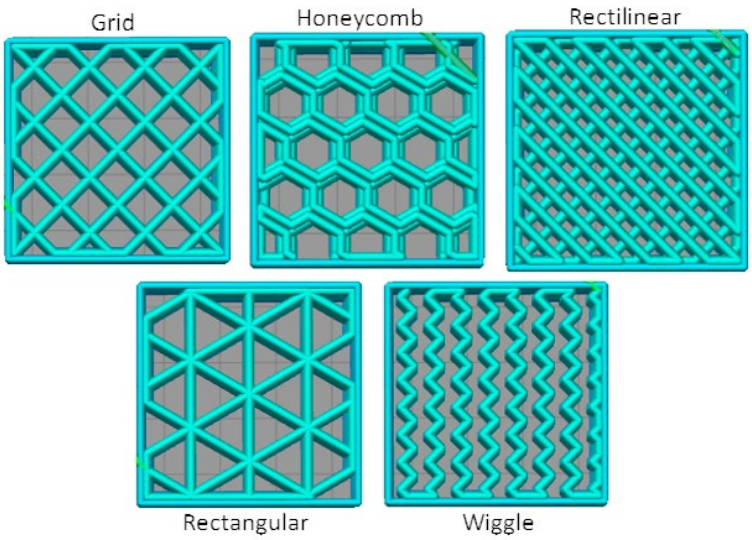

Figure 2.4. Various patterns to fulfil inside the sample.

2.1.6. Printing velocity

The printing velocity defines the linear speed of the extruder head traverses in the XY plane of the build platform. While different printing speed could vary the wide or diameter of the extruded wire, so it can be interesting to consider its effectiveness on the mechanical properties of the printed parts. Sera Ertay et al. present an integrated methodology for planning of tangential path velocity, material deposition rate and temperature control of the extruded material which is deposited along curved paths. The tangential velocity along the path is smoothed and optimized while respecting the heater's and extruder's capacities, as well as the feed drives' jerk, acceleration and velocity limits. The extrusion rate is controlled proportional to the tangential path velocity while keeping the temperature of the deposited thermoplastic material at the desired temperature by adaptively controlling current supply to the heater. The experimentally proven algorithm leads to more uniform material deposition at sharp curvatures and resulting improved dimensional accuracy of printed parts [29].

Also there are other parameters which are not objected in this study and kept constant during this research such as raster angle, air gap, extruder temperature, etc.

Consequently, it is clearly observable that using this technology in order to achieve certain product specifications is not a simple task and the factor of great relevance for the final characteristics and production of the piece is the manufacturing strategy. Hence, it is so important to set the best combination of the parameters for the desired mechanical properties. Abovementioned parameters such as (build orientation, nozzle diameter, layer height, fill density, and infill pattern) have shown more influence in the

literature reviewed. Accordingly, these parameters are considerable to find their effectiveness on the mechanical properties of this innovative material as well.

2.2 Mechanical properties and materials

One of the most the most significant issues for engineers to design a structure is selecting the material according to a suitable set of mechanical properties. These properties could be determined using accepted measurement standards which define the material behavior due to the resistance at load. Large strain plasticity, as observed in various materials, is one of the well-known phenomena requiring combined geometric and material nonlinear analysis of solids [30, 31]. As the stress increases, materials begin to fail via plastic deformation (non-linear stress vs. strain) or brittle fracture. One approach to quantify failure behavior is by determining yield strength, ultimate strength, and impact strength. Each one of these may be defined in relationship to the mode of loading: tension, compression, flexure, shear, or torsion [32]. Additionally, polymers are critical for AM because they represent the greatest market penetration and user accessibility [33]. The use of polymeric materials has become very popular in engineering applications. As a result, a continuous improvement in fiber/matrix, development of innovative fabrication technologies, advanced polymeric composite offers possibilities for major leaps in design, manufacturing, energy conservation, product utility and diversity [34]. The current repertoire of polymer materials available for power bed fusion (PBF) includes: ABS, polycarbonate (PC) polymer blends based on ABS and PC, polyamide (PA), PLA, polyvinyl alcohol (PVA), PEEK, thermoplastic flame retardant (FR) compounds, epoxies, etc. AM also allows combinations of plastics with carbon fiber and polymer matrix composites (PMC) [35]. Many of these materials are toughened to improve impact and fracture performance, but it is not clear whether AM takes full advantage of these properties. These materials are mainly employed for prototyping designs and the creation of low performance parts, but the demand for new higher performance polymer materials and composites is growing. For many polymers used in additive manufacturing, some mechanical, chemical, and physical properties are often reported in the technical specification sheet in tension or compression loading modes. On the other hand, these parameters do not adequately characterize materials that fail by the propagation of cracks. To describe this behavior requires fracture parameters that are often not reported in the technical sheet [36].

Of all mechanical properties, there have been a number of reviewed papers noticed tensile strength. In 2000 Es-Said et al. [37], examined the effect of layer orientation on the mechanical properties of rapid prototype ABS P400 samples by performing tensile, three-point bending, and impact tests. The highest results of this work for ultimate tensile strength, yield, flexural strength, and absorbed energy value of impact strength

are 20.6 MPa, 16.3 MPa, 44.4 MPa, and 4.12 J respectively. In contrast, other authors analyzed and compared the tensile and bending mechanical properties and the surface quality of treated with a solution of 90% Dimethylketone and 10% water and untreated FDM prototypes of ABS. Through this work, they found the maximum strength of 21.21 MPa and 44.35 MPa for tensile and flexural respectively. In order to treated filament changed into 20.09 MPa tensile strength and 45.29 MPa flexural strength. In conditions of reduced roughness, a minor reduction of the tensile strength was found but a greater ductility was found [38].

On the other hand, B.M. Tymrak et al. [39], quantified the basic tensile strength/stress, and elastic modulus of printed PLA and ABS components using realistic environmental conditions. The results found average tensile strengths of 28.5 MPa for ABS and 56.6 MPa for PLA with average elastic modulus of 1807 MPa for ABS and 3368 MPa for PLA. In the other side, the mechanical behavior of FDM parts by the classical laminate theory (CLT) is described by Caterina Casavola et al. [40]. In order to reach this objective, the values of the elastic modulus in the longitudinal and transverse directions to the fiber (E_1, E_2), the Poisson's modulus (ν_{12}) and the shear modulus (G_{12}) have been experimentally measured. Finally, the comparison between the CLT and the experimental results, conducted on ABS and PLA, has been carried out on symmetric and balanced specimens. The classical laminate theory allows to calculate the elastic behavior of a multi-layer orthotropic material using the constants that describe the mechanical behavior of the single layer E_1, E_2, ν_{12}, G_{12} and thickness h_c. E_1 and E_2 are the elastic modulus in the longitudinal and transverse directions to the fibers, ν_{12} is the Poisson's ratio, G_{12} is the shear modulus and thickness h_c is the layer thickness. The tests on the wire show that the PLA has a Young's modulus and UTS values that are about twice the values of ABS. However, even if PLA is stronger than ABS it is more brittle. Indeed, the deformation at fracture is 0.079 mm/mm for the PLA and 0.16 mm/mm for the ABS. Moreover, the most important disadvantages of PLA compared to ABS are the lower capacity to endure higher temperature than room temperature and the lower durability due to its biodegradability.

In [41], the influence of layer thickness and raster angle on the mechanical properties of 3D-printed polyether-ether-ketone (PEEK) is studied. Samples with three different layer thicknesses and raster angles were built using a PEEK 3D printing system and their tensile, compressive and bending strengths were tested. To evaluate the printing performance of PEEK samples, a comparison was made between their mechanical properties and ABS parts and the results are shown in table 2.1.

Table 2.1. Mechanical properties of PEEK and ABS [41].

Property	PEEK	ABS
Tensile strength	100.0 MPa	37.0 MPa
Elastic limit	72.0 MPa	31.0 MPa
Compressive strength	118.0 MPa	37.0 MPa
Compressive modulus	3.8 GPa	2.3 GPa
Bending strength	163.0 MPa	53.0 MPa
Bending modulus	4.0 GPa	2.2 GPa

Very recently, Travieso-Rodriguez et al. [42], analyzed the influence of the different manufacturing parameters on the flexural resistance and fatigue performance of PLA specimens built though fused filament fabrication. This work resulted Young module 3.7 GPa elastic limit 95.3 MPa maximum tension 120 MPa, and maximum elongation 6.21 from the flexural test. The most effective parameters' level to maximize the responses are indicated in table 2.2. It should be mentioned that the maximum stress achieved form the fatigue test is around 78 MPa obtained by the optimal set of parameters and levels.

Table 2.2. Parameters and levels to maximize the responses [42].

Factor	**Young's Modulus (E)**	**Yield Strength ($Rp_{0,2}$)**	**Maximum Tension (σ_{max})**	**Maximum Elongation (ε)**
Filament width	0.6 mm	0.6 mm	0.6 mm	0.2 mm
Layer Height	0.1 mm	0.1 mm	0.1 mm	0.2 mm
Infill density	75%	75%	75%	75%
Printing Velocity	20 mm/s	20 mm/s	20 mm/s	30 mm/s
Layer Orientation	Y	Y	Y	X
Infill pattern	Honeycomb	Honeycomb	Honeycomb	Rectilinear

Accordingly, influence of printing parameters on fatigue response of ABS parts built through FFF has been studied to achieve the optimal set of parameter and levels [43]. The results of this work shows that the highest lifespan, using the rectilinear infill pattern, was obtained when layer height, nozzle diameter, and infill density were at their highest level. On the other hand, the lowest variance was obtained when the infill density was at the lowest level, and the layer height and nozzle diameter at their middle or highest level, due to the lower difference shown. In case of honeycomb infill pattern, the nozzle diameter and layer height

maximized the lifespan at their middle and highest level and, like the rectilinear pattern, the infill density at its highest. The lowest noise was observed when the layer height was at its middle or highest level, nozzle diameter at its middle level, and infill density at its lowest. The optimal set of parameters and selected levels to achieve higher fatigue resistance is shown in table 2.3.

Table 2.3. Optimal combination of factors and levels to maximize the expected cycles to failure [43].

Parameters	Levels
Infill pattern	Honeycomb
Fill density	75 %
Nozzle diameter	0.4 mm
Layer height	0.2 mm

The ABS is frequently used for the automobile interior parts due to its excellent impact strength in combination with good balance of other requisite properties. These unique properties are originated from the specific components in the copolymer. ABS contains rubber-rich phase composed of Polybutadiene (PB) and PB grafted with Styrene–Acrylonitrile random copolymer (SAN) which is dispersed in rigid SANrich matrix. The PB moiety mainly determines the toughness of ABS, while the tensile and flexural strength depends on primarily on the SAN matrix [44]. In the other side, the PLA has good mechanical properties comparable to those of Polypropylene in many aspects [45]. PLA is considered to be an environmentally benign material, because it is usually synthesized by polymerizing lactic acid produced through the fermentation of renewable resources such as corn [46-50]. Because a lot of corn is to be consumed to produce bioethanol, which should provoke serious environment concern about the indiscreet deforestation to expand the arable land for the corn cultivation running counter to the CO_2 reduction, efforts are under way to investigate to use grass instead of grain as the source of the lactic acid production [51]. Fermentation by using genetically engineered microbes is another interesting route for a direct PLA synthesis [52, 53]. Therefore, ABS and PLA due to the low cost, high availability, and basic printer requirements are most common within the RepRap 3D printing industry and most extruders are capable of easily extruding these materials reliably [54].

In order to explain the fluctuation of tensile strengths of the large sample set of RepRap prints and better inform designers on RepRap print properties [55], determined the effect of color and processing temperature on material properties of deposited PLA in various colors. Five colors (white, black, blue, gray, and natural) of commercially available filament processed from Ingeo 4043D pellets PLA is tested for crystallinity with X-ray Diffraction (XRD), tensile strength following ASTM D638 standard and the microstructure is

evaluated with environmental scanning electron microscope. The results of this work are summarized in table 2.4, and clearly show that percent crystallinity of 3-D printed parts is color dependent.

Table 2.4. Ultimate tensile strength, maximum strain, and percent crystallinity as a function of color for PLA [55].

Color	Ultimate tensile strength (MPa)	Yield strength (MPa)	Maximum strain (%)	Crystallinity (%)
Natural	57.16 ± 0.35	52.47 ± 0.35	2.35 ± 0.05	0.93 ± 0.06
Black	52.81 ± 1.18	49.23 ± 1.18	2.02 ± 0.08	2.62 ± 0.09
Gray	50.84 ± 0.23	46.08 ± 0.23	1.98 ± 0.04	4.79 ± 0.10
Blue	54.11 ± 0.30	50.10 ± 0.30	2.13 ± 0.02	4.85 ± 0.15
White	53.97 ± 0.26	50.51 ± 0.26	2.22 ± 0.04	5.05 ± 0.18

Composite materials have a wide range of uses, and their use is rapidly increasing. Natural fibers are also increasingly used as reinforcements for thermoplastic composites. AM is a common material extrusion process using bio polymers reinforced with natural fibers. However, there is a lack of understanding of the effect of printing parameters on the mechanical properties involved in this new process [56]. A few studies have reported the mechanical properties of PLA composite materials reinforced by natural fibers of printed parts influenced by various processing parameters. Wood fiber-reinforced PLA composites (WFRPCs) were used as a filament to manufacture the unidirectional WFRPC components by means of FDM. The physic-mechanical properties of the WFRPC components printed at different extrusion temperatures (200, 210, 220, and 230 °C) were determined by Teng-Chun Yang [57]. The results of this study shows that most of the physical properties (moisture content, surface roughness, water absorption rate, and thickness swelling rate) of the printed WFRPC component were not significantly influenced by extrusion temperature, while its density and color difference increased as the extrusion temperature increased. Additionally, the tensile and flexural properties of the FDM-printed WFRPC component decreased when the extrusion temperature was more than 200 °C, whereas the compressive strength and internal bond strength increased by 15.1% and 24.3%, respectively, when the extrusion temperature was increased from 200 to 230 °C. Additionally, the microstructure and mechanical performance of wood-based filament is investigated using experimental and numerical approaches on the parts printed by FDM technique [58]. Wood-based filament made of PLA/PHA matrix reinforced by wood particles is printable in a wide range of temperatures ranging from 210 °C to 250 °C. Only a limited improvement in the tensile performance is obtained when the printing temperature is increased from 210 °C to 230 °C. Higher printing temperatures above 230 °C are not suitable, as the tensile properties can be affected by the thermal degradation of wood particles that occurs between 210 °C and 370 °C. Mirko Kariz et al. [59], have investigated the effect of

wood content in 3D printing materials on the properties of 3D printed parts. Six filaments using PLA with varying loading levels of wood particles from 0% to 50% by weight were produced and used for 3D printing. The density of the filaments and 3D printed parts used in this study slightly decreased with increasing wood content. The tensile strength of the filaments increased from 55 MPa to 57 MPa with an addition of 10% wood, but decreased with higher levels of wood content to 30 MPa for filaments with 50% wood content. In [60], the viability of a recycling and reusing process for end-of-life glass fiber reinforced wind turbine blades is validated. In this work short glass fibers from scrap turbine blades are reclaimed and mixed with PLA through a double extrusion process to produce composite feedstock with recycled glass fibers for FFF. For 25 weight % reinforcement, the samples showed up to 74% increase in specific stiffness compared to pure PLA samples, while there was a reduction of 42% and 65% in specific tensile strength and failure strain, respectively. For the composite specimens out of reinforced PLA with recycled glass fibers, it was found that the specific modulus and tensile strength are respectively 18% and 19% higher than those of samples reinforced with virgin glass fibers.

Despite of the variable printing parameters, geometrical characteristics of the fibers play an important role in the mechanical properties of composites [61]. In [62] a better understanding of the relationships between processing method, fiber characteristics, and composite behavior on the properties of wood-plastic composites (WPC) is provided. WPC were manufactured using extrusion or injection molding (IM) and fibers with different length-to-diameter (L/D) ratios. The IM process resulted in better composite physical and mechanical properties than the extrusion process, but higher density was obtained with the extrusion process. In the study by Ke-Chang Hung et al. [63], four kinds of lignocellulosic fibers (LFs), namely, those from Chinese fir (*Cunninghamia lanceolata*), Taiwan red pine (*Pinus taiwanensis*), India-charcoal trema (*Trema orientalis*) and makino bamboo (*Phyllostachys makinoi*), were selected as reinforcements and incorporated into high-density polyethylene (HDPE) to manufacture wood-plastic composites WPCs by a flat platen pressing process.

In contrast to the aforementioned references this dissertation does not aim to design a new material, but to assess the characteristics of one already existing and manufactured and distributed by a real company, by applying extensive experimental tests following a Taguchi orthogonal array.

Herein the material which is selected to investigate its properties is a commercial material entitled Timberfill developed and manufactured by Czech company Filamentum Ltd (Fig. 2.5). This material is developed as a composition of biodegradable PLA polymer reinforced by wood particles in a 5%-10% ratio. Since the initial mechanical parameters could be defined by the terms of yield tress/yield strength, ultimate strength, maximum deformation at break, durability, etc. the majority of studies have focused on the tensile strength, flexural strength, and fatigue performance to investigate the mechanical properties of printed parts

through FFF process of in variable strategies on different materials. Consequently, to introduce this material, applying tensile strength, flexural strength, and fatigue tests could be helpful to achieve the mechanical properties of the Timberfill material. Furthermore, finding the best combination of selected printing parameters and levels to obtain higher resistance of printed part is another important point of this work. Additionally, some technical information based upon the manufacturer is illustrated in figure 2.6.

Figure 2.5. Timberfill spool, left) Champagne, right) Rosewood.

Physical properties	**Typical Value**	**Test Method**	**Test Condition**
Material density	1,26 g/cm³		20 °C
Melt volume index	25 cm³/10 min	ISO 1133	190 °C, 2,16 kg
Diameter tolerance	± 0,10 mm		
Weight	750 g of filament (+ 250 g spool)		
Mechanical properties	**Typical Value**	**Test Method**	**Test Condition**
Tensile strength	39 MPa	ISO 527	at break, 5 mm/min
Elongation at break	2 %	ISO 527	5 mm/min
Tensile modulus	3200 MPa	ISO 527	1 mm/min
Charpy impact strength	22 kJ/m²	ISO 179/1eU	23 °C, unnotched
Hardness	77 Shore D	ISO 7619	
Thermal properties	**Typical Value**	**Test Method**	**Test Condition**
Melting temperature	145-160 °C		
Heat distortion temperature	48 °C	ISO 75	method B, 0,45 MPa
Printing properties	**Typical Value**	**Test Method**	**Test Condition**
Print temperature	170-185 °C		
Hot pad	40-50 °C		

*Figure 2.6. Initial technical data sheet of the Timberfill material [**https://fillamentum.com/**]*

The thermal stability of PLA and Timberfill was considered through Thermal gravimetric analysis (TGA) as a method of thermal analysis that the mass of a sample was measured over time as the temperature changes. Since part of Timberfill is constituted by wood and PLA, the results proved that wood compartment was decomposed around 345±1 °C and the second which might be related to PLA specimens in the structure of Timberfill was peaked near 393±1 °C. The higher decomposition temperature of PLA offered it as a better alternative than Timberfill. Also performed thermogravimetric tests on the material evidences the composition ratio as 8±1% of wood fibers.

On the basis of these observations, the specific objectives of this dissertation can be formed as follow to drive the activities undertaken inside the framework.

2.3 Developed models to characterized mechanical properties

In the process of FFF, the combination of manufacturing parameters and find the optimal set of them with appropriate levels is difficult to understand [39, 54]. That is why a large number of studies have been investigated the effects of these parameters on the mechanical properties of different materials [19, 42, 43, 64], by means of FEM techniques. The study [55], combined the use of FFF with finite element analysis (FEA) to enhance the understanding of certain manufacturing parameters (i.e. material, infill density, infill pattern, and outer vertical shell) in the design process of a lumbar fusion cage. Three FFF materials with distinct mechanical properties namely polycarbonate (PC), acrylonitrile butadiene styrene (ABS), and PLA were tested. Three infill densities (i.e. 25%, 50%, 75%) were investigated along with two different infill patterns (i.e. rectangular and honeycomb). Compressive modulus and compressive yield strength values obtained from standard mechanical analysis were used as input for FEA to assess numerically the mechanical performance of a lumbar fusion cage under physiological static loading. The results of FEA analysis indicated that both PC and ABS can be adopted to fabricate a porous cage with a 50% infill density and a honeycomb infill pattern, without the need of a vertical outer solid shell. In the paper [doc20], a novel approach of voxelization modelling-based Finite Element (FE) simulation and process parameter optimization for FFF is presented. In the approach, firstly, a general meshing method based on voxelization modelling and automatic voxel element sorting is developed. Then, FE based simulation for the FFF process is conducted by combining the ANSYS Parametric Design Language (APDL) with the element birth and death technique. During the simulation, the influence of key process parameters on the temperature field, including scanning speed, molding chamber temperature and nozzle temperature, is analyzed in detail. Results showed that among the process parameters, the molding chamber temperature had the most significant effect on the warping deformation of the FFF parts. The optima parameters for the FFF process

with ABS under the analyzed conditions were 50 mm/s for the scanning speed, 80 °C for the molding chamber temperature of, and 180 °C for the nozzle temperature, respectively. Courter, B. et al. [65], have simulated the FFF process by the commercial finite element software package Abaqus. A Mobius arm part is used to illustrate the simulation procedure and a sequentially coupled thermo-mechanical analysis is performed. The heat transfer analysis calculates the temperature history which is mapped onto and used to predict residual stress and potential part distortion in the subsequent structural analysis. Independent tool path events are characterized using event series data such as time, location and bead cross-sectional area. Abaqus solves for dependent events such as progressive element activation, local material orientation, and evolution of cooling surfaces, temperature profile, stress and distortion. The results show that FE simulations effectively capture the interaction between tool path and thermomechanical physical processes and their impact on the final state of the printed part.

2.4 Conclusions from the state of the art

The main conclusions should have obtained from the state of the art are described following:

1. There is no sufficient technical information of the commercial composite materials in case of engineering operations. A few publications can be found which are investigated the mechanical characterizations of laboratorial made compositions.
2. There is a set of optimal combination of parameters and levels to apply in FFF process to maximize the mechanical resistance of the specimens. These influential parameters and levels could be selected regarding to the literature reviewed and previous experiences for each one of the responses.
3. There are no enough comparison studies between the FFF processes with traditional techniques. The applicability's of this young manufacturing technology and its functional end-use parts have been evaluated and compared to injection-molded results on the same material.
4. None of the reviewed research have considered the behavior of the material by modeling its properties and comparing to the real experimental test. In present work the experimental results are validated through finite element modeling which this method could be used to predict the mechanical behavior of any innovative material.

Chapter 3

Case study:

Study of the manufacturing process effects of fused filament fabrication and injection-molding on tensile properties of composite PLA-wood parts

Abstract

The present study evaluates the effects of manufacturing parameters on the tensile properties of a commercial composite material based upon polylactic acid (PLA) with wood fibers known as Timberfill. The specimens are built through fused filament fabrication (FFF) and the influence of four printing parameters (Layer height, Fill density, Printing velocity, and Orientation) are considered through a L_{27}Taguchi orthogonal array in order to reduce experimental runs. Tensile test is applied to obtain the response variable used as output results to perform the ANOVA calculations. Results show that fill density is the most influential parameter on the tensile strength, followed by building orientation and layer height, whereas the printing velocity shows no significant influence. The optimal set of parameters and levels is found, being 75% fill density, 0°Z-axis orientation, 0.4 mm layer height, and 40 mm/s velocity as the best combination. Applying this combination obtained 9.37 MPa in maximum tension. Separately, five solid injection molded Timberfill specimens are tested as well and the results compared to the printed samples. The values of the elastic modulus, elastic limit, and maximum tension of the injected samples were almost twofold of those were obtained for the FFF samples, but the maximum elongation of injected specimens was fell sharply.

Keywords: Additive manufacturing, 3D printing, Fused Filament Fabrication, Young's module, Tensile strength, Timberfill, PLA

Nomenclature

AM- Additive manufacturing

FFF - Fused filament fabrication

DOE - Design of experiments

ANOVA - Analysis of variance

3.1. Introduction

Additive manufacturing (AM) has already gained traction in the aerospace and biomedical industries and is now being explored as a viable manufacturing method in the construction sector. Fused Filament Fabrication (FFF) or 3D printing is one of the most common AM technique to fabricate complex three-dimensional components to a near-net shape. The mechanical performance of FFF 3D printed parts depend on several manufacturing process and design parameters. Examples of manufacturing process parameters include machine tolerances, feedstock material, filament diameter, nozzle diameter, nozzle temperature, bed temperature, cooling rate (i.e. fan speed), and printing velocity [1,2]. On the other hand, there are examples of design parameters such as building orientation, raster angle, layer thickness, and infill percentage [19, 54, 66, 67].

Numerous studies have investigated the effects of aforementioned parameters on the tensile strength and the other mechanical properties of applicable materials. Es-Said, O.S. et al. [37] have examined the effect of layer orientation on the mechanical properties of rapid prototype ABS P400 samples by performing tensile, three-point bending, and impact tests. The tensile data of the ABS samples with different orientations indicate that the ultimate and yield strengths were the highest in the orientation where layers were deposited along the length of the sample (0° in X-axis), followed by those where the samples are built at 45°, -45° and 90° in descending order. In [68] influence of five important process parameters such as layer thickness, orientation, raster angle, raster width and air gap on three responses such as tensile, flexural and impact strength of test specimen are considered. In this study the desirability function concept have been used to determine optimal factor levels for improving tensile, flexural and impact strength independently and all three strengths simultaneously. In another study Fernandez-Vicente, M. et al. [69] the influence of two controllable variables, such as pattern and density of the infill of samples produced using an open-source 3D printer on the tensile mechanical behavior has been evaluated. The results obtained

show that the influence of the different printing patterns causes a variation of less than 5% in maximum tensile strength, although the behavior is similar. The change in infill density determines mainly the tensile strength. The combination of a rectilinear pattern with a 100% infill shows the higher tensile strength, with a value of 36.4 MPa, with a difference of less than 1% from raw ABS material. A study made by John J. Laureto et al. [70] characterized the mechanical property variations of ultimate tensile strength (UTS) and yield strength of FFF printed components of ASTM D638-14 Type I and Type IV tensile bar specimens, and multiple parameter types were evaluated for PLA material. The results show that the influence of different printing patterns varies the maximum tensile strength less than 5%. The combination of a rectilinear pattern in a 100% infill shows the higher tensile strength, with a value of 36.4 MPa, with a difference of less than 1% from raw ABS material.

Cwikła, G. et al. [71] have concluded the infill pattern, fill density, shell thickness and printing temperature influence on the selected mechanical properties of the standardized samples, printed with low-cost standard materials (ABS), using a low cost 3D printer. The results show that, where the objective is to have both, a lightweight and durable element, the best set of parameters is the use of a honeycomb pattern with fill density of about 40-50%, and a shell thickness of 2-3 layers/lines. If the maximum strength is the priority, shell thickness should be increased. The use of an infill pattern other than the honeycomb can accelerate the printing time at the expense of its strength. Tensile test has also shown that the extrusion multiplier parameter should not be set less than 0.9, because strength of the sample decreases disproportionately to filament savings. Marat-Mendes, R. et al. [72] have studied the influence of FFF processing parameters such as extrusion temperature and raster angle upon mechanical properties and microstructural features of processed PLA parts. In this research the fill density, layer thickness and printing velocity were kept constant at 60 %, 0.2 mm and 40 mm/s, respectively. The results indicate that mechanical performance is higher when material is stored under controlled atmosphere before use, and when material deposition direction is aligned with applied load. Increasing the extrusion temperature also increases performance, by increasing deformation ability of PLA molecules. In a study focused on the influence of nozzle temperature and infill line orientations for parts made with short carbon fiber (CF)-reinforced PLA by El Magri, A. et al. [73]. Results have shown the influence of nozzle temperature on the mechanical properties, with an optimum temperature maximizing the tensile properties. Infill orientations also play a significant role in achieving good mechanical properties, with the proper combination of orientation enabling the tailoring of properties along a specific axis.

To reduce the consumption of petroleum-based resources and thereby enhance the eco-friendliness of the material, it could be interesting to replace ABS parts with other materials such as PLA or other composites and renewable materials for same purposes. To this extend other researches have compared mechanical

characterizations of different materials. The results of study quantifying the basic tensile strength and elastic modulus of printed components using realistic environmental conditions for standard users of a selection of open-source 3D printers from [39] shows that parts printed from tuned, low-cost, open-source RepRap 3D printers can be considered as mechanically functional in tensile applications. For this reason, recently natural fibers have been introducing as the filler adding to common filaments.

PLA composition reinforced with natural fibers such as hemp, wood, kenaf, and flax has already been studied [13-16]. Although there are a few studies on PLA-based composites, the majority of the available literatures did not use significant commercial filaments. A summary of the filler, content, and test have been done by these researches is provide in table 3.1.

Table 3.1. Mechanical tests on different non-commercial composite.

References	Filler	Fiber content (%)	Test
Tisserat *et al.,* 2015 [17]	Paulownia wood	25	Tensile
	Orange wood	25	//
Zhao *et al.,* 2016 [18]	Bamboo	20	-
Daver *et al.,* 2016 [19]	Cork powder	5	Tensile
Tao *et al.,* 2017 [20]	Aspen sawdust	5	Tensile
Xie *et al.,* 2017 [21]	Poplar wood	30	Tensile
Gkartzou *et al.,* 2017 [22]	Pine lignin	5	Tensile
Filgueira *et al.,* 2017 [23]	thermomechanical pulp (TMP)	10-20	Flexural-Tensile
Stoof *et al.,* 2017 [24]	Hemp	0-30	Tensile
Kariz *et al.,* 2018 [25]	Wood powder	0-50	Flexural-Tensile
Guo *et al.,* 2018 [26]	Poplar wood	10	Flexural-Tensile-Impact
Depuydt *et al.,* 2019 [27]	Bamboo-Flax	15	Flexural-Tensile

Additionally some researchers observed mechanical behavior of parts fabricated with different manufacturing technologies [40, 64, 74], and different treatments [38, 65, 75, 76] to achieve higher resistances of mechanical properties.

However, it is essential to characterize and understand the performance of FFF-processed Timberfill parts while many drawbacks could control by carefully choosing the processing parameters [35]. That is why the aim of the current investigation is to examine the effects of various printing parameters on innovative commercial material submitting tensile test to obtain mechanical properties. To avoid manufacturing a big number of specimens an experimental design of Taguchi L_{27} orthogonal array was applied that refers to

how participants are allocated to the different conditions. Then to evaluate the achieved characteristics of printed Timberfill samples, a comparison was made between injection-molded and printed sample applying the same procedure. This provides a point of comparison to assess the properties achieved by the printed specimens. It is also another forte of this paper, since there are few reported studies in the literature that discuss the differences between the properties of 3D printed parts and those obtained by other conventional manufacturing technology using the same base material.

3.2. Materials and methods

Timberfill "Rosewood" filament of 1.75 mm diameter developed and manufactured by company Filamentum Ltd. located in the Czech Republic was used to manufacture specimens for this study. Timberfill was developed with a purely aesthetic purpose that of imitating objects with a wood aspect. To achieve this goal, the company developed a composition of biodegradable PLA polymer combined with wood fibers in a 5-10 % ratio. Therefore, Timberfill can be proven to be a feasible material for some practical purposes in low-scale manufacturing environments.

Timberfill is a relatively new PLA-wood composite material that exhibits similar mechanical features as ABS or PLA. Models printed with this material have a genuine appearance of wood. It is provided as a commodity material, with the purpose of becoming a commonly used material in FFF machines for various applications.

3.2.1. Tensile testing and specimens

The tensile specimens in this work were manufactured according to ASTM D-638 standard test method for tension of plastics and composites utilizing dog-bone shape as shown in Figure 3.1, with 7mm thickness. In this study, Elastic modulus (Young's modulus), Elastic limit (Yield stress), Tensile strength, and maximum Elongation to break are calculated to characterize the mechanical behavior of Timberfill pieces submitted to tensile loads.

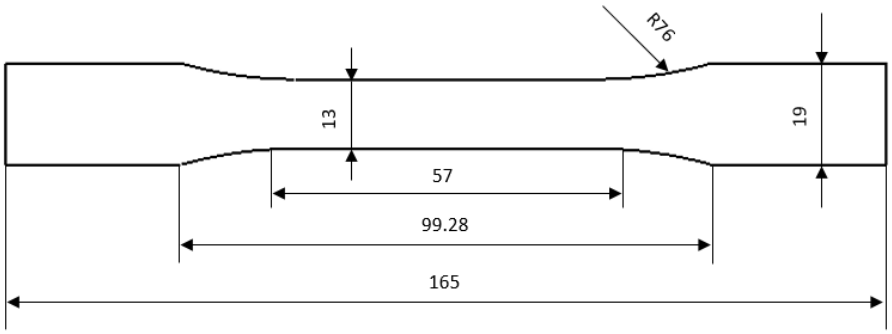

Figure 3.1. Geometrical drawing of specimens for tensile test.

3.2.2. Taguchi experimental design

To carry out the study, design of experiment (DOE) has been applied based on Taguchi method which is a robust optimization technique to make experiments to predict responses and optimize the FFF process conditions in accuracy level [77]. The factors and levels shown in Table 3.2, have been chosen taking into account their high effectiveness on mechanical properties rely on previous researches [37], printer configurations, and material manufacturer recommendations. Since Timberfill is a composition of PLA polymer with wood fibers, the manufacturer has recommended to use the nozzle with minimum 0.5 mm diameter. Finally, it has been decided to select layer height, fill density, printing velocity, and building orientation (Table 2).

Table 3.2. Factors and levels used for the DOE.

Parameters	**Level**		
	1	2	3
Layer height (mm)	0.2	0.3	0.4
Fill density (%)	25	50	75
Velocity (mm/s)	30	35	40
Orientation	X-axis	45º X-axis	Z-axis

To clarify the selected parameters, figure 3.2 shows a definition of different orientations that used in the slicer software for print the samples. The cut section of the samples which indicates the different orientation with 50% density of grid infill pattern (Fig. 3.2. A), but the support has been applied under the thinner part of the samples in Z-axis orientation. In figure 2B, the height of the Layers depositing on top of the previous one is shown.

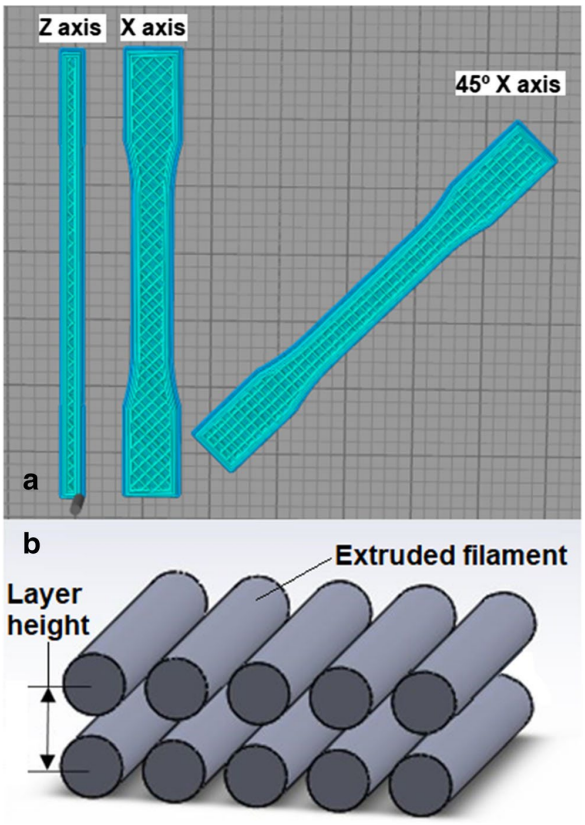

Figure 3.2. A) Different orientation and cut section of the samples with 50% density in grid infill pattern. B) The height of the extruded layers.

To analyze the influence of the selected factors and levels a L_{27} Taguchi orthogonal array has been applied using Minitab 18 software for statistical calculations (Table 3.3).

Table 3.3. L27 Taguchi orthogonal array of DOE.

Runs	Layer height (mm)	Fill density (%)	Velocity (mm/s)	Orientation
1	0.2	25	30	X-axis
2	0.2	25	35	45º X-axis
3	0.2	25	40	Z-axis
4	0.2	50	30	45º X-axis
5	0.2	50	35	Z-axis
6	0.2	50	40	X-axis
7	0.2	75	30	Z-axis
8	0.2	75	35	X-axis
9	0.2	75	40	45º X-axis
10	0.3	25	30	45º X-axis
11	0.3	25	35	Z-axis
12	0.3	25	40	X-axis

13	0.3	50	30	Z-axis
14	0.3	50	35	X-axis
15	0.3	50	40	45º X-axis
16	0.3	75	30	X-axis
17	0.3	75	35	45º X-axis
18	0.3	75	40	Z-axis
19	0.4	25	30	Z-axis
20	0.4	25	35	X-axis
21	0.4	25	40	45º X-axis
22	0.4	50	30	X-axis
23	0.4	50	35	45º X-axis
24	0.4	50	40	Z-axis
25	0.4	75	30	45º X-axis
26	0.4	75	35	Z-axis
27	0.4	75	40	X-axis

It should be mentioned that for each manufacturing parameter set or run included in the array, 5 specimens were manufactured individually and tested, to guarantee the repeatability of the results. Therefore, the rest of the parameters that are not object of study have been kept constant among all specimens (Table 3.4).

Table 3.4. Main constant printing parameters used in the experiments.

Nozzle diameter	Raster angle	Nozzle temperature	Infill pattern	Skirt layer
0.5 mm	45º	180ºC	Grid	2 layers

3.2.3. Specimens manufacture

According to the above-mentioned test method the sample was designed by the Catia V5 software with the actual shape and dimensions and has been exported to an STL format, so that it can be read and interpreted by the printing parameterization software. In this project the Repetier-Host (Slic3r) software has been used which the G-Code is obtained to be able to print. All of the specimens were printed using Prusa i3 printer.

Five specimens were also manufactured through the injection process. The same raw material used for the printed specimens was used for this. In this way the results obtained can be comparable. These specimens were manufactured in the condition which are defined in table 3.5.

Table 3.5. Manufacturing conditions of the injection-molding samples.

	Injection property				
Quantity	Injection pressure	Temperature	Injection time	Maintaining time	Cooling duration

	35-65 bars	200°C	76 s	30 s	10 s

3.2.4. Experimental setup

Once all the samples were manufactured, they have been measured to achieve the average area by calculating from the width and thickness of four different sections of samples using digital micrometer.

The universal Microtest EM2/20 machine has been used for these tensile tests equipped with a 25 kN load cell at a 1 mm/min displacement rate, 50 mm extensometer, a Spider and Microtest data acquisition system, two S1 pneumatic jaws, and the Microtest SCM3000-Catman 4.5 control software. In the other side, this setup consists of a set of a High Definition (HD) camera that records the test video at 60 Hz sampling frequency, which is also connected to the spider data logger. The camera has been applied to illuminate the test area and to synchronize the data using a switch-controlled flash (Fig. 3.3).

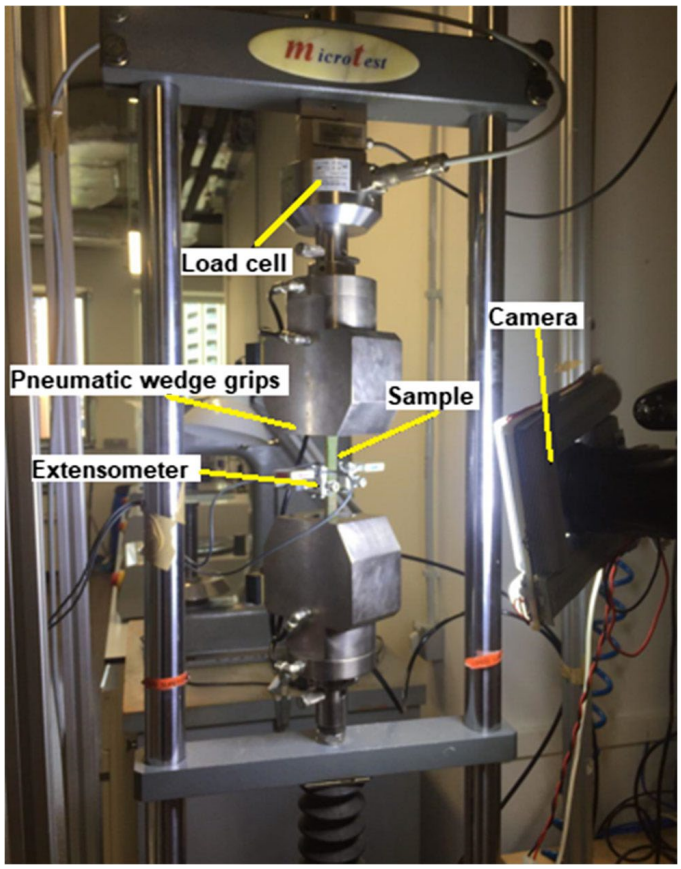

Figure 3.3. Universal testing machine with camera and load equipment.

Once all the setup is equipped and adjusted, the tests are carried out for all of the 135 FFF specimens and the 5 injected samples.

3.2.5. Analysing process

After each test has been completed, two different files are achieved from the data logger. First, a file that includes the force collected from the load cell and displacement of the extensometers, as well as the recorded voltage versus time. Second, the video recorded by the camera that provided graphical information to compute the strain of the specimen at every stage of the test.

To obtain the defined mechanical properties such as Young's modulus (E), yield strength ($Rp_{0.2}$), maximum strength (σ_{max}), and maximum deformation (ε), Matlab R2018b software is used to analyze the data. To perform this analysis, several steps have been followed. First of all, the HD video was processed to obtain each photo frame during the test. In the second step, the photo frames and the recorded data are synchronized by means of a Matlab script. Next, a rectangular grid pattern is generated in the initial frame of the test sample dotted in red crosses (Fig. 3.4. A). This gridding recognizes the displacement on the section of samples while the deflection occurs (Fig. 3.4. B). During the next step, the marked pixels are tracked and deflection is computed consequently based on the differences between the initial and final position. By finishing this step, two scroll files have been generated which can be used for the deflection script to transfer the values of the points into real deformations. After using the deflection obtained in this step, the process continues to calculate the deformation and create the stress-strain curve.

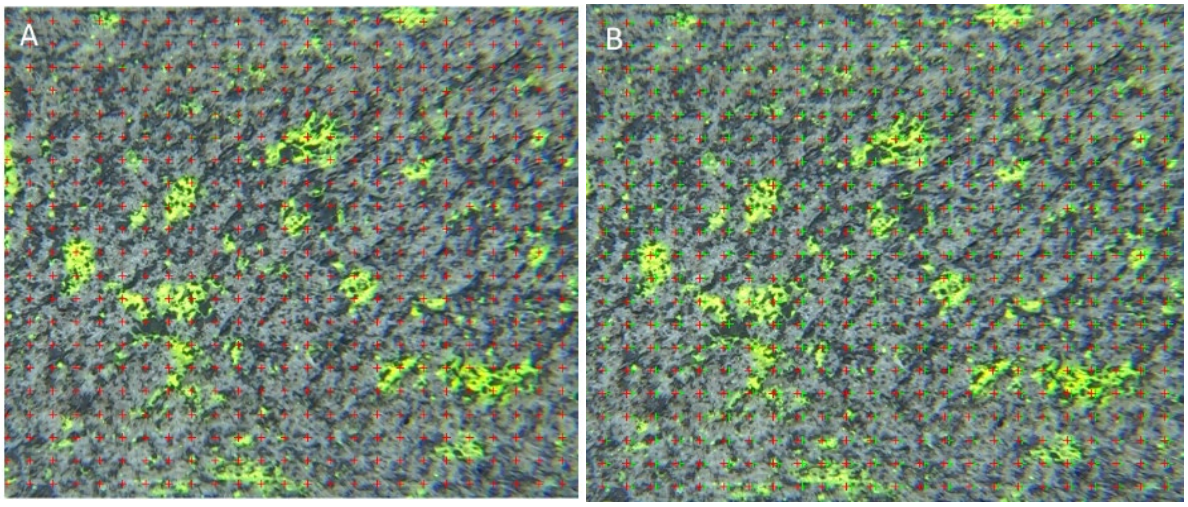

Figure 3.4. A) Rectangular grid generated on the test section of sample tracking with red points. B) Initial points and displaced points.

3.3. Results and discussion

Table 3.6 includes the average results of the five repetitions for each manufacturing configuration.

Table 3.6. Results obtained for experimental runs. E: Young's modulus, Rp0.2: yield strength, σmax: maximum strength, ε: maximum deformation with standard deviation for each property.

	E (GPa)	$S_{0.2}$ (MPa)	σ_{max} (MPa)	ε_{max} (%)
1	0.65 ± 0.06	4.50 ± 0.48	4.93 ± 0.60	1.34 ± 0.25
2	0.60 ± 0.03	4.21 ± 0.02	4.84 ± 0.22	2.03 ± 0.21
3	0.71 ± 0.02	4.97 ± 0.24	5.16 ± 0.40	1.06 ± 0.17
4	0.64 ± 0.00	4.98 ± 0.14	5.73 ± 0.29	2.0 ± 0.50
5	0.80 ± 0.03	5.54 ± 0.06	5.97 ± 0.16	1.42 ± 0.27
6	0.72 ± 0.02	4.83 ± 0.17	5.39 ± 0.22	1.90 ± 0.19
7	1.06 ± 0.07	7.07 ± 0.15	7.81 ± 0.13	2.01 ± 0.10
8	0.93 ± 0.06	6.03 ± 0.31	6.73 ± 0.31	1.77 ± 0.15
9	0.91 ± 0.03	6.84 ± 0.41	8.17 ± 0.52	2.63 ± 0.35
10	0.58 ± 0.02	4.31 ± 0.26	5.05 ± 0.26	2.23 ± 0.45
11	0.74 ± 0.05	5.61 ± 0.7	6.17 ± 0.55	1.78 ± 0.37
12	0.68 ± 0.01	4.78 ± 0.13	5.26 ± 0.12	1.65 ± 0.11
13	0.98 ± 0.06	7.02 ± 0.24	7.37 ± 0.19	1.28 ± 0.09
14	0.79 ± 0.02	5.74 ± 0.18	6.36 ± 0.19	2.34 ± 0.15
15	0.69 ± 0.05	5.43 ± 0.48	6.43 ± 0.57	3.03 ± 0.60
16	0.81 ± 0.02	5.67 ± 0.11	6.34 ± 0.12	2.36 ± 0.25
17	0.81 ± 0.03	6.19 ± 0.20	7.63 ± 0.25	3.56 ± 0.50
18	1.21 ± 0.05	8.95 ± 0.30	9.37 ± 0.27	1.42 ± 0.12
19	0.72 ± 0.00	5.25 ± 0.10	5.67 ± 0.17	1.41 ± 0.15
20	0.77 ± 0.02	5.82 ± 0.23	6.35 ± 0.16	1.75 ± 0.29
21	0.65 ± 0.02	4.84 ± 0.19	5.58 ± 0.26	2.69 ± 0.37
22	0.87 ±0.02	6.61 ± 0.14	7.22 ± 0.18	1.95 ± 0.25
23	0.70 ± 0.01	5.68 ± 0.19	6.55 ± 0.25	2.35 ± 0.29
24	1.13 ± 0.20	7.61 ± 0.48	8.15 ± 0.37	1.13 ± 0.10
25	0.88 ±0.04	6.71 ± 0.18	7.94 ± 0.31	2.35 ± 0.43
26	1.20 ± 0.07	8.90 ± 0.32	9.11 ± 0.42	1.27 ± 0.23
27	1.06 ± 0.03	7.82 ± 0.09	8.55 ± 0.04	2.42 0.50

- Analysis of variance

Once the results were obtained, the statistical calculation through analysis of variance (ANOVA) was performed on the dataset included in the Taguchi experimental array, for each parameter that describe the mechanical behavior of the evaluated specimens by the Minitab 18 software. To validate the statistical significance of the parameters included in the model on each of the responses, the p-value associated to the ANOVA, was compared to a significance level of 5%. In addition, the interactions between the different parameters were analyzed which leads to the conclusion that if there is significant interaction among the pairs of selected values or not, since the p-values of each pairs should be less than 0.05.

- Young's modulus

In this case, it can be concluded that the most significant parameters, due to their p-values, are the fill density and orientation as shown in Fig. 3.5. This graph evidences that the fill density results have a direct relation with the Young's modulus that means higher values of density results in a higher elastic modulus that can be clearly due to the solidity percentage of inside the samples. As it can be seen from the figure, the samples built in Z-axis orientation have shown higher elastic module and the most significant reason could be depositing layers more than the other building directions. Based on the obtained p-values, layer height also can be taken into account because the value is not so much bigger than 0.05, but printing velocity does not show a significant effect on the Young's modulus.

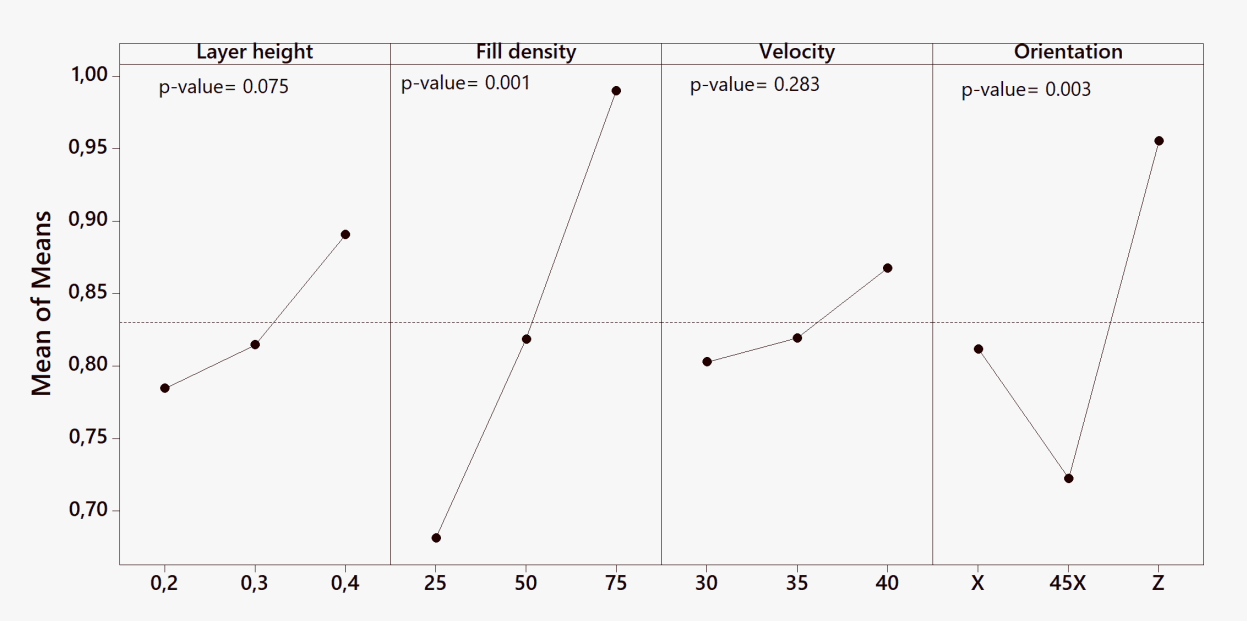

Figure 3.5. Main effect for means calculated through ANOVA. Response variable: Young's module.

In this case obtained p-values of parameters interactions were more than 0.05, it means that the selected parameters in this study are independent of each other, at least in the analyzed value ranges for Young's modulus.

- Yield Strength

It is necessary to analyze the effects of the variation of the different factors on the yield strength, which is indicated in graph of main effects for the averages (Fig. 3.6). The most significant parameters on the yield strength according to the p-values are fill density, followed by orientation and layer height. The effectiveness of these parameters have been repeated due to the fact that occurred to in case of Young's

modulus. So that to achieve the bigger yield strength, the bigger values of layer height and fill density in Z-axis orientation should be selected.

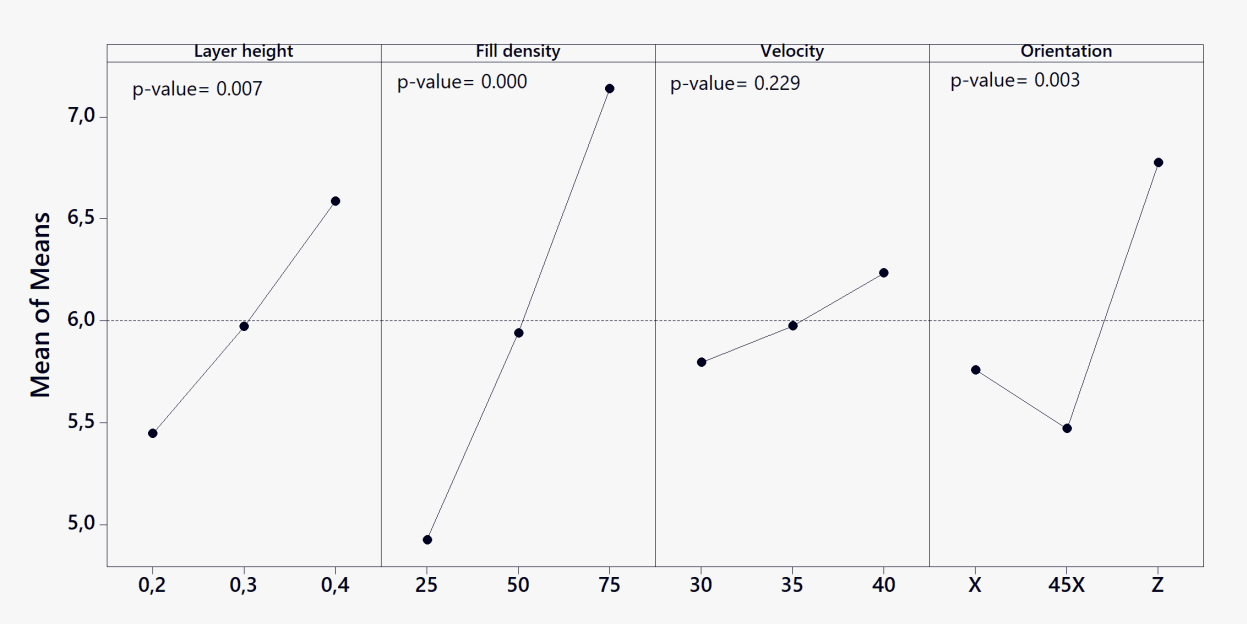

Figure 3.6. Main effect for mean effects calculated through ANOVA. Response variable: yield strength.

Similar to the interaction between parameters on Young's modulus, the p-value does not show significant on yield strength. It means, there is no influential interaction between parameters.

- Maximum stress

Regarding the obtained p-values from the factors on maximum stress as shown in Fig. 3.7, the most significant parameters are fill density, layer height, and orientation in descending order. Printing velocity has not as significant effect on this property. The higher maximum stress obtained by more fill density and bigger height of the layers. In order to orientation, the higher values are achieved from the printed samples in Z-axis. These parameters have exhibited the same effectiveness of Young's modulus and yield strength to the maximum stress as well.

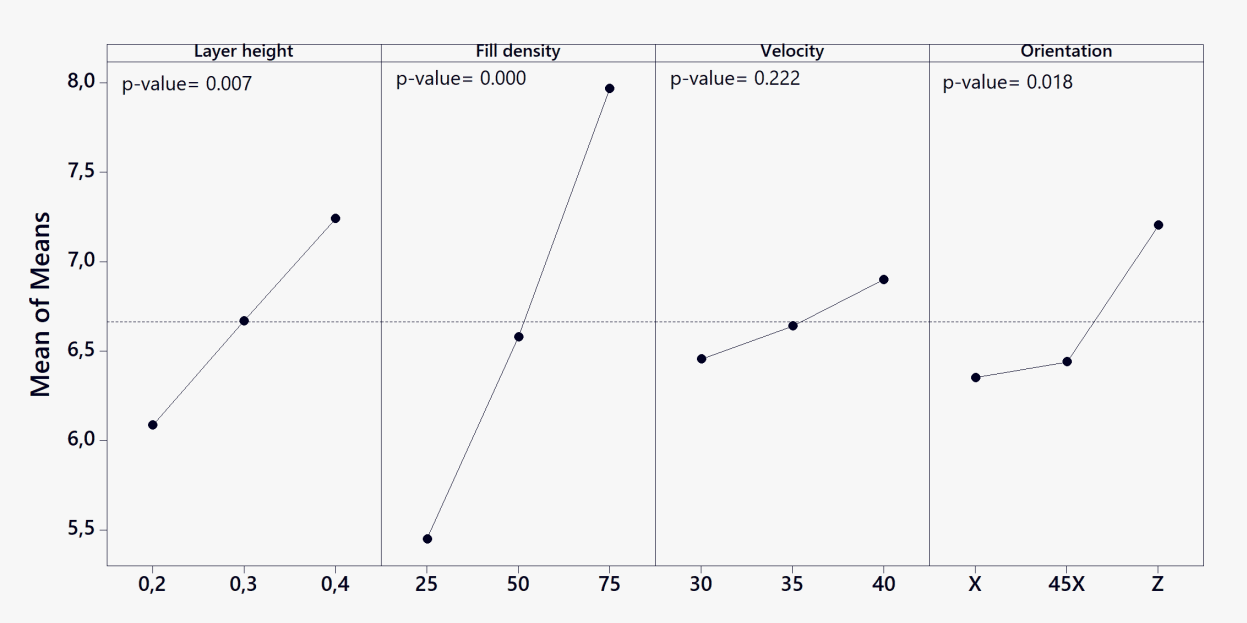

Figure 3.7. Main effect for mean effects calculated through ANOVA. Response variable: maximum stress.

The obtained p-values of interaction are higher than 0.05, therefore the interaction between parameters should not be taken into account as a significant, like in the previous properties analyzed.

- Maximum deformation

In case of maximum deformation, the fill density, layer height and velocity are not influential parameters whereas building orientation has shown remarkable effect on the maximum deformation according to the p-values. The higher maximum deformations are obtained from those specimens printed at 45° in X-axis orientation as shown in Fig. 3.8. In this case the correlation between the raster angles to generate the honeycomb shape and the tensile test direction could be mentionable in order to obtained higher maximum deformation of the samples printed in this this orientation. Also the obtained p-values of interaction for this response are higher than 0.05, therefore the interaction between parameters should not be taken into account as a significant.

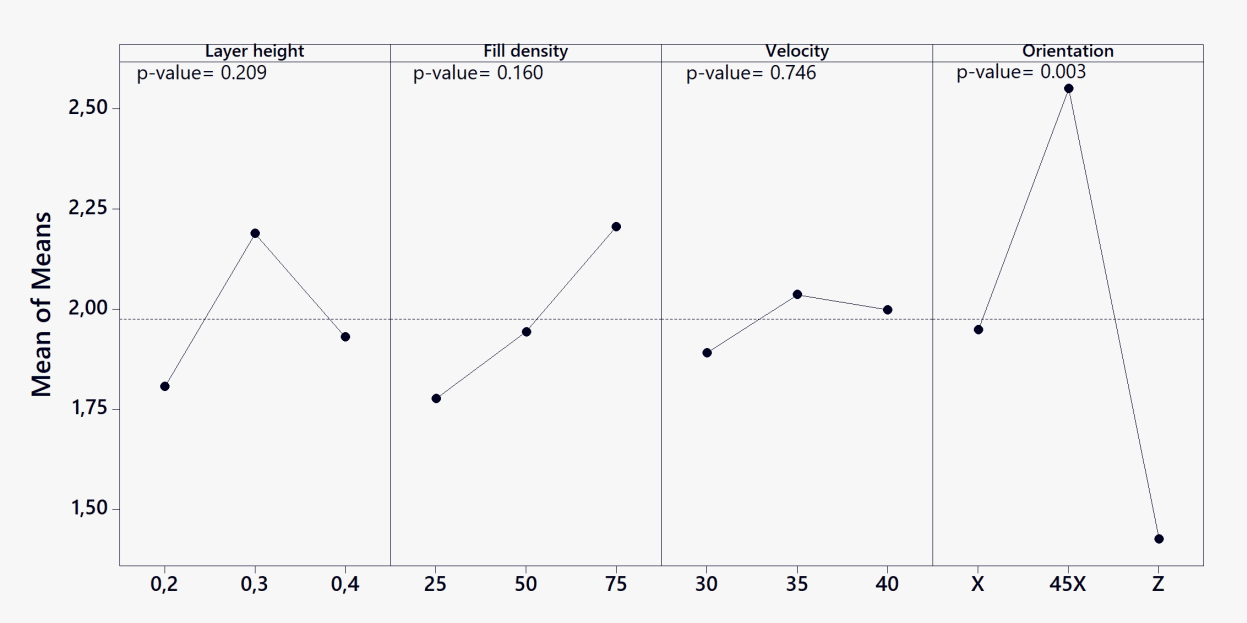

Figure 3.8. Main effect for mean effects calculated through ANOVA. Response variable: maximum deformation.

3.3.1. Results discussion

An overview of the results is summarized in table 3.7. Based on the p-values the most influential parameters and the levels on the responses are indicated in the relevant cells.

Table 3.3. Summary of significances on responses.

Response		Influential Parameter
Young's Modulus (E)	Elastic properties	Fill Density: 75% Orientation: Z-axis
Yield Strength ($S_{0,2}$)		Fill Density: 75% Orientation: Z-axis Layer height: 0.4
Maximum Stress (σ_{max})	Plastic properties	Fill Density: 75% Layer height: 0.4
Maximum Deformation (ε)		Orientation: 45°X-axis

These results evidence that each of the analyzed parameters is related to a different stress-strain functional regime of the FFF Timberfill material. Since the deposited layers direction in building Z-axis orientation is aligned to the test axis, it causes the material to endure the stress and the effectiveness of this parameter in elastic regime.

The obtained optimal set of parameters are shown in table 3.8. It is worth mentioning that, as the printing velocity is not influential in any case, the lowest value has been taken for the sake of productivity.

Table 3.4. Optimized set of parameters and their levels.

Factor	level
Layer height (mm)	0.4
Density (%)	75
Printing velocity (mm/s)	30
Orientation	Z-axis

3.3.2. Comparison between FFF and Injected results

Engineering stress-strain curves achieved from printed and injected samples are shown in Fig. 3.9. The average of achieved values of Young's modulus, yield strength, maximum stress, and maximum deformation from the FFF manufactured samples are almost ½ of obtained from the injected samples, while the maximum deformation average of injected samples is lower than FFF samples observably (Table. 3.9), meaning the injection process enhances the overall behavior of the material.

Figure 3.9. Strain-stress curve of FFF and injected Timberfill.

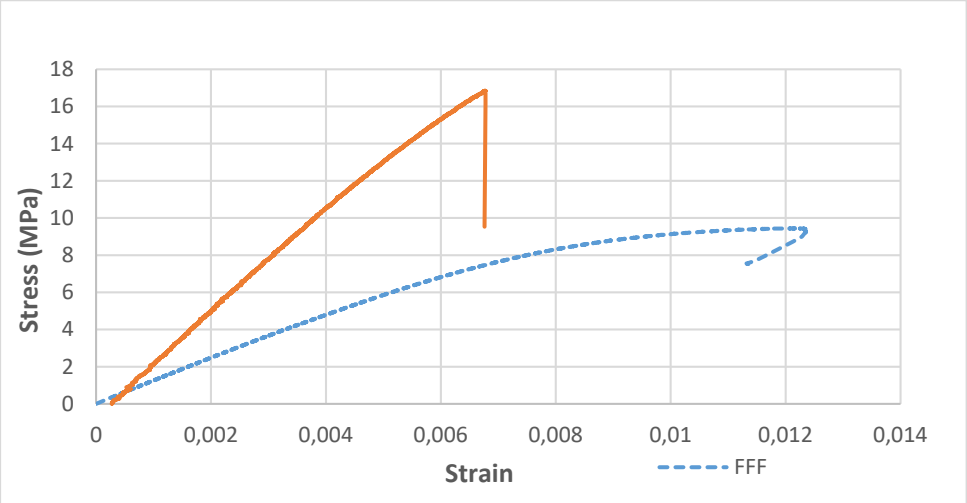

Table 3.9. Comparison of maximum values of all mechanical properties achieved for injected and FFF results.

Maximum values		
Timberfill	**Printed**	**Injected**
Young's Modulus (GPa)	1.21	2.81
Yield Strength (MPa)	8.95	16.47
Maximum Stress (MPa)	9.37	16.95
Maximum Deformation (%)	3.56	0.51

Since the tensile stresses are produced across the whole cross section, the injected specimen demonstrated higher strength to the tension than printed specimens when they are submitted to tensile test. The printed

sample meets smaller mean failure which agrees to the solidity percentage of the samples. In contrary, the higher the maximum deformation of printed sample can be due to the disengagement of the extruded wires one by one.

3.3.3. SEM Fractography

To clarify the failure mode submitted to tensile test for both injected and printed samples, scanning electron microscopy images of broken zone have taken (Fig. 3.10). According to the nature of the material, both different manufactured parts shown brittle behavior to which there are no sign of extending zone due to plasticity. The main reason of this phenomenon could be the poor tenacity of the wood fibers to matrix that causes an interruption to the molecular chain of the matrix. Also the smooth surface of the fibers can make lower interference with the matrix so that make lower resistance versus the applied load subsequently.

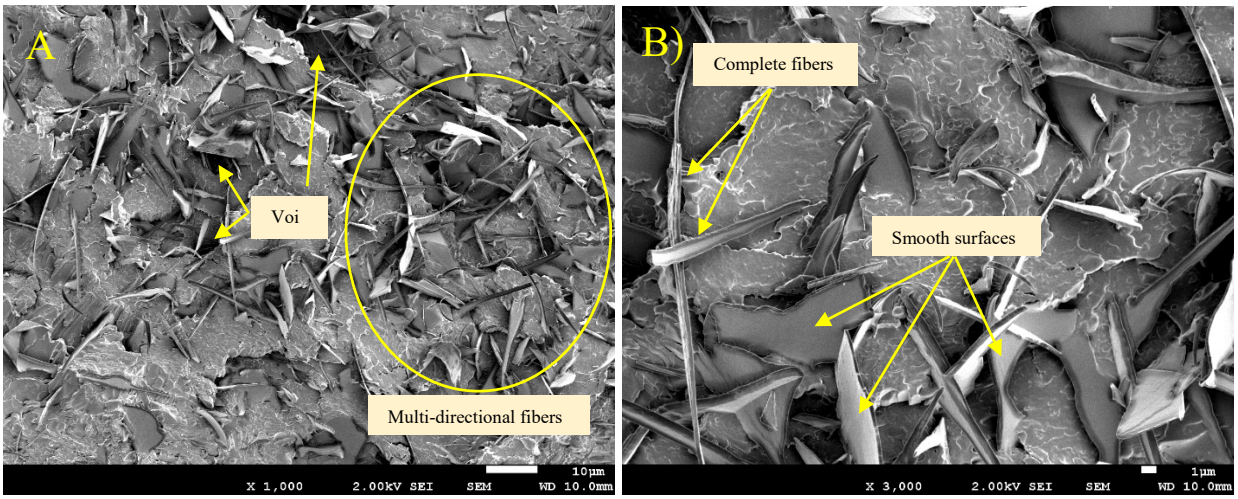

Figure 3.10. SEM image of the fractured zone of the samples.

Secondly the existence particles with smaller size less than 10 µm (wood flour) might have decreased the viscosity of the semi-melted material and caused the porosity in the extruded wires which this factor did not happened for the injected samples that can be another reason of the lower resistance of the printed specimens than the injected ones and subsequently than the obtained results for pure PLA.

Thirdly from the material science point of view, the fiber volume ratio or the fraction of fiber reinforcement plays a very important role in determining the overall mechanical properties of the composites as that a higher fiber volume fraction typically results in better mechanical properties of the composite [38]. Therefor Timberfill is not except of this rule neither. Based on the manufacturer statements the volumetric percentage of the fibers to matrix is in the range of 5-10 %, so increasing this percentage can arise the resistance of the material.

3.4. Conclusions

This study shows the effects of different printing parameters on the mechanical properties of wood-reinforced PLA (Timberfill) material. The selected parameters in this work are: Layer height, fill density, printing velocity, and orientation. The mechanical properties that are object of this research are Young's modulus, Yield Strength, Maximum Stress, and Maximum Deformation. Firstly, it was found that a combination of 75% fill density, Z-axis orientation, and 0.4 mm layer height exhibits the best mechanical properties with their effectiveness in descending order, regardless of the printing velocity. Although:

- The most effective printing parameters are building orientation, fill density, and layer height in the descending order, but there was no significant interaction between them.
- Considering the obtained p-value, printing velocity has no critical influence on the responses.
- The achieved Young's modulus, yield strength, and maximum stress of the injection molded parts were higher than printed ones taking into account the solidity percentages of the samples. Maximum deformation of the printed samples was considerably higher than injected samples.
- Altogether, the achieved values for the responses of this material are not high enough as a thermoplastic composite which the composition percentage of the fibers to matrix could be one reason of its deficiency. Also, creating a good interface between matrix and fibers by performing chemical treatments can be a great career on this field.

Chapter 4

Case study:

Experimental analysis of manufacturing parameters' effect on the flexural properties of wood-PLA composite parts built through FFF

Abstract

This paper aims to determine the flexural stiffness and strength of wood-particle reinforced polylactic acid (PLA) composite (Timberfill) parts manufactured through fused filament fabrication (FFF). The influence of four printing factors (layer height, nozzle diameter, fill density, and printing velocity) is studied through a L_{27} Taguchi orthogonal array. The four-point bending method is applied to carry out the tests and obtain the response variables used as output results to perform the analyze of variance (ANOVA) calculations. Layer height is the most influential parameter on the flexural strength, followed by nozzle diameter and infill density, whereas the printing velocity shows no significant influence. The optimal set of parameters and levels is found, being 0.2 mm layer height, 0.7 mm nozzle diameter, 75% fill density, and 35 mm/s velocity the best combination to process the material. This combination shows that the highest flexural resistance achieved experimentally is 47.26 MPa. The results are supported with microscopic photographs of rupture sections, and validated by comparing them with previous studies performed on pure PLA material, proving that the introduction of wood fibers in PLA matrix reduces the resistance of pure PLA matrix by hindering the cohesion between filaments and generating voids inside it. Lastly, five solid Timberfill specimens manufactured by injection molding were also tested to compare with the printed samples. The value of the elasticity module for the FFF specimens was almost 25% lower than of injected specimens result, and the resistance was reduced with regards to the additive-manufactured specimens.

Keywords: additive manufacturing, 3D printing, fused filament fabrication, Young's module, flexural strength, Timberfill.

Acronyms

AM - additive manufacturing

FFF – fused filament fabrication

DOE - design of experiments

ANOVA - analysis of variance

4.1. Introduction

Among all the additive manufacturing (AM) technologies available, the most popular is Fused Deposition Modeling (FDM), also referred to as Fused Filament Fabrication (FFF). This is due to its economic accessibility, ease of use, and variety of materials commercially available [78]. These kind of technologies offer the potential for significant cost savings due to reduced material waste and the production of intricate geometries. Therefore, they have gained considerable attention during the last decades. The Fused Filament Fabrication (FFF) process, which is also termed Fused Deposition Modeling (FDM), is one of the most popular AM methods [79]. The increase in accessibility of fused filament fabrication (FFF) machines has inspired the scientific community to work towards the understanding of the structural performance of components fabricated with this technology. A FFF printer generates a 3-dimensional object by extruding a stream of heated and semi-melted thermoplastic material, which is deposited onto layer upon layer, working from the bottom up. This process is performed by means of a heated print head that is oozing out a permanent flow of that semi-molten plastic. The deposited material will almost immediately harden upon leaving the hot print head, thus materializing in a small period of time the desired workpiece [80].

Recently, numerous researches have focused on studying the influence of the building parameters on different mechanical properties. Recently, numerous researches have focused on studying the influence of the building parameters on different mechanical properties. There is a variety of parameters, and it is not easy to choose these for a part for final use with mechanical requirements. Usually, operators choose these parameters under their experience and acquired knowledge, but there is not enough comprehensive information to determine suitable manufacturing parameters [17]. M. F. Afrose et al. have done an experimental analysis of fatigue characteristics by considering the effect of different build orientations. It was observed that the ultimate tensile stress of PLA samples built in X-direction (PLA-X) was found to be

the highest at 38.7 MPa and ranged from 60 to 64 % of raw PLA material, while for PLA -Y and PLA -45, the values were lower at 31.1 and 33.6 MPa, respectively [81]. Giovanni Gomez-Gras et al. [19] have studied The influence of fill density and pattern, nozzle diameter, layer height and printing speed on fatigue performance of cylindrical specimens. A combination of 75% infill density, 0.5 mm nozzle diameter and 0.3 mm layer height results in the highest fatigue life. For that combination of factors, a lower threshold for the fatigue endurance limit has been found at 35.8 MPa. In this research also the honeycomb infill pattern is advised to manufacture FFF parts, as it enables a longer lifespan with regards to specimens manufactured using a rectilinear infill. A study made by Es Said et al. [37] shows that raster orientation causes alignment of polymer molecules along the direction of deposition layers during fabrication. Consequently, tensile, flexural and impact strength were significantly influenced by orientation. Wenzheng Wu et al. [41] devoted a study to the influence of layer thickness and raster angle on the mechanical properties of 3D-printed polyether-ether-ketone (PEEK) pieces. Samples with three different layer thicknesses (200, 300 and 400 μm) and raster angles (0°, 30° and 45°) were built using a PEEK 3D printing system and their tensile, compressive and bending strengths were tested. The optimal mechanical properties of the samples were found at a layer thickness of 300 μm and a raster angle of 0°. To evaluate the printing performance of PEEK samples, a comparison was made between the mechanical properties of them and acrylonitrile butadiene styrene (ABS) parts. The results suggest that the average tensile strengths of PEEK parts were 108% higher than those for ABS, compressive strengths were 114% and bending strengths were 115%. However, the modulus of elasticity for both materials was similar. These results indicate that the mechanical properties of PEEK parts are superior to ABS parts.

Shabat et al. [6] have performed the mechanical and structural characterization of FDM of ABS modeling material by visual testing, light microscopy investigation and mechanical testing. The test results revealed different mechanical properties (in terms of stresses and displacements) as well as different fracture surfaces, according to the building strategies. The relationship between the mechanical properties and the fracture morphology of printed ABS material and the FDM process parameters was examined. The measured deflection of the first set of specimens was higher for those manufactured along the X direction, indicating greater ductility for specimens built horizontally. The experimental result of the second set revealed that high-angled specimens have lower displacement values.

Anoop Kumar Sood et al [68] have considered the influence of five important process parameters such as layer thickness, orientation, raster angle, raster width and air gap on three responses such as tensile, flexural and impact strength of test specimen. Araya-Calvo et al. [82] have conducted mechanical characterization of AM technology based on Composite Filament Fabrication (CFF); which utilizes a similar method of layer by layer printing as FFF, by design of experiment (DOE) as a statistical method, to investigate the

effect of fiber pattern, reinforcement distribution and print orientation on compressive and flexural mechanical properties of polyamide 6 (PA6) reinforced with continuous carbon fiber (CF). In this work Maximized flexural response is achieved with 0.4893 Carbon Fiber volume ratio, concentric reinforcement and perpendicular to the applied force, resulting in a flexural modulus of 14.17 GPa and a proportional limit of 231.1 MPa. Another study focused on the influence of nozzle temperature and infill line orientations for parts made with short carbon fiber (CF)-reinforced polylactic acid (PLA). Results have shown the influence of nozzle temperature on the mechanical properties, with an optimum temperature maximizing the tensile properties. Infill orientations also play a significant role in achieving good mechanical properties, with the proper combination of orientation enabling the tailoring of properties along a specific axis [83].

To reduce the consumption of petroleum-based resources and thereby enhance the eco-friendliness of the material, it could be interesting to replace of parts of ABS with other materials such as PLA or other composites and renewable materials for same purposes. To this extend other researches have compared mechanical characterizations of different materials [8, 84, 85]. B.M. Tymrak et al. [39] quantifies the basic tensile strength/stress, and elastic modulus of printed ABS and PLA components using realistic environmental conditions for standard users of a selection of low-cost, open-source 3-D printers. The results show that the average tensile strength of RepRap printed parts is 28.5 MPa for ABS and 56.6 MPa for PLA with average elastic module of 1807 MPa for ABS and 3368 MPa for PLA. These results indicate that the 3-D printed components from RepRaps are comparable in tensile strength and elastic modulus to the parts printed on commercial 3-D printing systems. While considerations must be made for the settings, tuning, and operation of each individual printer as well as the type, age, and quality of polymer filament used, functionally strong parts can be created with open-source 3-D printers within the bounds of their mechanical properties.

Also several researchers considered different mechanical behaviors of parts fabricated through another different manufacturing technologies [40, 64, 74], and different treatments on the raw materials and building conditions [38, 65, 75, 76], to achieve higher resistances of mechanical properties, many contradictions still need to be considered, including the high costs associated with these commercial machines, their material restrictions, and the difficulty to study process parameters [86].

As observed in the presented state of the art, the exploration of mechanical properties of workpieces generated through additive manufacturing has been extensively tackled with. However, references only focus on the typical PLA and ABS materials, neglecting the existence of other raw materials that can be manufactured through FFF. For this reason, the aim of this work is to study the influence of printing parameters on an innovative PLA-wood composite, provided by Czech company Filamentum under the

commercial name of Timberfill. Results shall be extracted from four-point bending tests to determine an optimal set of parameters to improve flexural strength. Taguchi L_{27} orthogonal array design is used in the experimental phase to avoid manufacture a large amount of runs. Then to evaluate the achieved characteristics of flexural property of printed Timberfill samples, a comparison was made between the mechanical properties of printed PLA and injected Timberfill parts using the same test procedure.

Timberfill is a relatively new material developed by Filamentum that exhibits similar mechanical features as ABS or PLA and models printed with this material have a genuine appearance of wood. To achieve that objective, the company developed a composition of biodegradable PLA polymer combined with wood fibers. It is provided as a commodity material, with the purpose of becoming a commonly used material in FFF machines for various applications. However, it is essential characterize and understand the performance of FFF-processed Timberfill parts.

4.2. Materials and methods

4.2.1. Four-point bending testing and specimens

The specimens are manufactured with 2.85 mm of diameter Timberfill Champagne, developed and manufactured by Filamentum Ltd. Originally, this material was developed with a purely aesthetic purpose that of imitating objects with a wood aspect. To achieve that objective, the company developed a composition of biodegradable PLA polymer combined with wood fibers in a 5%-10% ratio. Therefore, Timberfill can be proven to be a feasible material for some practical purposes in low-scale manufacturing environments.

In this research, a four-point flexural test has been performed, with prismatic samples with dimensions according to the ASTM D6272 standard [87]. This testing method details the procedure to determine the flexural properties of unreinforced and reinforced plastics, including high-modulus composites and electrical insulating materials in different forms. Hence its adequacy for the purposes of these works with a composite material.

The test consists on a bar of rectangular cross section resting on two supports, which is loaded at two points by means of the respective loading noses, each one an equal distance from the adjacent support point. The distance between the noses (the load span) is either one third or one half of the support span (figure 4.1). A support span-to-depth ratio of 16:1 shall be used. The loading noses and supports shall have cylindrical surfaces. In order to avoid excessive indentation or failure due to stress concentration directly under the

loading noses, the radii of the loading noses and supports should be 5 ± 0.1 mm. According to this method the distances between support spans and load spans shall be 64 mm and 21.3 mm respectively.

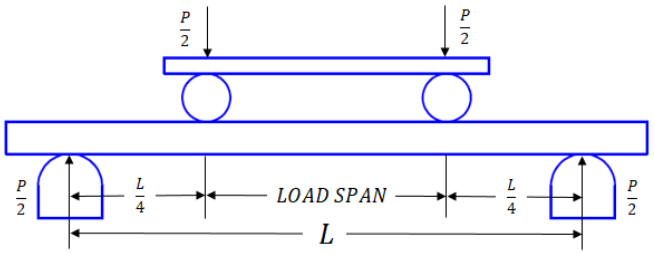

Figure 4.1. Geometry and loading system of the four-point bending test.

The machine is adjusted as near as possible to that calculated rate for the load span of one third of the support span. Once the conditions are determined, displacement rate of 19 mm/min and maximum displacement of 10.98 mm are achieved.

4.2.2. Taguchi experimental design

The Design of Experiments (DOE) technique has been used to carry out the study. In this work, four parameters varying in three levels are included in the model. Table 4.1 shows the factors and their selected levels to be developed based on a Taguchi experimental design method which is a robust optimization technique to make experimental to predict responses and optimize the FFF process conditions in accuracy level [77]. These factors and levels were selected based on a preliminary set of tests out of the experimental design of this paper, to confirm and adjust the recommendations given by the material manufacturer.

Table 4.1. Factors and levels used for the DOE.

Parameter	Levels		
	1	2	3
Layer height (mm)	0.2	0.3	0.4
Nozzle diameter (mm)	0.5	0.6	0.7
Fill density (%)	25	50	75
Printing velocity (mm/s)	25	30	35

To analyze the influence of these factors, a L_{27} Taguchi orthogonal array was used to conduct the experimental phase (Table 4.2). Of each manufacturing parameter set or run included in the array, 5 specimens were manufactured and tested, to guarantee the repeatability of the results. Once the results were obtained, the statistical calculations were performed by the Minitab 18 software, and the interactions between the different parameters were analyzed which leads to the conclusion that if there is significant

interaction among the pairs of selected values or not, since the p-values of each pairs should be less than 0.05.

Table 4.2. L27 Taguchi orthogonal array of DOE.

Run	Layer height (mm)	Nozzle diameter (mm)	Fill density (%)	Printing velocity (mm/s)
1	0.2	0.5	25	25
12	0.2	0.5	50	30
3	0.2	0.5	75	35
4	0.2	0.6	25	35
5	0.2	0.6	50	30
6	0.2	0.6	75	25
7	0.2	0.7	25	35
8	0.2	0.7	50	25
9	0.2	0.7	75	30
10	0.3	0.5	25	30
11	0.3	0.5	50	35
12	0.3	0.5	75	25
13	0.3	0.6	25	35
14	0.3	0.6	50	25
15	0.3	0.6	75	30
16	0.3	0.7	25	25
17	0.3	0.7	50	30
18	0.3	0.7	75	35
19	0.4	0.5	25	35
20	0.4	0.5	50	25
21	0.4	0.5	75	30
22	0.4	0.6	25	25
23	0.4	0.6	50	30
24	0.4	0.6	75	35
25	0.4	0.7	25	30
26	0.4	0.7	50	35
27	0.4	0.7	75	25

It should be taken into account that all of the samples are printed with honeycomb infill pattern. Therefore, the rest of the parameters that are not object of study have been kept constant among all specimens (Table 4.3).

Table 4.3. Main constant manufacturing parameters used in the experiments.

Building orientation	Raster angle	Nozzle temperature	Infill pattern	Skirt layer
0-*X*	45º	180ºC	Honeycomb	2 layers

4.2.3. Specimens manufacture

According to the ASTM testing method, the specimens may be cut from sheets, plates, or molded shapes, or may be molded to the desired finished dimensions. The actual dimensions and shape can be seen in figure 4.2.

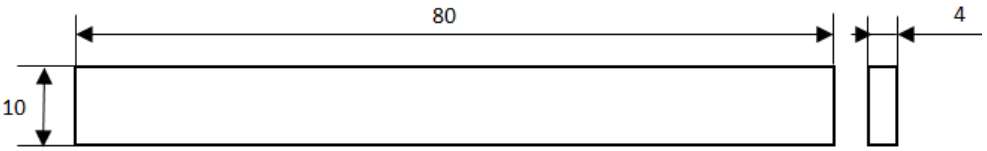

Figure 4.2. Schematic view of four-point bending test specimens.

4.2.4. Experimental setup

The four-point bending experiments were conducted using a ZwickRoell Z020, electromechanical multi-space machine shown in figure 4.3. a, with a maximum load of 20 kN. A 500-N load cell was connected to a Spider 8 data acquisition system to record the force applied every sampling instant during the test and transfer the data to the computer. On the other hand, the specimen was recorded through an HD camera at 60-Hz sampling frequency. The camera was also equipped with a switch-controlled flash to illuminate the test area and to synchronize the data (figure 4.3. b). Like that, strain was computed as a result of a Matlab routine based on image processing functions through which the frames were translated into displacement.

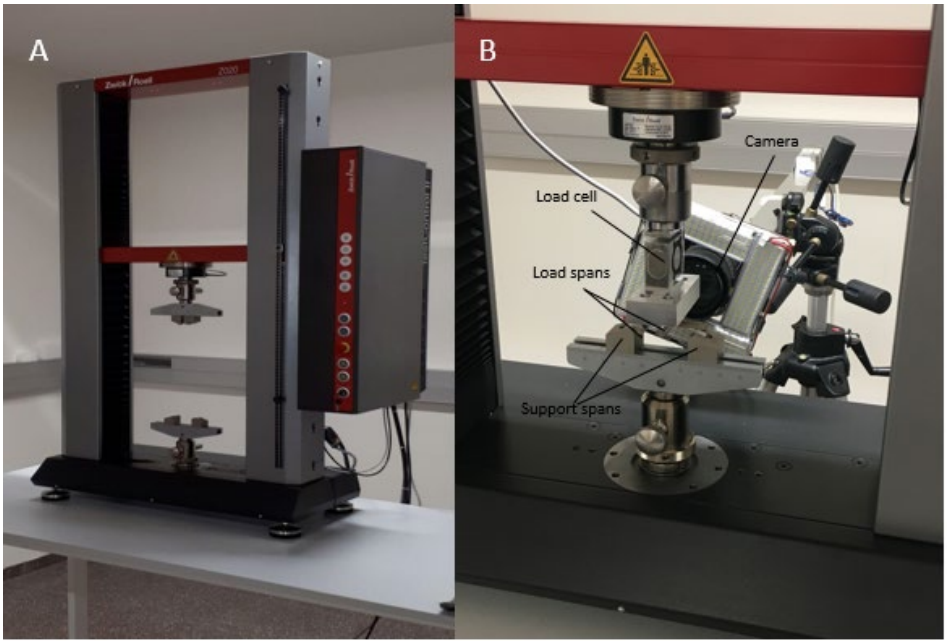

Figure 4.2. a. Universal material testing machine ZwickRoell Z020 used to conduct the tests. b. Camera and load equipment assembly.

4.2.5. Analyzing process

The described equipment was applied to carry out the tests on all of the 135 FFF samples. Furthermore, five additional specimens were manufactured with the same raw material through injection, to compare the results of additive-manufactured parts with a reference value. After each test was completed, two different files were generated. Firstly, a file that contains the force collected from the load cell, as well as the recorded voltage versus time. Secondly, the video recorded by the camera, that provided graphical information to compute the strain of the specimen at every stage of the test.

The constructed stress-strain figure for every specimen was used to extract different mechanical descriptors used as response variables for the ANOVA model. These were the Young's modulus (E), the elastic limit ($S_{0.2}$), the maximum stress or flexural strength (σ_{max}), and maximum elongation (e_{max}). A self-designed Matlab routine was executed in a Matlab R2018b software. Essentially, the routine performs the following steps:

1. The input data is the HD video processed during the test, and it is firstly divided into its different frames. Since the camera captures 60 frames per second, and the average duration of the test is 50 seconds, the average number of frames to process for each test is 3000.
2. The video frames and the recorded force data are synchronized. When the test starts, the flash is activated and sends a 0 V signal to the DAQ Spider system to launch data recording. Subsequently, the Matlab script synchronizes the dark frame of the video and the spider data recorded alongside at the same time. Then, it detects the points until the maximum bending position before the sample will be broken.
3. A grid is generated in the initial frame of the test sample. This gridding consists of a straight line divided by 50 points at the outer fiber and two rectangular grids at the support spans (figure 4.a). It is important that the linear grid extends the space between both loading points.
4. Deflection is computed by tracking every marked pixel, based on the differences between the initial and final position. The results are converted into an array at the X-axis and Y-axis separately. The difference between the positions in the current frame (in red) and the starting position (in green) is shown in figure 4.b. By finishing this step, two scroll files were generated and introduced into a specific script to compute the real deformation of the specimens' outer fibers.
5. All deformations for every frame is calculated as described in the previous point, and the whole flexural curve is created. The pixels that have been measured by Matlab are converted in millimeters. The GIMP 2.10.8 software is used to do this, as can be seen in figure 4.c.
6. By means of another Matlab script, the voltage and the deformation are calculated for the specimen second by second, and the results are synchronized with the deformations value that have been calculated previously. Finally, a .txt format file is generated with voltage, deformation versus time. Consequently, the stress is calculated by the Euler-Bernoulli equation for a rectangular section beam subjected to pure bending stress (Eq. 1)

$$S = \frac{PL}{bd^2} \qquad (1)$$

where S is the stress applied to the external fiber, P is the load, L is the specimen length, b is the specimen width and d is the specimen thickness.

Here the average value of thickness and width are defined by measuring manually the specimen before the test with a micrometer.

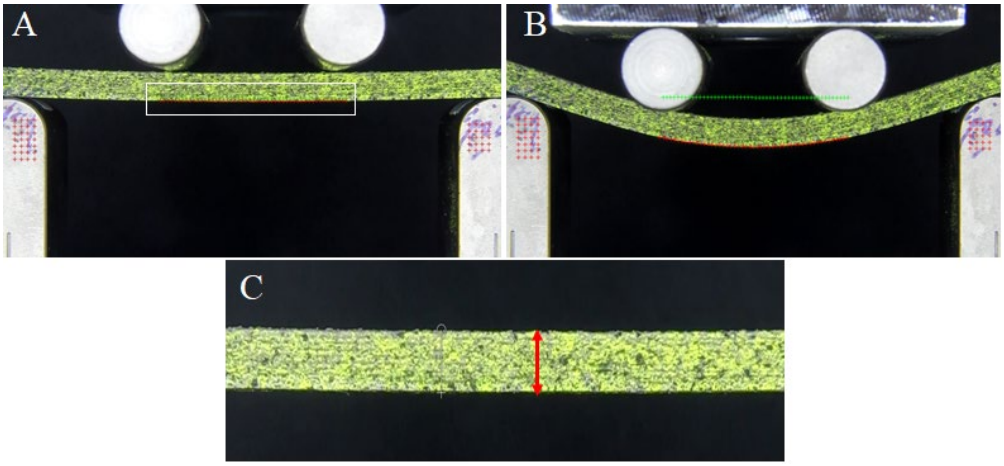

Figure 4.3.a. Generated grid with Matlab ® script. b. Image processing protocol. c. Calculation of the pixel/mm ratio.

4.2.6. Comparison between Timberfill and PLA

Since Timberfill is a composite of PLA and wood fibers, it is interesting to compare the results achieved on Timberfill material with its base material, as it is an extended material and is often cited in the bibliography. The used data to carry out the comparison are obtained from [88] which has been done in the same condition of current work in this research group. Both materials were characterized through a tensile stress, and their stress-strain curves are compared. Fractographies taken with a Moticam 3 digital camera through a Motic SMC binocular loupe shall also lead to further detail about the differences between fracture modes. Finally, microscratch tests were conducted in a Scratch tester unit (CSM-Instruments) using a spherical diamond indenter with a radius of 200 µm, to compare wear resistance of both materials. Tests were done under linearly increasing load, from 0 to 120 N in case of Timberfill and from 0 to 70 N in case of PLA, at a loading rate of 10 mm/min and in an interval length of 5 mm, according to ASTM- C1624-05 standard [25]. These tests were conducted along both the longitudinal and transversal printing direction to observe the main plastic deformation mechanisms induced. Surface damage induced during scratch tests were observed by a desktop scanning electron microscopy Phenom XL from ThermoFisher Scientific.

4.2.7. Comparison between FFF Timberfill and Injection-molded Timberfill

Finally, a comparison between the flexural properties of the printed and injected Timberfill was conducted, to evaluate the effects of the additive manufacturing strategy on the material's properties.

4.3. Results analysis

The average results of the five repetitions of each manufacturing configuration, including the standard deviation are included in Table 4.4.

Table 4.4. Results obtained for each experimental run.

	E (GPa)	Std. dev.	$S_{0.2}$ (MPA)	Std. dev.	δ_{max} (MPa)	Std. dev.	e_{max} (%)	Std. dev.
1	2.07	0.08	30.66	0.56	35.34	0.34	2.77	0.34
2	2.13	0.04	33.48	0.77	39.52	1.25	3.49	0.33
3	2.17	0.04	34.19	0.42	41.15	0.88	4.65	1.78
4	2.03	0.08	31.56	0.91	37.82	0.49	3.46	0.08
5	2.12	0.04	31.83	0.97	39.76	0.93	4.35	0.00
6	2.16	0.05	32.96	0.47	40.45	0.64	3.92	0.45
7	2.29	0.15	36.28	0.56	44.17	1.82	4.07	0.68
8	2.24	0.08	35.73	0.56	45.40	0.99	5.34	1.62
9	2.41	0.04	38.06	1.17	47.26	0.86	4.24	0.31
10	1.76	0.07	28.45	1.05	34.29	0.68	3.80	0.32
11	1.89	0.05	29.54	0.81	36.26	0.58	4.70	1.68
12	1.77	0.06	29.56	0.71	36.24	0.64	4.72	1.99
13	1.82	0.07	36.58	1.62	34.94	1.37	3.80	0.73
14	1.87	0.08	29.69	0.52	37.46	0.66	4.07	0.14
15	1.82	0.06	28.97	1.05	35.51	2.40	3.96	0.61
16	1.84	0.07	29.27	1.24	36.64	1.29	4.48	0.44
17	1.91	0.08	29.49	1.07	37.01	1.83	3.86	0.44
18	1.94	0.08	30.40	1.62	40.17	1.67	4.89	0.37
19	1.70	0.09	26.60	1.78	26.04	2.03	3.15	1.76
20	1.81	0.08	27.53	0.31	33.19	0.70	3.62	0.31
21	1.73	0.11	27.74	0.64	35.14	1.43	4.57	0.62
22	1.41	0.08	23.32	1.78	27.05	2.25	3.59	0.76
23	1.69	0.11	27.23	0.94	32.97	2.14	4.04	0.50
24	1.89	0.20	29.43	5.46	35.64	7.74	3.88	0.90
25	1.86	0.03	30.71	0.53	37.99	0.81	4.64	0.24
26	1.91	0.09	31.35	1.21	39.79	1.54	4.79	0.26
27	1.95	0.15	31.09	1.61	40.27	1.23	4.80	0.53

4.3.1. Analysis of variance

An analysis of variance (ANOVA) was performed on the dataset included in the Taguchi experimental array, for each parameter that describe the mechanical behavior of the evaluated specimens. To validate the statistical significance of the parameters included in the model on each of the responses, the p-value associated to the ANOVA, was compared to a significance level of 5%.

- *Young's module*

In this case, it can be concluded that the most significant parameters, due to their p-values, are the layer height and the nozzle diameter as shown in figure 4.5. This graph evidences that the layer height results have an inverse relation with the Young's module, but higher values of nozzle diameter and density results in a higher elastic module. Based on the obtained p-values, density can be taken into account because the value is not so much bigger than 0.05, but printing velocity does not show a significant effect on the Young's module.

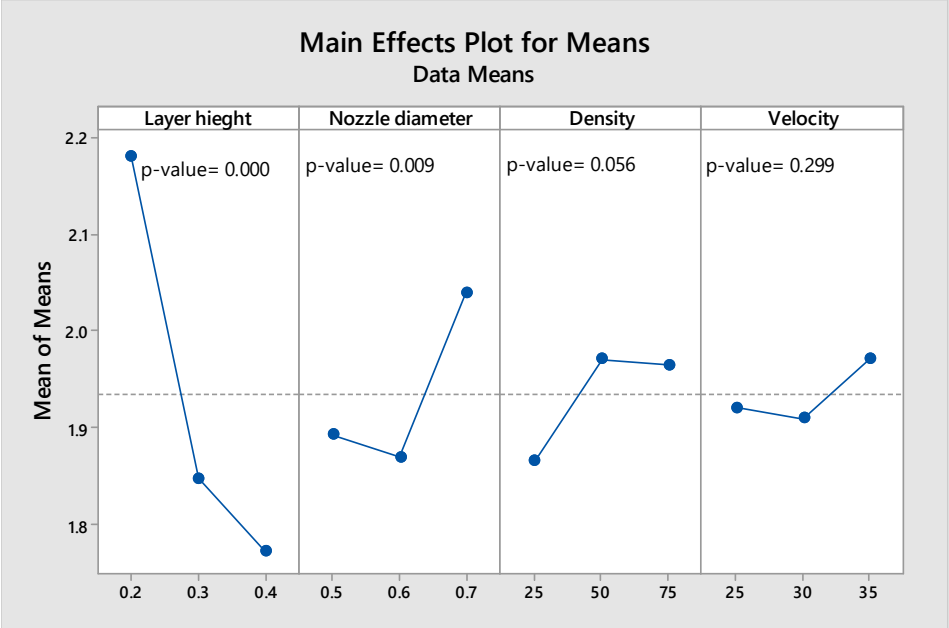

Figure 4.4. Main effect for means calculated through ANOVA. Response variable: Young's module.

In this case obtained p-values were more than 0.05, it means that the selected parameters in this study are independent of each other, at least in the analyzed value ranges for Young's module.

- *Elastic limit*

It is necessary to see how the variation of the different factors affect the elastic limit, which is indicated in graph of main effects for the averages (figure 4.6). As already mentioned the most significant parameter due to the p-value on elastic limit is layer height; that it should be lower to obtain the bigger elastic limit,

which in this work is 0.2 mm. On the other side, the nozzle diameter has a direct proportion with the elastic limit; it means the bigger diameter the higher elastic limit. Fill density and printing velocity did not show a significant effect on elastic limit.

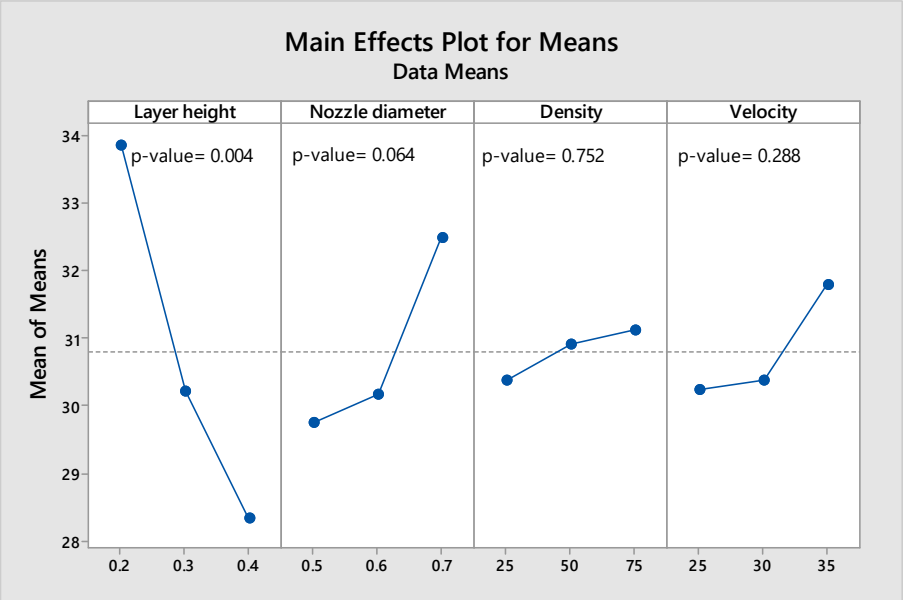

Figure 4.5. Main effect for mean effects calculated through ANOVA. Response variable: elastic limit.

Similar to the interaction between parameters on Young's module, the p-value does not show significant on limit elastic. It means, there is no influential interaction between parameters.

- *Maximum stress*

Based on the obtained p-values from the factors, it can be mention a notable significance of layer height, nozzle diameter, and infill density on the maximum stress. Following, the best levels of these factors are shown in figure 4.7.

Figure 4.6. Main effect for mean effects calculated through ANOVA. Response variable: maximum strength.

In order to the selected variations of the factors in this work, the best level of the layer height, nozzle diameter, and infill density to be influent on the maximum stress are 0.2 mm, 0.7 mm, and 75 % respectively.

The obtained p-values of interaction are higher than 0.05, therefore the interaction between parameters should not be taken into account as a significant.

- *Maximum elongation*

In this case, the layer height is not an influential parameter whereas infill density and nozzle diameter have shown significances p-value on the maximum elongation. In figure 4.8, the best level of these factors could be found.

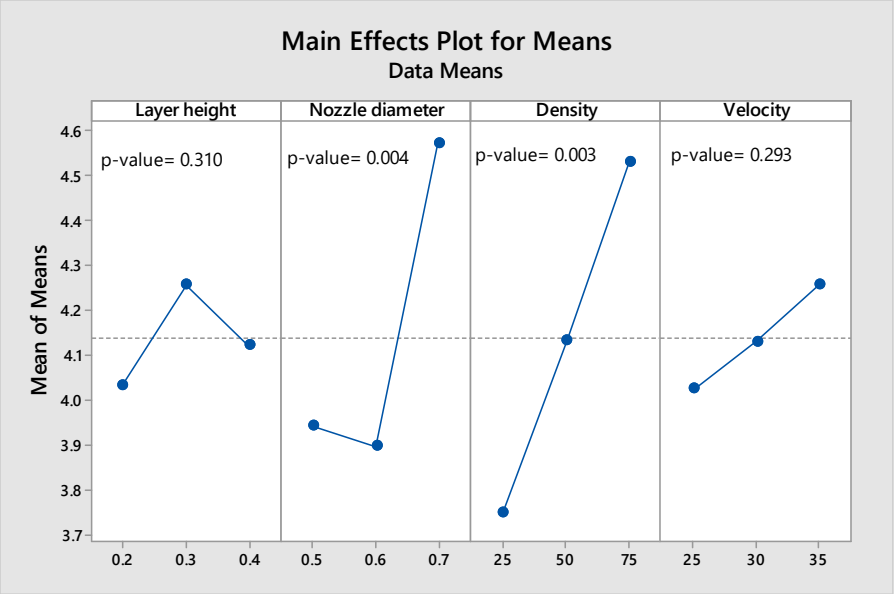

Figure 4.7. Main effect for mean effects calculated through ANOVA. Response variable: maximum deformation.

In order to the selected variations of the factors in this work, the best level of the infill density and nozzle diameter to influence on the maximum elongation are 75 % and 0.7 mm respectively. It can be seen from figure 4.9 that could be different infarctions between the parameters and levels. As already mentioned, to consider influential the interaction of parameters, the p-value has to be taken into account. In this case is lower than 0.05 for the interaction between nozzle diameter and density, meaning that the interaction between the levels of both parameters can influence the maximum elongation value.

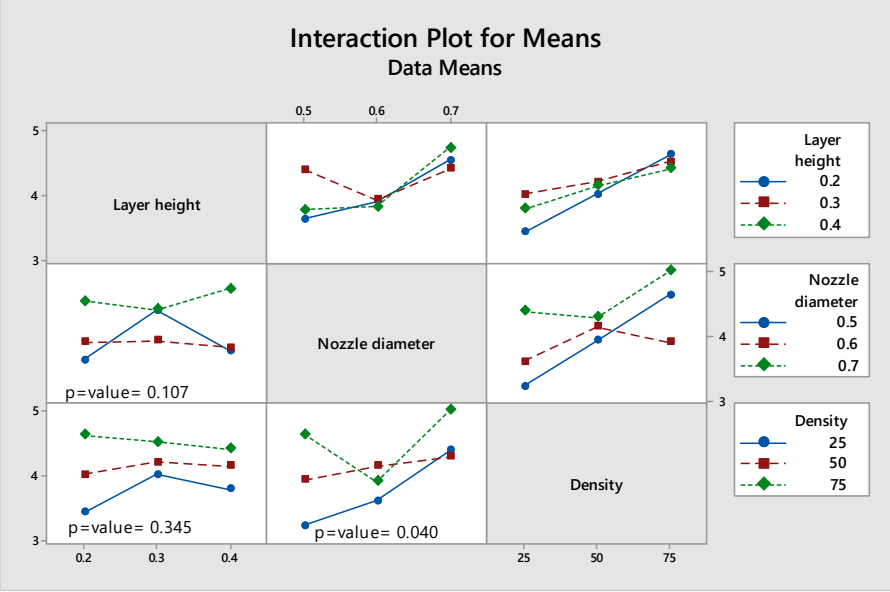

Figure 4.8. Main effect for interactions calculated through ANOVA. Response variable: maximum deformation.

4.3.2. Results discussion

An overview of the results is summarized in Table 4.5. Based on the p-values the most influential parameters on the responses are shown with arrow symbol, the yellow cells illustrate the threshold factors, and not significant ones are not defined. In the other side, the best selected level of each parameter is indicated in the cells.

Table 4.5. Summary of significances on responses. ↑: most influential parameters. n.i.: non-influential parameters.

Factors	Responses			
	Elastic properties		Plastic properties	
	Young's Module (E)	Elastic Limit ($Rp_{0,2}$)	Maximum stress (σ_{max})	Maximum elongation (ε)
Layer Height (mm)	0.2 ↑	0.2 ↑	0.2 ↑	n.i.
Nozzle Diameter (mm)	0.7 ↑	0.7	0.7 ↑	0.7 ↑
Fill Density (%)	50	n.i.	75 ↑	75 ↑
Printing Velocity (mm/s)	n.i.	n.i.	n.i.	n.i.

These results evidence that each of the analyzed parameters is related to a different stress-strain functional regime of the FFF Timberfill material. Whereas the layer height seems to determine how the material endures the stress to which it is subjected during the whole test, the nozzle diameter and the fill percentage are clearly more influential in how the Timberfill works in its plastic regime, as well as its failure mode as proves the maximum elongation registered in the tests. For this reason, a single optimal parameter set cannot be defined. In this situation, the criteria that will be followed in order to define the best level for each parameter is based on the following two conditions:

- If a parameter delivers the best response at the same level in all cases, it is chosen.
- In case of divergence, then the level with lowest p-value in the ANOVA test is chosen.

Table 4.6 shows the final result for the optimized set of parameters. It is worth mentioning that, as the printing velocity is not influential in any case, the highest value has been taken for the sake of productivity.

Table 4.6. Optimized set of parameters and their levels.

Factor	level
Layer height (mm)	0.2
Nozzle diameter (mm)	0.7
Density (%)	75
Printing velocity(mm/s)	35

4.3.3. Comparison between Timberfill and PLA

Table 4.7 shows the best combination set of parameters obtained for PLA and Timberfill material. The results related to PLA specimens has been extracted from previous research published by the authors in [88].

Table 4.7. Comparison of factor levels leading to best results for PLA and wood-reinforced PLA.

Factor	Material	
	PLA	Timberfill
Layer height (mm)	0.1	0.2
Nozzle diameter (mm)	0.6	0.7
Density (%)	75	75
Printing velocity (mm/s)	20	35

The direct comparison of both materials proves that they demand a low value of layer height combined with a higher nozzle diameter, and a 75% infill density, so that their mechanical properties are enhanced. Indeed, by decreasing the height between layers and increasing the material flow, as well as depositing each filament with the lowest offset to the adjacent one, leads to a net increase of the enduring material, thus enhancing the overall resistance of the material. On the other hand, printing velocity results are reversed, although it must be highlighted that 20 mm/min resulted in better results for the PLA, and was non-influential in the Timberfill material. The presence of wood could be the cause to this divergence.

Although the direct comparison of the optimal levels has proved a similar influence of both materials, it is also necessary to compare the absolute results represented by two respective illustrative strain-stress curves (figure 4.10). The absolute values are shown in Table 4.8. The introduction of wood in the PLA matrix is clearly detrimental to the mechanical behavior of the Timberfill.

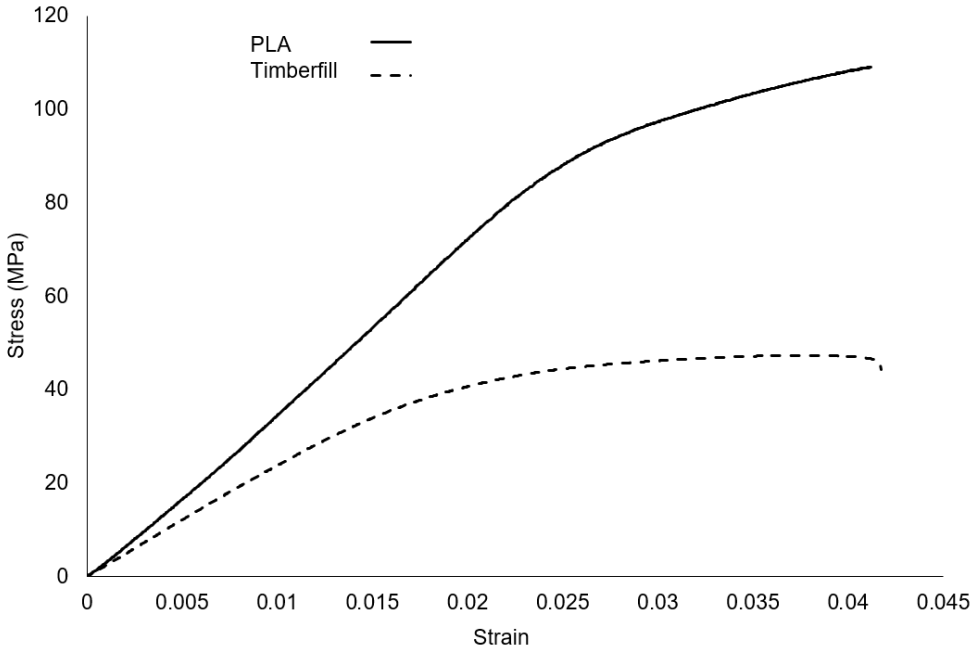

Figure 4.9. Strain-stress curve of PLA and wood-reinforced PLA.

Table 4.8. Comparison of maximum values of all mechanical properties achieved for PLA and wood-reinforced PLA.

Material	Timberfill	PLA
Young's Modulus (GPa)	2.41	3.70
Elastic limit (MPa)	38.06	90.80
Maximum stress (MPa)	47.26	109.50
Maximum elongation (%)	5.34	6.21

The examination of a fractography can lead to further information about this phenomenon. Indeed, the wood fibers create discontinuities in the matrix causing lower ductility in Timberfill respect to PLA. That is also corroborated by the microscopy pictures of fracture cross-section taken by the same camera (figure 4.11).

As a first approach, the presence of wood inside the PLA matrix could lead to think that it increases the inner friction of the material, thus increasing it resistance and restricting its deformation. However, the wood fibers are actually acting as an anchor that transfers the load to the PLA matrix and its fibers. Therefore, the crack is forced to advance through these particles, which are perpendicular to the stress, with a consequent stress concentration, and an overall decrease of the mechanical resistance to bend of Timberfill material.

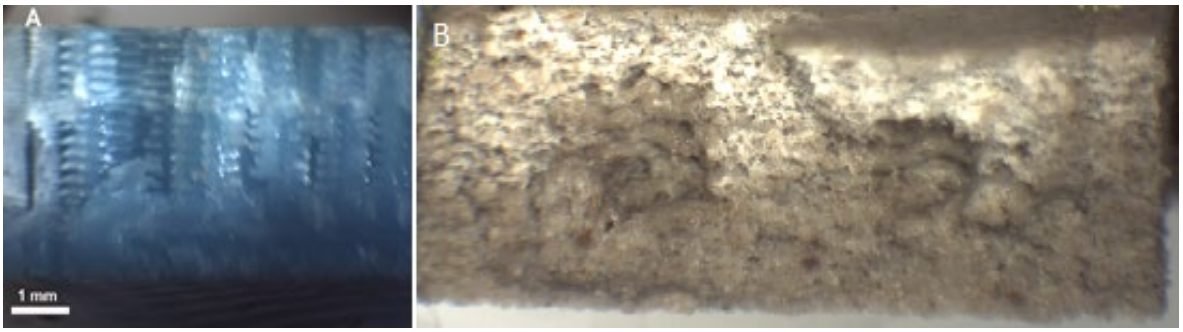

Figure 4.10. Fracture section of specimens. a. PLA specimen with a layer height of 0.1 mm and filament width 0.3 mm. b. Wood-reinforced PLA specimen with layer height 0.2 mm and filament width 0.7 mm. Both in 75 % infill density.

To better understand the fracture behavior, micro scratch tests were performed on both materials. (Figure 4.12). It is confirmed that Timberfill is formed as a porous material, as discussed above. The base PLA deformed by the scratch partially covers the remaining pores of the sample. Up to the tested force in both materials (120 N for Timberfill, 70 N for PLA), they both show a ductile behavior, without evidencing cracking in the base material. Neither of them shows remarkable adhesive wear. On the other hand, there are no disclosures between filaments in any of the materials, fact that implies that the adhesion between filaments in the same layer is enough to resist the efforts applied during the test.

What is clearly different between the two materials is the obtained friction coefficient, being 0.4 for Timberfill, twice than for the PLA. In both cases, the value is kept constant throughout the test. At sight of the obtained results in the scratch tests, it can be stated that the introduction of the wood inside the PLA

matrix to create the Timberfill composite increases the friction of the material, what could be interesting for certain future applications of the material.

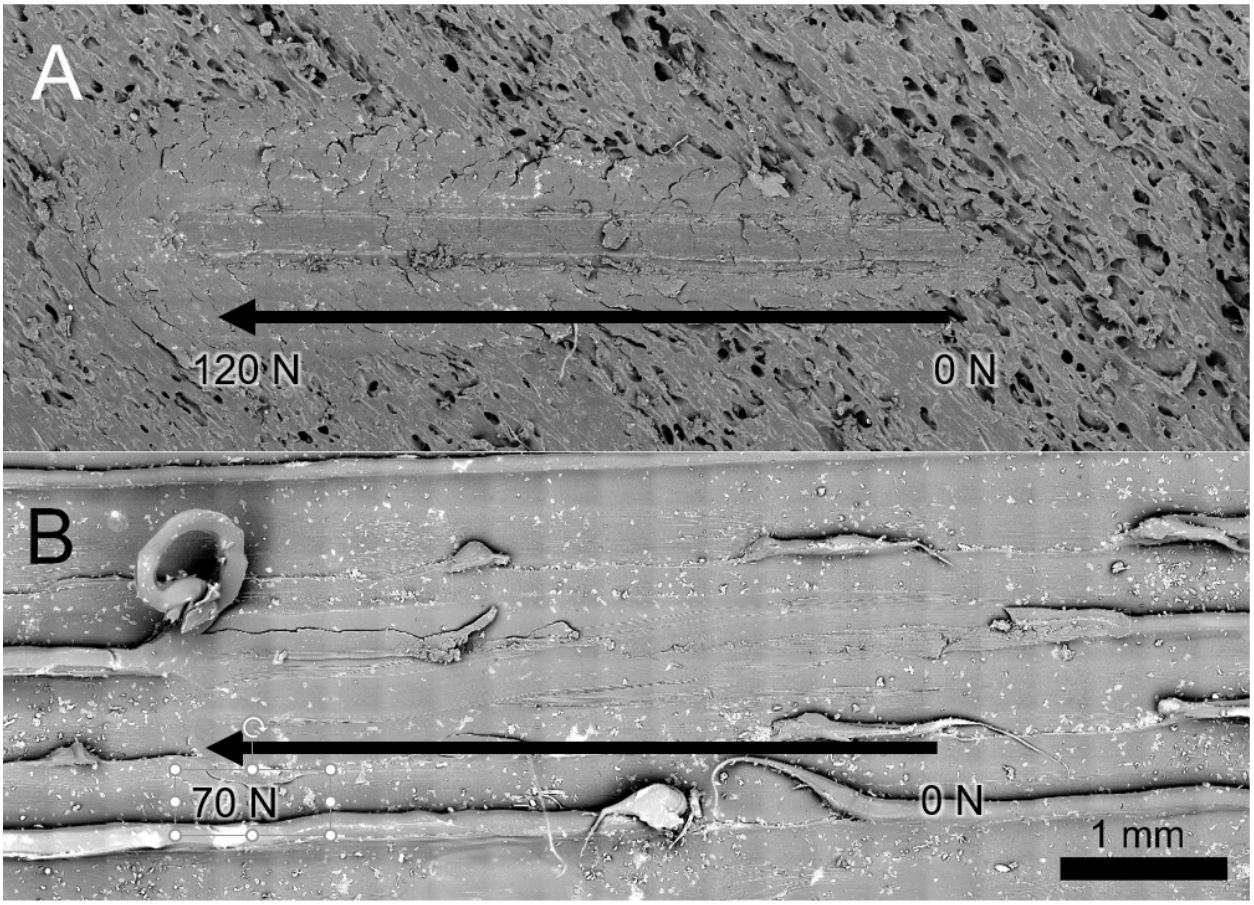

Figure 4.11. Microscratch tests. A. Wood-reinforced PLA. B. PLA.

4.3.4. Comparison between FFF Timberfill and Injected Timberfill

Bending engineering stress-strain curves for printed and injected samples are shown in figure 4.13. The Young's module of the additive-manufactured samples was 2.41 GPa, almost 75% of the injected samples (3.11 GPa), but the other properties were higher in the FFF specimens than on the completely solid ones. For example, the average values of flexural strength were 38.06 MPa and 24.62 MPa for printed and injected samples respectively (Table 4.9), meaning that the processing the Timberfill material by FFF enhances the overall behavior of the material.

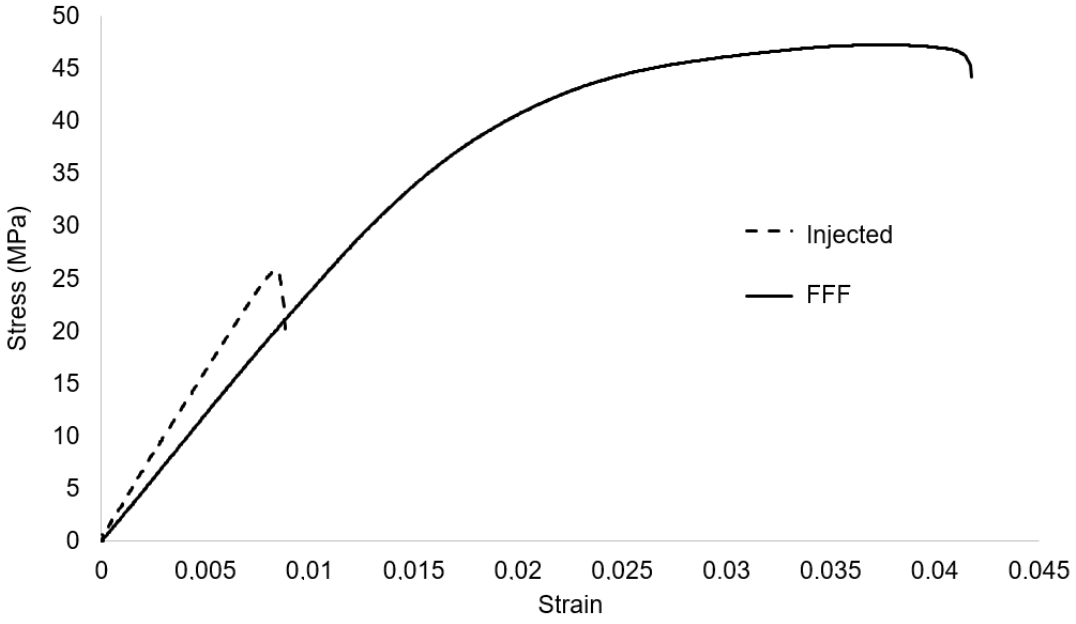

Figure 4.12. Strain-stress curve of FFF and injected wood-reinforced PLA.

Table 4.5. Comparison of maximum values of all mechanical properties achieved for injected and FFF wood-reinforced PLA.

Maximum values		
Timberfill	**Printed**	**Injected**
Young's Modulus (GPa)	2.41	3.11
Elastic Limit (MPa)	38.06	24.62
Maximum Stress (MPa)	47.26	25.62
Maximum Elongation (%)	5.34	1.02

To specify this observation, microscopic examinations of the specimens' cross-section were performed. Figure 4.14.a shows the specimen with honeycomb pattern at a 75 % infill density, and figure 4.14.b shows the injected sample. The brightened zones represent the area subjected to tensile effect. Regarding to the obtained values for responses (Table 4.9) and the behavior shown in the fracture, it is noticeable that the specimen generated by successive filaments shows a higher ductility due to the fact that these filaments have higher mobility one with respect to the other. Thus, the crack grows property which occurs in the outer fiber of the sample can decrease the ductility of injected parts, because this phenomenon should repeat for each layers of printed parts. Likewise, lower height of the layers and bigger diameter of the nozzle help adhesion between consecutive layers. This can consequently increase the maximum stress and flexural resistance of the printed samples.

Finally, the printed specimens demonstrated more resistance than injected samples when they are submitted to bending forces. This means that the FFF process must be recommended over the classical injection method to manufacture wood-composite PLA pieces, which are expected to be loaded according to bending moments.

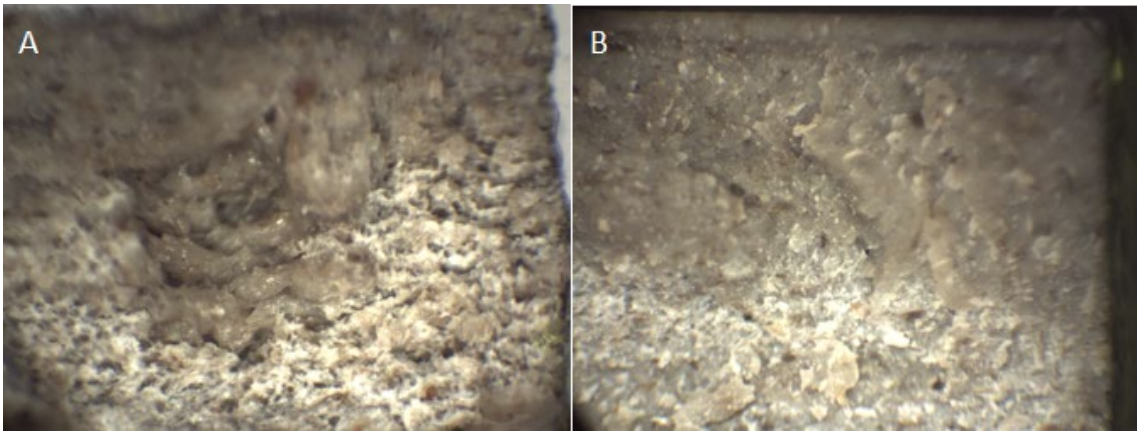

Figure 4.13. Fracture zone of wood-reinforced PLA parts. a. FFF. b. Injected.

4.4. Conclusions

The experiments conducted through the research explained in this paper have enriched the knowledge about an innovative wood-reinforced PLA material used for additive manufacturing systems. Firstly, it was found that combining 0.2-mm layer height, 0.7-mm nozzle diameter and 75% infill density, the material exhibits the best mechanical properties, regardless of the printing velocity set to the system. Of all those parameters, the layer height proves to be the most influential one, followed by the nozzle diameter, whereas no interaction between them seems to be important to determine the mechanical behavior of the obtained specimens.

Valuable information about the wood-reinforced material has been found when comparing it to simple PLA, as wood particles have proved to hinder the mechanical resistance of the material, as they increase the void between filaments and prevents neck growth between them. For this reason, the introduction of wood as a mechanical enhancer should be unadvised, and the wood-reinforced PLA should only be used in applications were mechanical properties are not relevant.

Finally, the comparison of FFF specimens to injected ones has also proved that the mechanical properties of wood-reinforced PLA or Timberfill material should be processed through additive manufacturing to maximize its properties. The maximum deformation experienced by FFF specimens were fivefold those obtained through injection, what could be caused by the interaction between filaments, that increase the ductility of the workpiece.

Chapter 5

Case study:

Fatigue behavior of PLA-wood composite manufactured by fused filament fabrication

Abstract

In this paper, the fatigue behavior of a polylactic acid-based composite reinforced with wood (trademarked as Timberfill) processed through fused filament fabrication is analyzed through rotating bending fatigue tests. Originally, this material was developed with the aim of enhancing the resistance of PLA by increasing the inner friction between polymer filaments. This work aims to confirm whether the inclusion of wood delivers the expected mechanical advantages from a functional point of view. The effect of wood on the mechanical behavior of the material is also assessed by comparing the results to similar experimental observed on non-reinforced PLA specimens. Firstly, the optimal set of parameters and levels resulting in the highest number of cycles to failure are determined, and compared to those found for PLA, by applying a Taguchi L27 experimental array. Layer height, infill level and nozzle diameter prove to be the most influential parameters on fatigue life. During a second phase, a set of specimens manufactured through the best parameter set were tested at different stress levels to represent the S-N curve. Infinite life was observed for specimens loaded with a maximum stress of 17.9 MPa. Therefore, this value can be considered as a lower threshold of the endurance limit for Timberfill cylindrical parts subjected to cyclic bending stress. SEM observations reveal that wood has a detrimental effect on the PLA matrix, as is reduces the cohesion of deposited filaments, and increases the ductile behavior of the base material.

Keywords: PLA; composite; additive manufacturing; fused filament fabrication; endurance limit; fatigue

Acronyms

AM - additive manufacturing

FDM - fused deposition modelling

FFF - fused filament fabrication

PLA - polylactic acid

ABS - acrylonitrile butadiene styrene

DOE - design of experiments

ANOVA - analysis of variance

SEM - scanning electron microscope

5.1 Introduction

One of the most extended additive manufacturing (AM) technique is Fused Filament Fabrication (FFF), or Fused Deposition Modelling (FDM) as patented in 1991 by Stratasys. FFF machines generate a 3D object by extruding a filament of a heated material, which is accurately distributed onto successive layers driven by a numerical control routine, thus constructing the workpiece from the bottom to the top. [1] The fact that the process is driven my thermal dynamics and change of state of the material [2], coupled with the fact that the process is characterized by numerous parameters that have to be determined manually by users in opens-ource and small scale 3D printing devices, the mechanical properties of parts obtained by means FFF are uncertain [3].

This paper deals with a wood-reinforced PLA material, commercially named as Timberfill. This material was developed to offer consumers a way of generating wood-looking parts, while also expecting an increase of the inner friction between the extruded filaments to enhance its resistance. The interest around the addition of natural fibers as fillers for common materials for additive manufacturing has risen in the last years, mainly due to sustainability reasons. For instance, furniture waste can be recycled by adding it to these materials, thus extending its lifecycle [4], and the use of highly available materials such as bamboo, makes it a sustainable idea [5]. The increase of biodegradability of the material is also noticeable when natural fibers, such as kenaf fibers, are joint to the base material [6]. The advantages are not only sustaibilitywise, but also related to an eventual enhancement of mechanical properties. For instance, kenaf-reinforced PLA has proved to increase its strength up to 50% with regards to the pure material [7]. But however interesting this combination might be, other researchers have highlighted the need to confirm the positive effect of wood addition, as not all fibers have the same affinity with the base material, as highlighted Huber & Müssig (2008) by observing different cohesion capabilities of hemp, flax and cotton fibers that derived in irregular PLA reinforcement [8].

The effect of reinforcement is also not totally characterized if it is attempted by adding particles instead of longitudinal fibers. Tao et al. (2017) [9] observed that the interfacial adhesion between aspen sawdust and

PLA was weak, what changed the thermal behavior of the composite, still adequate to be subjected to FFF. On the contrary, Kariz et al. (2018) [10] observed an increase of the tensile strength of wood-reinforced PLA from 55 MPa to 57 MPa with an addition of 10% wood, but a detrimental effect if that amount was higher, evidencing the high variability of results and the need to characterize specific materials for specific purposes. Lin et al. (2019) [11] also explored the ultraviolet aging as a means of improving the mechanical behavior of wood-reinforced PLA, finding that its effect is not positive at all. Therefore, as previous results go in different directions, it is necessary to understand the interaction between wood particles and PLA and assess its impact, whether positive or negative, as is done in this paper. The proliferous literature related to wood-reinforcement of PLA evidences the interest on the topic.

Most of research developed in this area has focused on tensile tests. Daver et al. (2016) [12] concluded that cork-reinforced PLA experienced an increase in ductility but lower mechanical properties as the percentage of cork increased, and that only a maximum of 5% of cork should be added to have a balanced effect. Gkartzou et al. (2017) [13] found that pine lignin dust is able to form heterogeneous systems with PLA, but again the adhesion can be detrimental. The effect of the reinforcement is also dependent of the length-to-diameter ratio of the particles. Depuydt et al. (2019) [14] conclude that short bamboo fibers increase twofold the elastic modulus of PLA, whereas the increase is more modest with dust-like fractions. Paulownia wood is also a feasible additive for PLA, and that it changes the tensile properties of the base material, as note by Tisserat et al. (2013) [15]. To a smaller extent, other mechanical properties of natural-fibers reinforcement of PLA have been tackled in bibliography. Guo et al. (2018) [16] deduced that a 10% addition of poplar wood could increase the impact strength of PLA by 7.75%. Flexural strength can also be increased by reinforcing PLA with thermomechanical pulp, with a higher chemical compatibility with PLA, as this enables better strength transfer from the material to the fibers [17]. In all cases, it seems that the extrusion temperature does not influence most of the physical properties of the material, at sight of the advances presented by Yang (2018) [18].

Other researchers have focused additional processing to make the reinforcement more effective, with diverse conclusions. Xie et al. (2017) [19] noted that the addition of plasticizers such as tributyl citrate can improve this adhesion and hence the mechanical properties and thermal stability of the composite. The positive effect of the addition of plasticizer was also supported by Stoof et al. (2017) [20], on hemp-reinforced PLA.

In contrast to the aforementioned references this paper does not aim to design a new material, but to assess the characteristics of one already existing and manufactured and distributed by a real company, by applying extensive experimental tests following a Taguchi orthogonal array. Furthermore, the study focuses on fatigue results, as this area of mechanical result has not been previously explored by other researchers on wood-PLA composite materials.

Focusing now on the FFF process itself, other authors have previously identified what are the most influential factors implicated that effectively define the mechanical behavior of workpieces. The revision

presented henceforth has been used by the authors to decide which factors are to be analyzed in the experimental execution of this paper. For instance, it has been clearly observed that the manufacturing orientation determines the main stress carrying direction and should ideally coincide with the expected in-service loads of the part to maximize its mechanical performance. Therefore, it is not worth considering it as a variable of study, but, on the contrary, as a fixed parameter [3,21].

All researchers agree that layer height is a very relevant parameter with impact on the mechanical properties of FFF parts, as it defines the neck growth that influences the cohesive forces between the deposited layers [22,23], especially when considering fatigue behavior. Tymrak et al. (2014) [23] concluded that by reducing the layer height to 0.2 mm, the tensile strength of PLA specimens was increased by 11.9 MPa, and the elastic modulus increased to 194 MPa. It also has a remarkable influence on the surface roughness and unitary cost of a piece, as show in their works Singh (2013a) [24] and Durgun & Ertan (2014) [25].

Another important aspect related to mechanical performance is how the infill is deposited to shape the overall geometry, defines the degree of porosity of the final part and the amount of bearing material [26]. Therefore, it accounts for the stiffness of the 3D printed part and its overall resistance [27]. How the infill is conformed actually depends on two different factors. On one hand, the infill density, that is, the space between filaments. And secondly, the infill pattern, as explains Wahl et al. (2012) [28].

Studies tackling with the fatigue performance of additive manufactured parts are scarce. Some references are found for laser sintered metal specimens in Spierings (2013) [29], Edwards & Ramulu (2014) [30] and Riemer et al. (2014) [31]. However, hardly have polymeric materials been previously explored. Afrose et al. (2016) [32], published a study dealing with the fatigue performance of PLA parts, where only one variable was considered, namely the manufacturing orientation. They found that specimens built at 45 degrees presented the highest fatigue life expected for every stress level tested. After that, Gomez-Gras et al. (2018) [3] used an experimental design to evaluate the fatigue performance of PLA. Both cases are an inspiration to this paper, especially the former that is used as a reference point to evaluate the effects of the introduction of wood particles in the PLA matrix to generate the Timberfill composite.

The issue arising from using innovative commercial materials such as the PLA-wood composite considered in this paper is dually tackled in this paper. On one hand, the parameters recommended by the manufacturer have not been tested or confirmed experimentally, and therefore, should be confirmed experimentally. On the other hand, most authors publish recommendations for extended materials such as PLA, ABS, and non-commercial. For this reason, this paper has been developed to continuous working on the knowledge about printing parameters, focusing on fatigue behavior as response mechanism. As fatigue properties are not usually explored for additive manufactured parts especially wood-PLA composite, the novelty delivered by this paper is both composed by the special material it includes, and the response system studied. The results obtained and explained in this contribution are of high relevance for the industry and low scale manufacturing environments, as from it arise technological recommendations for the application of a

composite material by means of open source devices, present nowadays in a high variety of economic sectors.

5.2 Materials and methods

The specimens used in this study were manufactured with Timberfill "Champagne" filament with 2.85-mm diameter, developed and manufactured by Filamentum. Timberfill is a composite material, 100% biodegradable, consisting of a PLA matrix with an 8±1% of wood fibers, as evidence thermogravimetric tests performed on the material. The tech specs provided by the manufacturer are included in Table 5.1. This material was developed with a purely aesthetic purpose, to imitate a wood appearance on objects, but also with the aim of enhancing resistance by increasing the inner friction between polymer filaments. This work aims to confirm whether the inclusion of wood delivers the expected mechanical advantages from a functional point of view.

Table 5.1. Reference mechanical properties and recommended manufacturing parameters specified by manufacturer for Timberfill material.

Property	Value	Property	Value
Material density	1.26 g/cm^3	Nozzle temperature	170-185 °C
Tensile strength*	39 MPa	Nozzle diameter	Min. 0.4 mm
Tensile modulus*	3200 MPa	Extruder velocity	20-30 mm/s

** Minimum guaranteed by the manufacturer*

5.2.1. Taguchi experimental design

Four main influential parameters on the fatigue performance of the Timberfill material were selected to perform the experimental design, namely the layer height, infill density, nozzle diameter and extrusion velocity. Three different experimental levels are considered to evaluate their influence on the fatigue lifespan response. The experimental execution was designed through a Taguchi orthogonal array. Each of the three levels selected for each factor are included in Table 5.2. This partial DOE method allows to combine numerous factors and levels and reduce the number of experiments.

Table 5.2. Factors and levels used for the DOE.

Factor		Code	Level 1	Level 2	Level 3
Layer height	[mm]	A	0.2	0.3	0.4
Nozzle diameter	[mm]	B	0.7	0.5	0.6
Infill density	[%]	C	25	50	75
Extrusion velocity	[mm/s]	D	25	30	35

Provided the number of factors and levels to be analyzed, the L27 array proves to be the most convenient to assess the first order influence of all factors, along with the mutual interactions among the first three ones [34]. Table 5.3 shows all the experimental runs described in the array. Each of them indicates the parameter

set to be applied for all specimens manufacturing. Five specimens were manufactured to repeat each manufacturing condition. The selection of these factors was decided based on previous results observed by the group and published before.

Table 5.3. Taguchi orthogonal array for the DOE.

#run	Layer height [mm]	Nozzle diameter [mm]	Infill density [%]	Extrusion velocity [mm/s]
1	0.2	0.7	25	25
2	0.2	0.7	50	30
3	0.2	0.7	75	35
4	0.2	0.5	25	35
5	0.2	0.5	50	30
6	0.2	0.5	75	25
7	0.2	0.6	25	35
8	0.2	0.6	50	25
9	0.2	0.6	75	30
10	0.3	0.7	25	30
11	0.3	0.7	50	35
12	0.3	0.7	75	25
13	0.3	0.5	25	35
14	0.3	0.5	50	25
15	0.3	0.5	75	30
16	0.3	0.6	25	25
17	0.3	0.6	50	30
18	0.3	0.6	75	35
19	0.4	0.7	25	35
20	0.4	0.7	50	25
21	0.4	0.7	75	30
22	0.4	0.5	25	25
23	0.4	0.5	50	30
24	0.4	0.5	75	35
25	0.4	0.6	25	30
26	0.4	0.6	50	35
27	0.4	0.6	75	25

The effect of two infill patterns (rectilinear and honeycomb) was also included as a focus of study (Fig. 5.1), however excluded from the experimental array that experimental design repeated twice, once for each pattern. Consequently, 270 specimens were manufactured (5 specimens for 27 conditions). Samples with the same conditions have been printed to confirm the repeatability of the obtained results and provide the results of statistical significance.

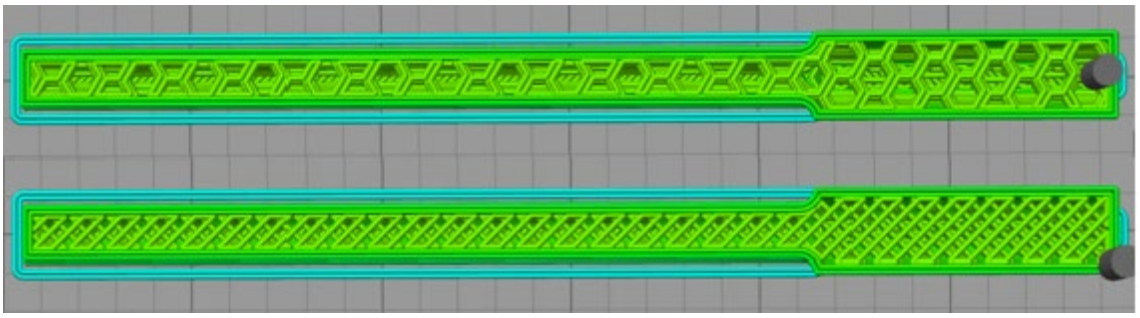

Figure 5.1. Top. Honeycomb infill pattern. Bottom. Rectilinear infill pattern. Blue lines: support material. Green lines: constitutive material of the specimen.

5.2.2. Specimens manufacture

All the specimens have been manufactured using a PYRAMID 3D Studio RepRap 3D printer. The specimen geometry was reproduced according to the ASTM D7774 standard [35] that describes the method to test the flexural fatigue properties of plastics (Fig. 5.2). This standard was taken as a reference because there is no specific reference material to evaluate laminated or additive-manufactured polymer materials.

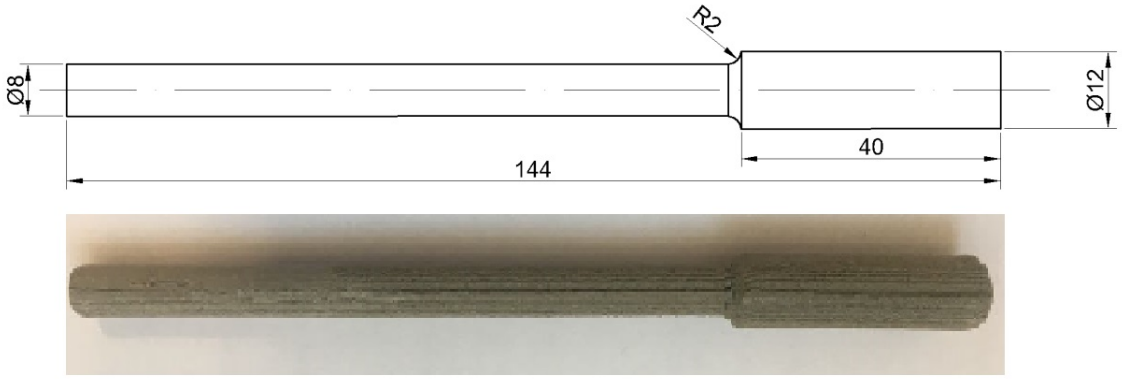

Figure 5.2. Top. Actual dimensions and shape. Bottom. Overview of the specimen manufactured.

The printing parameters that are not object of study such as building orientation, raster angle, temperature, etc., were kept constant during the manufacturing process (Table 5.4). At the bottom layers, the volume was supported with a rectilinear gridded structure that was removed before the fatigue testing. Also, the specimens were manufactured with external perimeters, solid layers at the top and the bottom of two layers.

Table 5.4. Printing parameters kept constant during the experiments.

Orientation	Raster angle	Nozzle temperature	Skirt layer	Bed temperature
0°-X	45º	180º C	2 layers	50º C

5.2.3. Experimental setup

A GUNTWP140 rotating bending stress machine has been used for the experiments (Fig. 5.3). The specimens were fixed to the chuck of the machine and rotated at a speed of 2800 min-1. The inverted stress

was applied by applying a load at its tip. The load was monitored during each test by a load cell installed at the loading mechanism. When the specimen fracture overcomes, the machine stops due to sensor displacement, and the number of cycles that each specimen endured is registered by a digital revolutions counter. The experimental setup was completed by a PCE-TC 3 thermographic camera with sensitivity of 32o C and precision of ±2o C to register the temperature of the specimen at its breaking point.

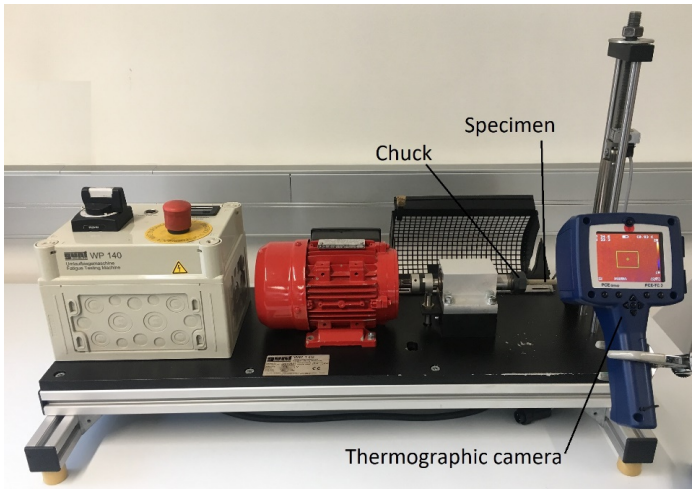

Figure 5.3. Overview of experimental setup.

5.3 Results and discussion

In the first experimental phase, a single 10-N force is applied to all specimens, in order to identify the parameter's set that leads to longer lifespan. Figure 5.4 shows the results of the average number of cycles for each run, along with its standard deviation. The parameter combination leading to maximum fatigue life was found for run number 21, in both infill patterns. That means that the recommended manufacturing parameters should be 0.4-mm layer height, 0.7-mm nozzle diameter, 75% infill density and 35-mm/s printing velocity

As for the observed temperature recorded the fracture point in a range of 28.5 to 32.5oC and no correlation was found between temperature and manufacturing conditions, it can be assumed that fatigue failure is not determined by yield of extreme temperature change.

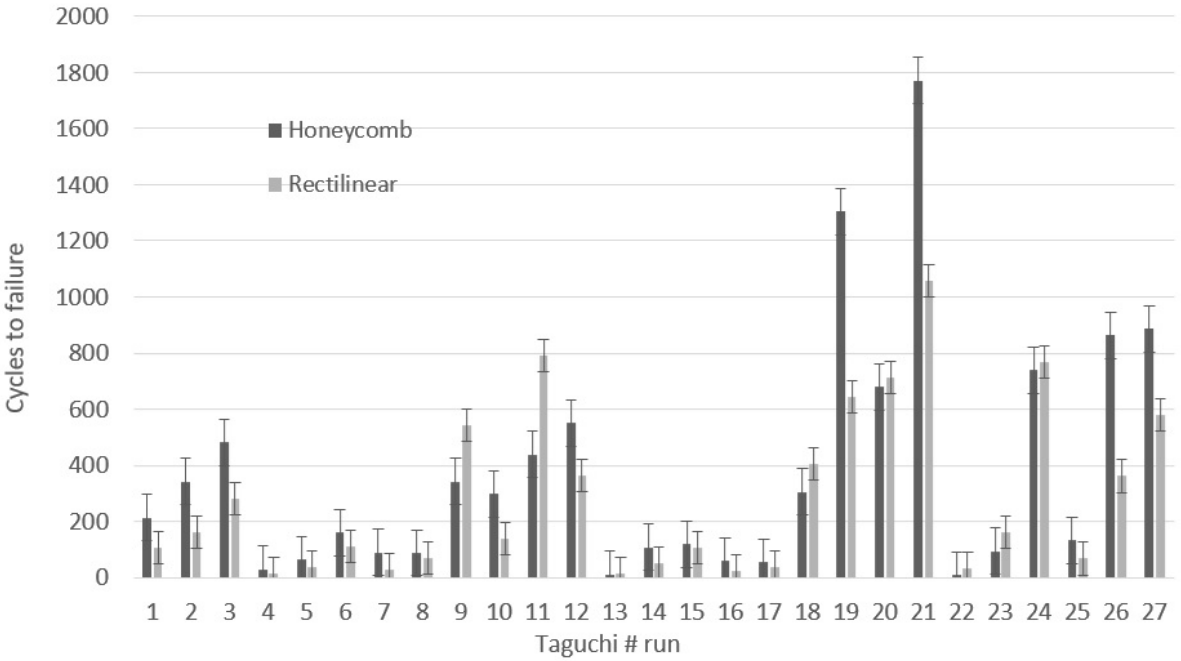

Figure 5.4. Average number of cycles to failure of each run.

5.3.1. Analysis of variance

The tested Taguchi arrays, for each infill pattern, were subjected to an analysis of variance (ANOVA) focusing on fatigue lifespan as response variable. To validate the statistical significance of the parameters included in the model, the p-value associated to each parameter included in the ANOVA was compared to a significance level of 5%. An Anderson Darling test was conducted to confirm the residual normality hypothesis of both sets of values was performed, to validate the ANOVA results, leading to a positive result.

Figure 5.5 shows the influence of the manufacturing factors used on the specimens' fatigue life, including the aforementioned p-values. It can be concluded that the statistically significant factors are layer height, the nozzle diameter, and the density. Furthermore, the honeycomb infill reveals a higher mean result for the expected lifespan, meaning that it should be preferred to the rectilinear infill. This result has already been observed in other materials such as PLA [3] and ABS) [23].

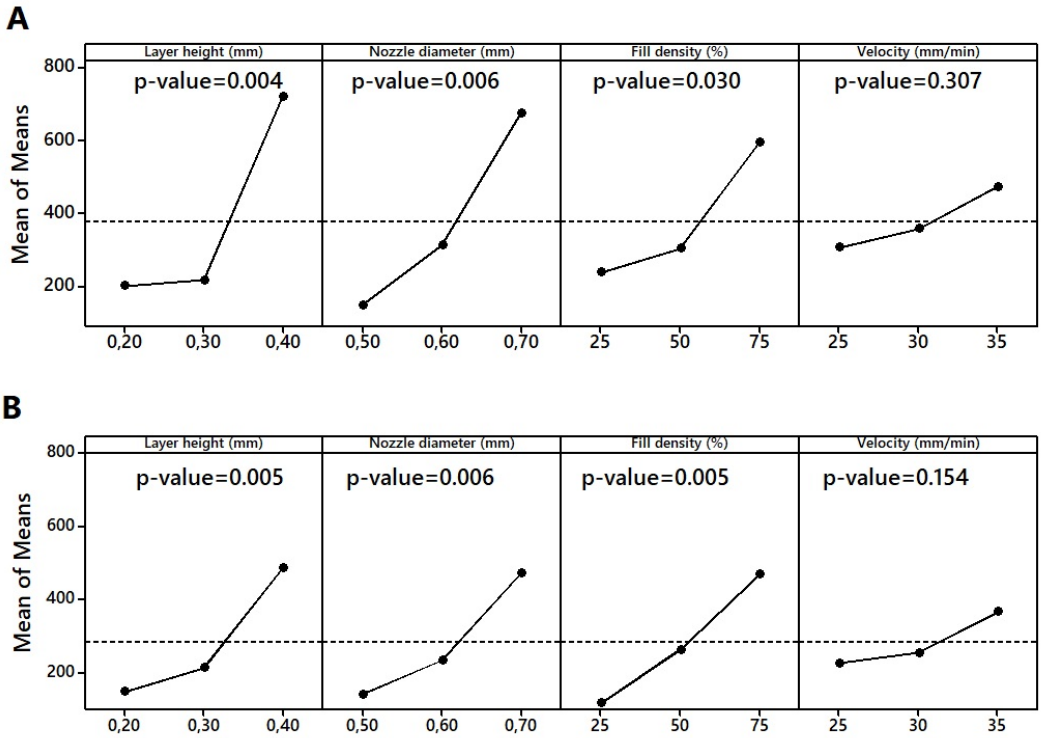

Figure 5.5. Main effects plot for the response variable number of cycles to failure and p-value associated to the ANOVA tests. A) Honeycomb infill. B) Rectilinear infill.

The layer height has the highest effect on the life of the samples. In addition, it can be seen that higher layer heights derive in longer life of the specimens. Compared to other factors, the slope that defines this feature is higher, meaning that the response variable is much more sensitive to this parameter.

In terms of nozzle diameter, it appears that the best value is 0.7 mm, as it gives a longer life. This result explains that a higher nozzle diameter allows to deposit more material in one pass and increases the contact between filaments of different layers and the penetration of neck growth. This statement is only true because the range of layer heights included in the study range from 0.2 to 0.4 mm. Experience dictates that increasing the layer height to a value near to the nozzle diameter would have a detrimental effect, as the porosity of the part world increase.

The infill density has direct influence on fatigue lifespan, and should be maximized to have a positive effect, as it was expected. Finally, the manufacturing velocity has a high p-value. For this reason, it can be concluded that this factor does not have significant effect on the specimens' fatigue life. This could be caused because the velocities range studied is not wide enough. This fact is not important because open source FFF machines, do not allow the user to modify these values to a higher extent.

Interactions between the layer height, the nozzle diameter and the infill density were also assessed through the ANOVA analysis. The p-values obtained from the ANOVA analysis, included in Table 5.5, prove that no interaction is statistically significant between factors. Therefore, it is useless to draw conclusions of the interactions between parameters.

Table 5.5. P-values for parameter interaction.

	Parameters interaction	p-value
Honeycomb infill pattern	Layer height - Nozzle diameter	0.167
	Layer height - Fill density	0.355
	Nozzle diameter - Fill density	0.697
Rectilinear infill pattern	Layer height - Nozzle diameter	0.147
	Layer height - Fill density	0.212
	Nozzle diameter - Fill density	0.366

5.3.2. Fractography

Fractographies can deliver more information about the failure mode of the Timberfill material. The cross-sectional view of broken samples of the rectilinear (Fig. 5.6A) and honeycomb (Fig. 5.6B) at a 75% infill were taken by a Moticam 3 digital camera through a Motic SMC binocular. Both infills show ductile behavior, with the presence of cavities and wooden particles separated by clearly distorted PLA walls. The distortion of the fracture surface is so remarkable that the deposited filaments can hardly be recognizable. Only the first and last printed layers show a less ductile pattern. This might be due to the fact that crack nucleation is originated at these zones.

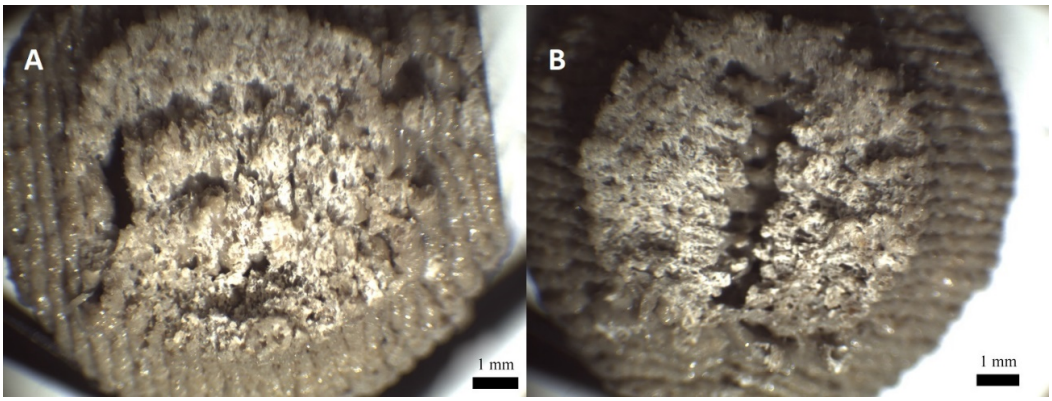

Figure 5.6. Fractographies of Timberfill specimens printed at 75% with infill pattern. A) Rectilinear. B) Honeycomb.

5.3.3. Wöhler curve for optimal printing conditions

The results described at section 3.1, evidence that there is a parameter set (Table 5.6) leading to higher fatigue lifespans. This parameter set was selected to manufacture a second set of specimens, in order to test them applying different stress levels to build the complete S-N curve, as indicates Table 5.7. As the FFF process improves the axial strength of the material due to the molecular alignment of the polymer chains,

the two highest tested stresses are slightly higher than the minimum tensile strength guaranteed by the manufacturer.

Table 5.6. Optimal combination of factors and levels to maximize the expected cycles to failure.

Parameter	Values
Infill pattern	Honeycomb
Fill density	75%
Nozzle diameter	0.7 mm
Layer height	0.4 mm

Table 5.7. Forces applied for the Wöhler curve tests and maximum stress levels.

F (N)	M_{max} (N·mm)	σ_{max} (MPa)
5.0	520	17.9
5.5	572	19.7
6	624	21.5
8.5	884	30.5
10.0	1040	35.8
11.5	1196	41.2
13.0	1352	46.6

Following the protocol established by Wirshing et al. (1980) [36], four repetitions were performed for each stress level, except for 35.8 MPa, which had been previously tested during the DOE phase. According to Burhan et al. (2018) [37], Palmgren's model in Eq. (1) represents the S-N curve for a composite material with an endurance limit.

$$S_a = S_f\left(2N_f\right)^b + S_\infty \qquad (1)$$

where Nf are the cycles to failure, Sf is a constant typical of each type of specimen, Sa is the maximum stress to which they are subjected during the fatigue test, and S∞ is the endurance limit.

The point cloud obtained from the previous testing was adjusted to a potential curve described by Eq. (1), obtaining a correlation with a Pearson's coefficient of 0.950. According to the executed tests, the specimens subjected to a maximum stress of 17.9 MPa did not experience failure before 106 cycles, hence this value being a lower threshold of the endurance limit of PLA-wood composite manufactured through FFF.

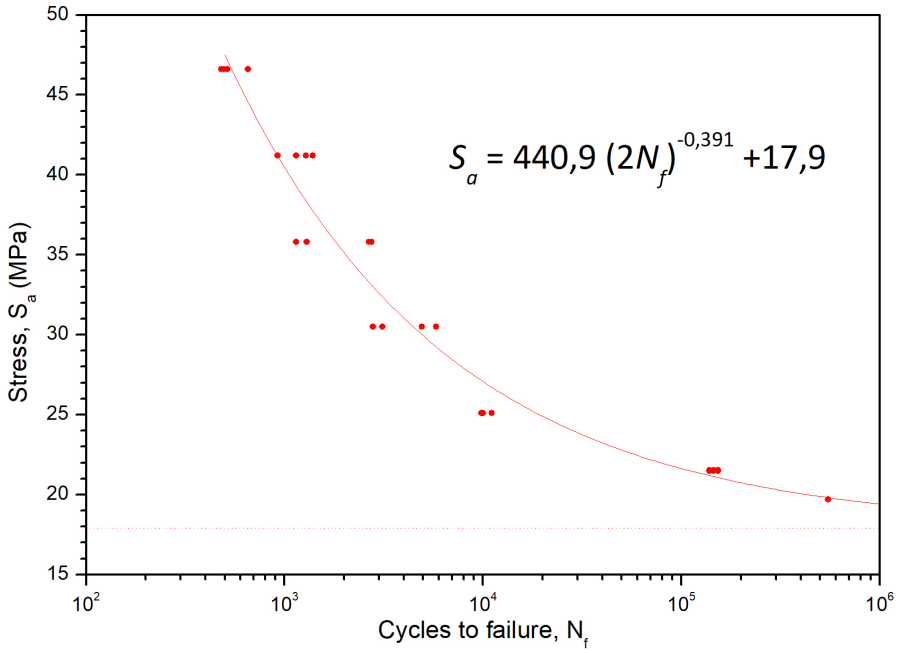

Figure 5.7. Wöhler curve for specimens manufactured with honeycomb infill, 0.4 mm layer height, 0.7 mm nozzle diameter, and 75% infill density.

5.3.4. Comparison between behavior of Timberfill and PLA

Since the Timberfill material is a composite based on a PLA matrix, it is of interest to compare the results included in this paper with their analogous ones regarding non-reinforced PLA [3]. It is important to mention that the machine used to manufacture the specimens and the test procedure followed in both works are the same. In addition, the printer used was the same, which makes this comparison significant. However, the stress tested in these two materials were different, due to the fact that both materials present different yield points. Table 5.8 shows the maximum stress levels applied to PLA specimens.

Table 5.8. Maximum stress levels included in the S-N curve of PLA specimens [4].

F (N)	M_{max} (N·mm)	σ_{max} (MPa)
10	1040	35.8
13	1352	46.6
15	1560	53.8
18	1872	64.5
20	2080	71.7
22	2288	78.8

The direct comparison of results show that the influence of each parameter on the fatigue life response shows the same behavior for both materials. The printing velocity shows no influence, where layer height, nozzle diameter and infill percentage all have a direct relation to fatigue lifespan increase. That means that

the PLA base in the composite material governs the general behavior of its derived composite, regardless of the wooden filling.

However, Timberfill seems more sensitive to the variation of the layer height, being this one the most relevant factor. On the other hand, the fatigue life for PLA specimens proved to be more influenced by the infill density. This difference could be explained by the fact that the wooden filling reduces the mobility between the polymer molecules, thus making the global infill density less relevant to achieve cohesion between all fibers. Meaning that, by having a PLA-wood composite, selecting the proper layer height has a higher influence to achieve the adequate resistance. In any case, the most important conclusion here is the similar influence of all parameters on the response.

Focusing now on the S-N curve, it can be observed that the exponent values differs about a 40% between both materials, being the expected life of Timberfill specimens lower than the one for non-reinforced PLA (Fig. 5.8). It is surprising that the introduction of wood as an additive in the PLA base is not positive, as one would expect that wood should improve resistance by acting as an anchoring point that limits polymer chain mobility. Instead, the wood seems to have the opposite effect: it does not act as a barrier for fracture prevention; much on the contrary, it weakens the PLA matrix.

This observation is confirmed through SEM inspection through JSM-7001F mode of JEOL machine, which

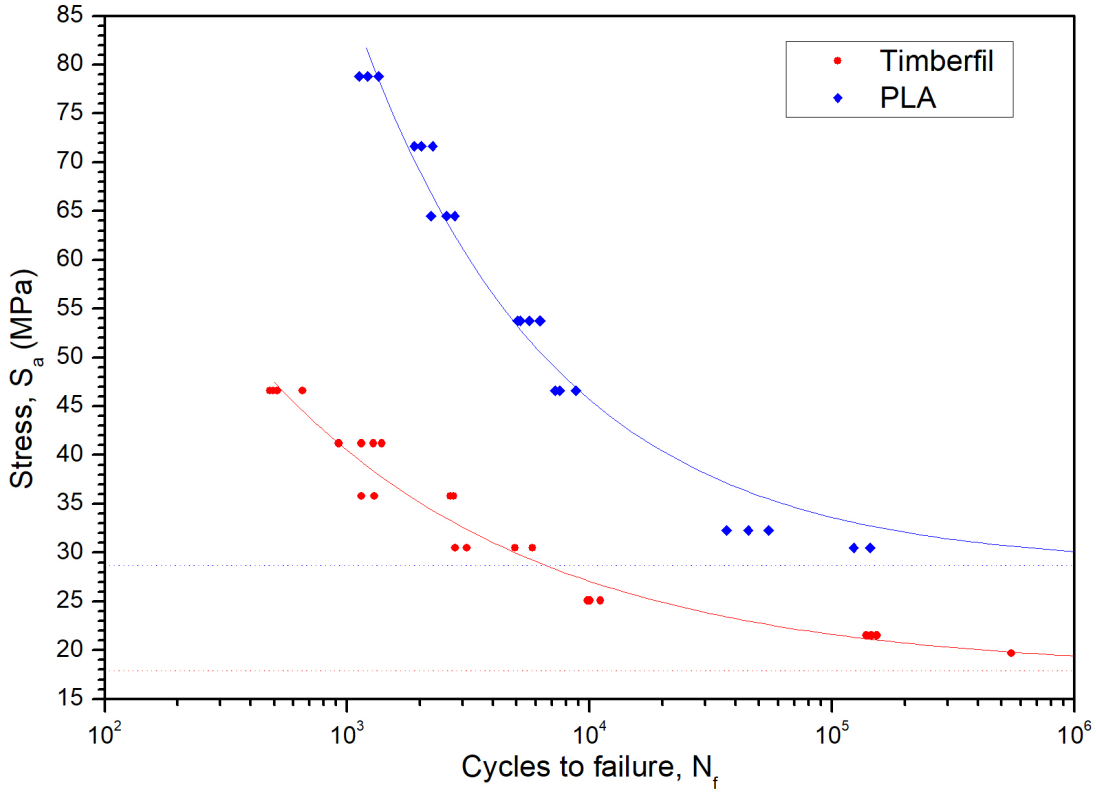

Figure 5.8. Wöhler curves for Timberfill and PLA.

shows that the adhesion between the wood and the PLA fibers is detrimental, and the voids among fibers are more conspicuous than what PLA shows (Fig. 5.9). These discontinuities act as stress risers inside the volume and reduce the mechanical properties of the base material. For this reason, the crack leading to failure in the pure PLA polymer specimens does not spread as fast as in the Timberfill material. Therefore, the utilization of Timberfill should be limited to workpieces where aspect is more important than function.

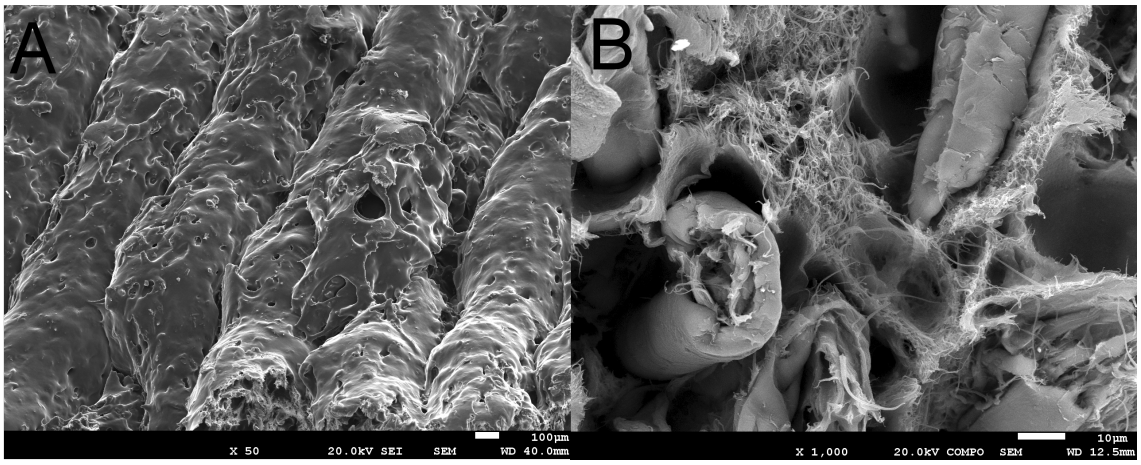

Figure 5.9. SEM images of Timberfil pieces. A) Lateral view. B) Detail of Fractography.

The comparison between the failure mode of the Timberfill (Fig. 5.7) and PLA (Fig. 5.10) is also very revealing about the effect of wood introduction in the material. Whereas the non-reinforced PLA reveals a brittle behavior, the incorporation of wood inside the matrix induces a ductile failure mode of the walls between them. This change in the fracture mode could be caused by the random distribution of voids and wood fibers that act as random oriented stress risers that change the local direction of the load inside the PLA matrix and prevents its failure by planes perpendicular to the nominal stress. Consequently, the matrix must tear between fibers and causes a much more ductile behavior.

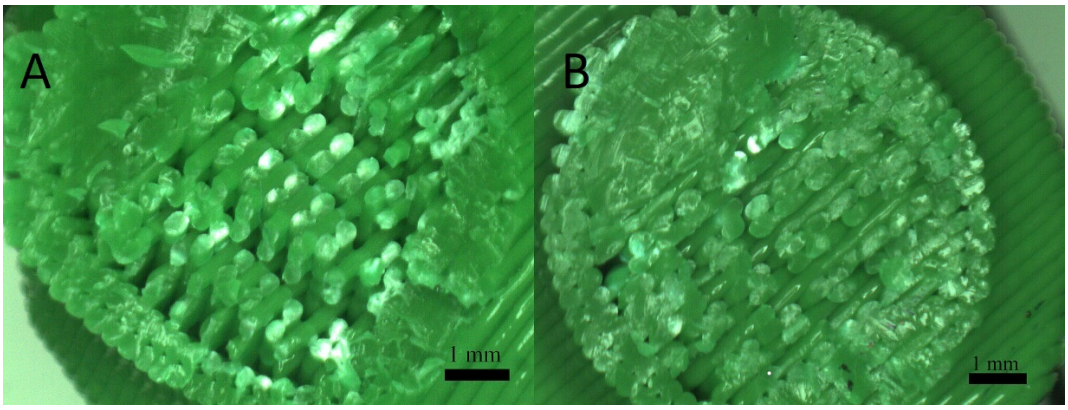

Figure 5.10. Fractographies of PLA specimens printed at the same conditions of Timberfill pieces with infill pattern. A) Rectilinear. B) Honeycomb.

5.4 Conclusions

A combination of three analyses, namely ANOVA performed on a Taguchi experimental design, the construction of an S-N curve, and microscopically observations was developed and explained in this paper to assess the mechanical behavior of a PLA-wood composite in terms of fatigue life. Only three parameters (nozzle diameter, layer height and infill density) out of four proved to be influential on the fatigue lifespan of cylindrical specimens subjected to rotating bending fatigue. The following conclusions can be extracted:

1. Specimens manufactured through a honeycomb pattern should be preferred to rectilinear ones to enhance fatigue life of PLA-wood parts. Furthermore, a combination of 75% infill density, 0.7 mm nozzle diameter and 0.4 mm layer height are recommended to manufacture this kind of workpieces.
2. The printing velocity does not show influence on the results.
3. A lower threshold for the endurance limit was found at 17.9 MPa, for Timberfill manufactured with a parameter set described in the first conclusion.
4. The introduction of wood fibers has a detrimental effect on the PLA matrix in terms of mechanical behavior, as they reduce the adhesion between fibers, and increase the voids among them. These voids act as stress risers reducing the efficiency of the base material but preventing its failure by planes perpendicular to the stress.
5. The usage of Timberfill should be limited to workpieces where aspect is more important than function.

Chapter 6

Finite element modeling to evaluate the Timberfill mechanical properties

The purpose of current chapter is to present the results of a FEM model to characterize the main Timberfill mechanical properties by considering that the workpiece manufactured through FFF can be considered as composed of two different sub materials: the skin and the infill. Although both of them are manufactured from the same raw material, the different ways through which they are deposited and how they are composed make them work differently, and, therefore, can be considered as different materials in terms of mechanical behavior. Consequently, the model explained below considers 4-point bending specimens as a composite made of material #1 in the infill, and material #2 composing the skin. Consequently, these parts are considered as a sandwich structure made of two different materials with different properties. Consequently, this research includes two sections: I) the experimental tensile test according to ASTM D-638 standard test method is carried out on the specimens manufactured by FFF under different conditions, II) the experimental results have been used as input data for Finite Element method (FEM) simulation to verify the flexural test analysis.

6.1 Experimental Tensile test

The Timberfill pieces obtained by FFF are composed by two different material configurations. The first one is their skin and the other one is the workpiece infill. To develop the proposed model, those material configurations are considered like two different materials. The model is therefore prepared to determine the contribution of each material on the final mechanical properties, considering that the source of variation of each part of the workpiece is not the raw material (which is common to both of them), but the way they are deposited. The workpiece is considered as a sandwich-structured part.

To introduce these properties as input data in the model, two different kinds of workpieces are manufactured, and then tested. First of all, dog-bone shaped tensile specimens according to the ASTM D-638 standard test (Figure 6.1) were manufactured without skin and with 7 mm thickness. Secondly, a

standard type skin was manufactured and tested independently. After testing both of them, the strain-stress curves were obtained, and the Young's modulus, elastic limit, tensile strength, and maximum elongation at break were computed.

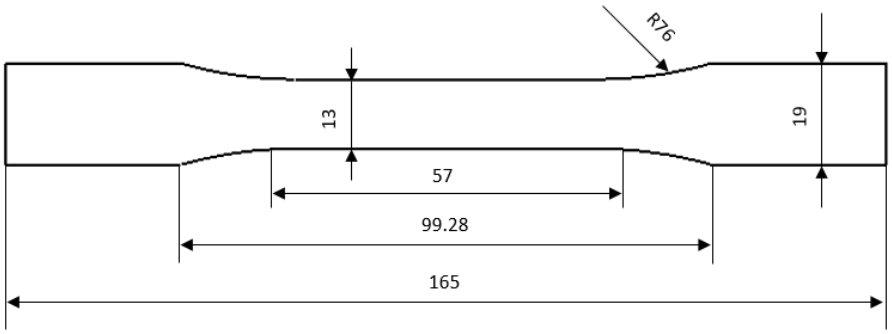

Figure 6.1. Dimension and geometrical shape of tensile sample.

6.1.1. Specimens fabrication

Regarding to the mentioned test method the sample was designed by Solidworks software with the standard shape and dimension, then has been exported as a STL format which can be read and interpreted by the printing parameterization software. In this work the Simplify 3D software has been applied to slice the drawing and generate the G-Code of sample to be able to print. To select the printing parameters, the information has been derived from the previous experimental study reported in chapter 3, in which the best manufacturing conditions for tensile properties were studied (Table 6.1).

Table 6.1. Printing parameters used in the experiments.

Nozzle diameter	Layer height	Fill density	Infill pattern	Printing velocity
0.5 mm	0.4 mm	75 %	honeycomb	40 mm/min

Since the selected material is composite of PLA with random wood particles, its properties should be those of an orthotropic material. Therefore, the same printing conditions were repeated to print the specimens in three different building orientation (0°-X, 0°-Y, and 0°-Z) and they were printed only with inside filling configuration without perimeter shell as shown in figure 6.2.A. Besides, the perimeter (skin) of the samples were printed separately with three layers in 0.4 mm height (Fig. 6.2. B). It should be mentioned that for each printing condition, 5 specimens were manufactured and tested to guarantee the repeatability of the results.

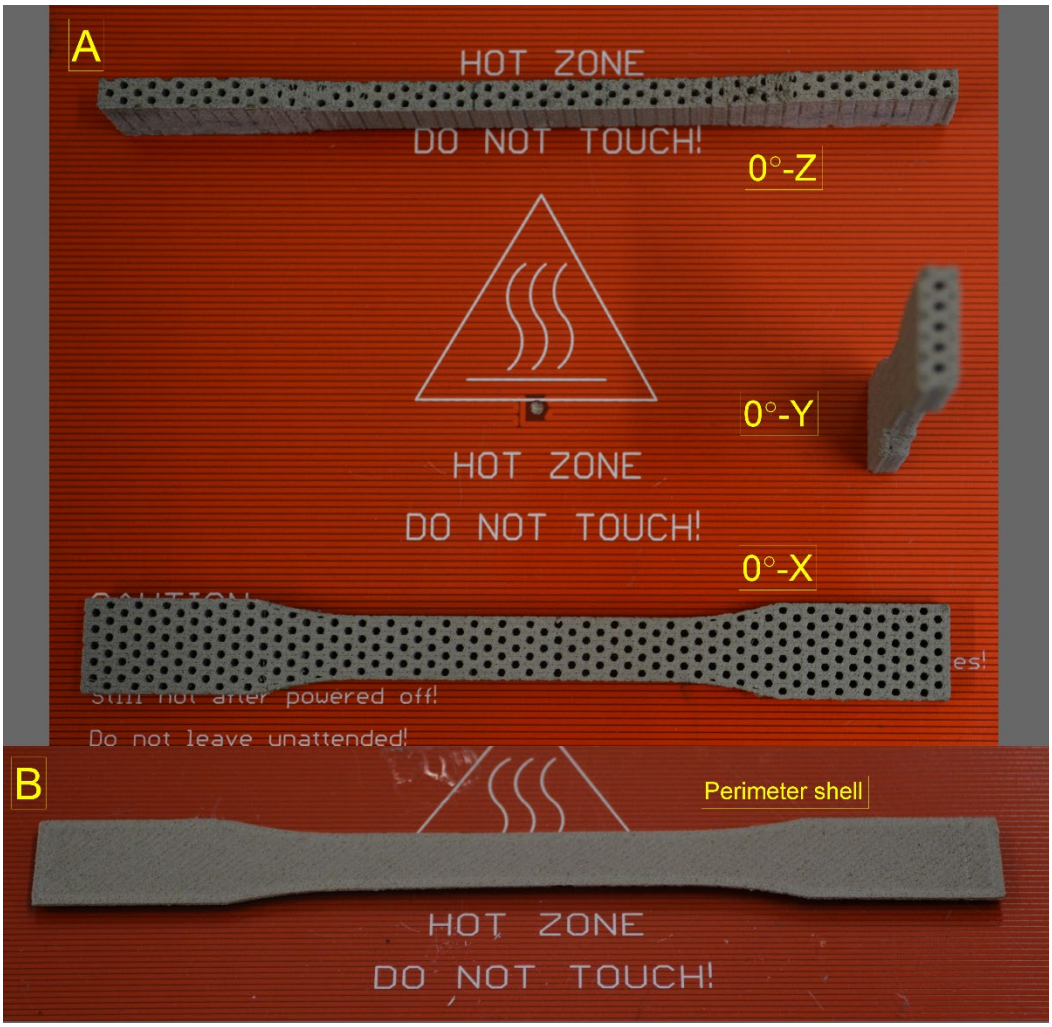

Figure 6.2. A) Different building orientations infill samples, B) outlier or skin

6.1.2. Experimental setup

The reader can refer to chapter 3 to know the experimental test methods and equipment used to that effect, as well as also the results analysis process. The tensile properties such as Young's modulus (E), yield strength (Rp0.2), maximum strength (σmax), and maximum deformation (ε) are defined for all 20 samples in total.

6.1.3. Experiment results

The average results of five repetition tests with the standard deviations of each printing filling conditions and the skin are indicated in the table 6.2. All data required to describe material's properties have been derived. This adaptation of information includes the Ej (young modulus in three-orthogonal directions), υij (Poisson ratio) for introducing orthotropic structure which is attributed to linear behavior of material. In order to define nonlinearity of behavior, experimental results of tensile tests were applied.

Table 6.2. E: Experimental results with the standard deviations. E: Young's modulus, $Rp_{0.2}$: yield strength, σ_{max}: maximum strength, ε: maximum deformation

#	E (GPa)	$Rp_{0.2}$ (MPa)	σ_{max} (MPa)	ε
0°-X	0.637 ± 0.025	4.257 ± 0.286	4.671 ± 0.476	1.36 ± 0.097
0°-Y	0.520 ± 0.059	2.452 ± 0.227	2.468 ± 0.378	1.11 ± 0.074
0°-Z	0.588 ± 0.027	3.051 ± 0.082	3.306 ± 0.164	1.01 ± 0.177
Skin	1.653 ± 0.039	12.658 ± 0.434	13.286 ± 0.436	1.57 ± 0.291

The Poisson's ratio as 0.5 for samples printed in 0°-X, 0°-Z and skin and 0.3 for those printed in 0°-Y have been determined.

6.2 Simulation

In order to simulate a four-point bending test, the mechanical behaviors of this innovative material is also investigated applying ANSYS Workbench which is based on (FEM). The values obtained from the tensile experimentation are prepared and exported into the ANSYS software as engineering data to specify the material.

6.2.1. Modeling process

Since the achieved data directly from the test contain a high amount of repeated values that the finite element program cannot assimilate, the polynomial trend line is made that fits the data correctly to make them as a set of data. This process is applied for all data of each filling samples and the skin tests results. Then these data are separately introduced to the ANSYS software to introduce a new material.

In the next step the geometrical model of the sample is created according to the ASTM D6272 standard [89]. This test method covers the procedure to determine the flexural properties of unreinforced and reinforced plastics, including high-modulus composites and electrical insulating materials in different forms. Hence its adequacy for the purposes of these works with a composite material. In this case the configuration has been modeled in three-layered structure, the bottom and top layers as skin and the central layer as infill so that they have been considered to be integrated. Whereas the applied test method has geometrical and enforcement symmetry, therefor using a vertical slide restriction for the central plane of the part can correctly represent the evolution of tensions (Fig. 6.3. A). Also the sample is divided into different segments for two reasons: 1) to make structured and regular mesh, 2) to define accurate contact between the spans and specimen (Fig. 6.3. B).

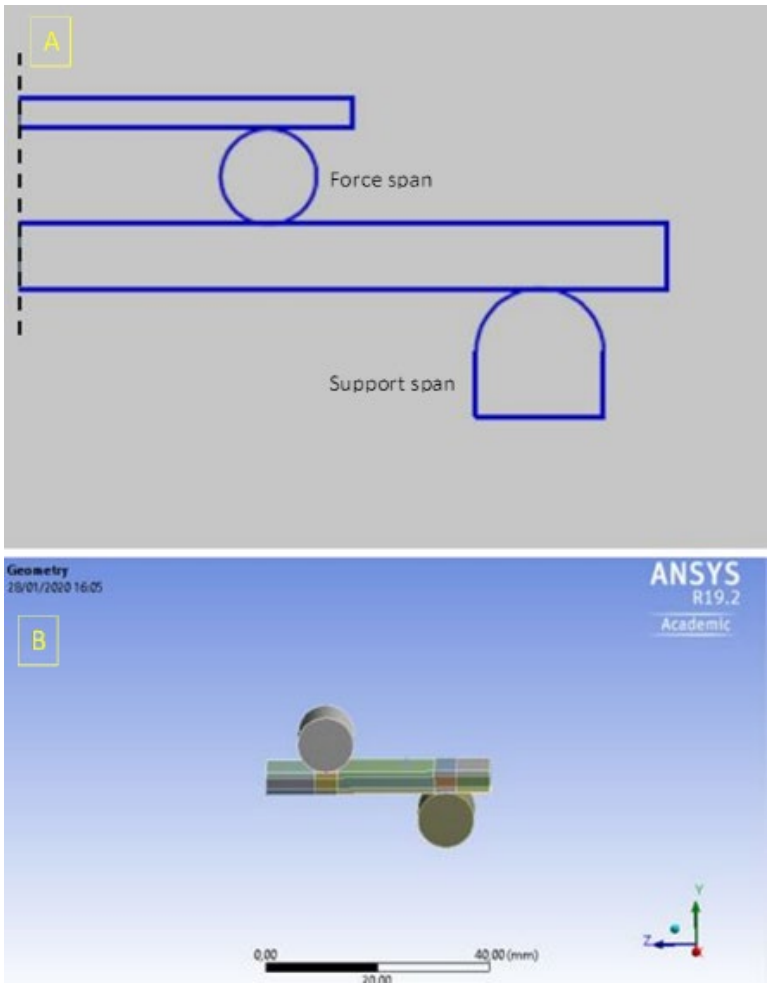

Figure 6.3. The finite element model corresponding to the experimental setup

A higher order 3D element composed of 20 nodes, named SOLID186. Each node has three degrees of freedom: translations in the nodal x, y, and z directions. Since this type of element exhibits quadratic displacement behavior, it is more accurate in estimating displacement than other elements with linear shape functions. It should be mentioned that frictionless has been considered as type contact between force span and specimen. To avoid lateral displacement in the middle plane of sample, constrain is determined in X direction and the supports span is limited at the bottom area in all directions. In order to apply uniform displacement into the force span, a reference point created and all degree of freedom of this body assigned to this point. All boundary conditions detail is demonstrated in figure 6.4.

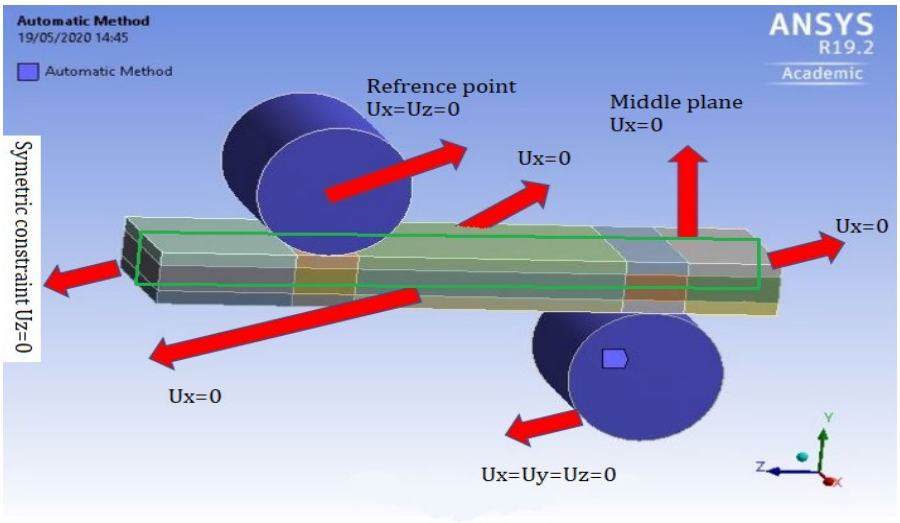

Figure 6.4. Defined boundary conditions on the sample

The assembly has been meshed as indicated in figure 6.5, in order to obtain different elements for both the skin and the filler and the supports that are sufficient to get plausible results. The analysis has been started by moving down the upper roller (force span) to simulate the force direction at which the experiments were performed at the same displacement rate while the other roller (support span) remains fixed.

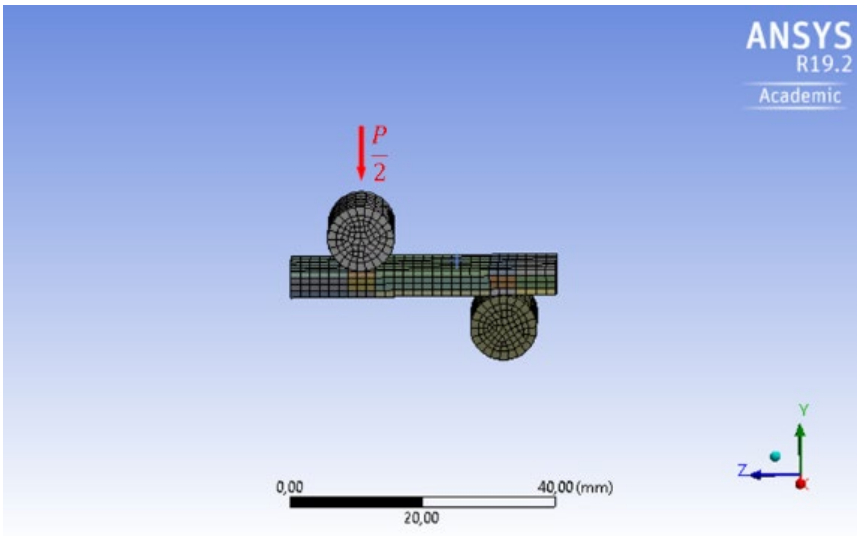

Figure 6.5. Mesh diagram of modeling assembly

6.2.2. Simulation results

Once the simulation process is finished, the mechanical properties such as equivalent stress, equivalent elastic strain, total deformation and force reaction versus time are achieved. Stress distribution extracted from element analysis of equivalent stress is indicated layer by layer in figure 6.6. As it was expected, the

maximum stress is distributed at the outliers of the sample between the force spans which the samples during the experimental test have experienced the similar behavior.

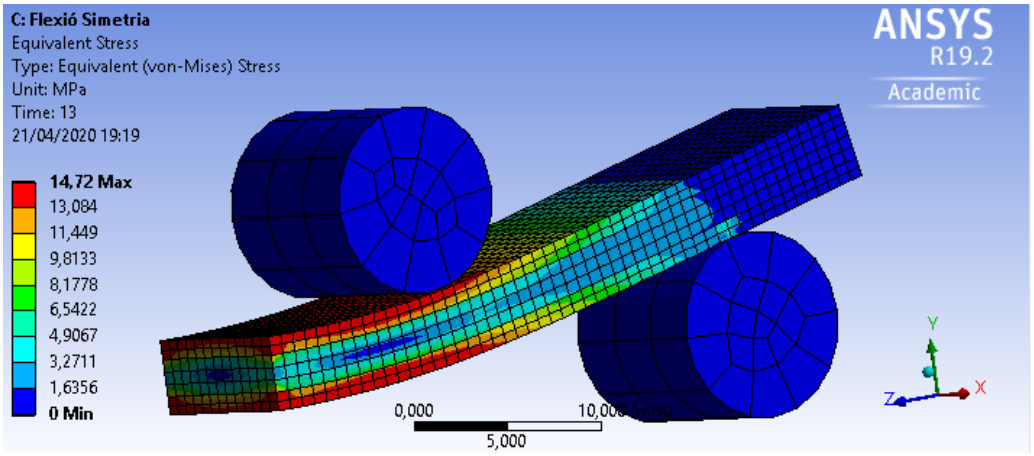

Figure 6.6. Damage development diagram of equivalent stress

The worth mentioning point is the obtained deformation curve of two experiments from the previous results of the samples printed with the same condition and manufacturing parameters versus the simulation results. This graph validates the experimental results evidencing the simulation by the coincidence of the deformation trajectory as shown in figure 6.7.

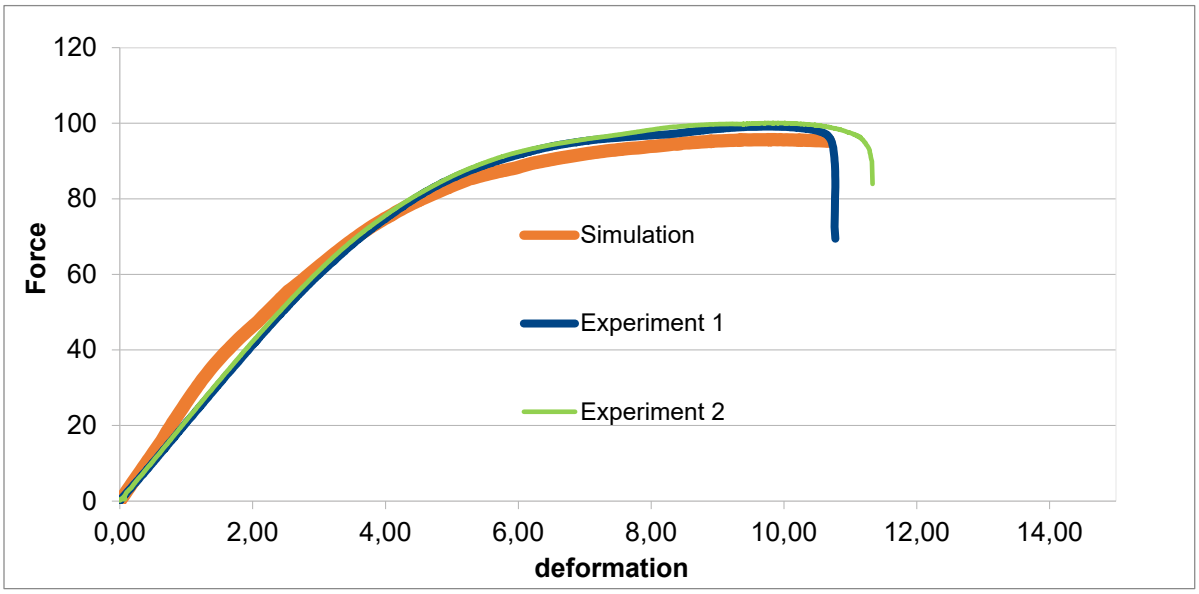

Figure 6.7. Deformation curves comparison of experiments and simulation

6.3 Conclusion

The mechanical properties of FFF manufactured Timberfill parts are investigated both experimentally and computationally to prevent the mechanical characteristics of this material. In the experimental phase the Young's modulus (E), yield strength (Rp0.2), maximum strength (σmax), and maximum deformation (ε) have been derived applying tensile test. To determine this material as an orthotropic composite the samples are printed in three different building orientation. The results have been introduced to the ANSYS simulation software to characterize both materials, and then the flexural properties have been modeled and compared to the previous experimental research to validate the results. The most important conclusion is that a valid model has been obtained to predict the deformation behavior of the material from the experimental phase, as a maximum error of 10% between the experimental and modelling results is evidenced, and taken as valid.

Chapter 7

Conclusions and future works

7.1 General conclusions

The aim of the present dissertation was characterizing a commercial wood-PLA composite material (Timberfill) carrying out standard mechanical tests on the specimens manufactured through FFF technology. Different printing parameters and levels selected as the manufacturing variables for printing the samples submitting the tensile, flexural, and fatigue tests to define the mechanical properties of this material. DoE method has been applied in the experimental phase of this study and the results are analyzed through analysis of variance (ANOVA) to determine the influence of printing parameters on each response. Besides of a comparison between the results obtained for this material and pure PLA, the results of Timberfill injection-molded samples applying the similar test procedure are compared as well. Also a simulation was conducted using a FEM to validate the experimental data.

Due to the fact that printing process parameters exhibit a significant effect on mechanical properties and one of the challenging aspects is improving material structure, this thesis concludes by arguing the influence of a number of parameters such as layer height, nozzle diameter, building orientation, fill density, infill pattern, and printing velocity on the mechanical properties. Although the results are discussed in detail for the responses in the relevant sections, the general conclusions are mentioned as follow.

1. Of all selected parameters layer height is the most influential parameter on the responses followed by nozzle diameter, fill density, building orientation, and velocity in the descending order. Since the lowest height of the layers with the biggest selected level nozzle diameter obtained better results for the responses, it can be mentioned that this composition makes a stronger adhesiveness between the layers and increases the solidity of the inside of the samples. It can be seen clearly that increasing the infill density would raise the endurance of the samples under the forces, furthermore the infill pattern could be effective which the honeycomb pattern eventuated the best results with the same filling percentage in compare to the other practical patterns. In the other hand, three different building orientation has been examined on the tensile strength test. Whereas the samples printed in the 0-Z orientation shown higher resistance, the reason could be that the deposition of

the material layers in a smaller area to generate the exact pattern that makes the samples more solid and more resistant. The printing velocity has shown no significant influent on none of the responses. Although none of the parameters could be defined as a significant individually.

2. According to the comparison between the injection-molded samples and FFF manufactured ones, the achieved results were various based on the different submitted tests. In order to the tensile strength test the obtained magnitude of the responses from the printed samples were lower than injected samples which the main reason is solidity of the injected specimens to endure more against the tension. In contrast the maximum elongation of the printed samples was significantly higher which can be due to the separation of the extruded filaments one by one and increases the ductility of the samples consequently. In case of the flexural test results, the obtained values for responses of the printed specimens are higher than the injected results meant that processing the Timberfill material by FFF enhances the overall behavior of the material. Due to the fact that in the bending test the initial force applies to the outlier of the specimen, the crack grows property which occurs in the outer fiber of the sample can decrease the ductility of injected parts, because this phenomenon should repeat for each layers of printed parts.
3. As it can be seen from the results of each executed tests (Tensile, Flexural, and Fatigue), the obtained mechanical properties of Timberfill parts shown lower resistances than pure PLA. Since the proportion of fiber to matrix or the fraction of fiber reinforcement plays a very important role in determining the mechanical behaviors of the composites as that a higher fiber volume fraction typically results in better mechanical properties of the composite. Therefore, regarding the Timberfill the volumetric percentage of the fibers to matrix is 8±1%, so increasing this percentage can arise the resistance of the material. Additionally, changing the actual composition of wood fiber inside the PLA matrix could be effective in turn positively effective on the resistance properties of the composite material.
4. On the other hand, the obtained results about the composite material comparing to non-reinforced PLA shows that wood particles have proved to decrease the mechanical resistance of the material due to the generated void between printed filaments and prevent neck growth between them. This phenomenon could be effected by the promiscuousness of the matrix and fibers together.
5. The obtained results of FEM analysis have concluded significantly that the deformation behavior of the material from the experimental test is resemble to the simulation results which indicates the validity of the experimental results.

7.2 Future works

A number of proposals for future research derived from this work are summarized as follow:

1. The works developed during this thesis have focused on some static and dynamic properties. However, the complete knowledge of how Timberfill works after being modified through FFF has not totally been explored. Other mechanical properties such as impact strength or compression could be explored in future works to complete the assessment of the material.
2. Since a small number of printing parameters were executed through this study, selecting another parameters and levels to perform the mechanical tests of the samples and understand their influence on the mechanical properties would be interesting.
3. Nowadays one of the serious subject under this field is roughness and relevant surface properties, finding the parameters and printing conditions to obtain better surface texture of the printed parts is recommended strongly.
4. Regardless, future research could continue to explore deeper analysis to find the exact portion of the fiber to matrix and apply better suggestions to improve the mechanical resistance of this material. Also improving the interface between matrix and fibers by performing chemical treatments can be a great career to achieve more resistant composite.
5. The FEM simulation can be applied to analyze the fatigue results and predict the other mechanical properties as well.

Bibliography

Bibliography of Chapter 1 and 2

1. Ahn, S.H., et al., Anisotropic material properties of fused deposition modeling ABS. Rapid Prototyping Journal, 2002. 8(4): p. 248-257.
2. Forster, A.M. and A.M. Forster, Materials testing standards for additive manufacturing of polymer materials: state of the art and standards applicability. 2015.
3. Jurrens, K. and E. Incorporated, Measurement Science Roadmap for Metal-Based Additive Manufacturing. Energetics Incorporated, Columbia, 2013.
4. Gao, W., et al., The status, challenges, and future of additive manufacturing in engineering. Computer-Aided Design, 2015. 69: p. 65-89.
5. Domingo-Espin, M., et al., Mechanical property characterization and simulation of fused deposition modeling Polycarbonate parts. Materials & Design, 2015. 83: p. 670-677.
6. Shabat, D., et al., Mechanical and structural characteristics of fused deposition modeling ABS material. Annals of “Dunarea de Jos” University, Fascicle XII, Welding Equipment and Technology, 2017. 28: p. 16-24.
7. Afrose, M.F., et al., Effects of part build orientations on fatigue behaviour of FDM-processed PLA material. Progress in Additive Manufacturing, 2016. 1(1-2): p. 21-28.
8. Cantrell, J.T., et al., Experimental characterization of the mechanical properties of 3D-printed ABS and polycarbonate parts. Rapid Prototyping Journal, 2017. 23(4): p. 811-824.
9. Akande, S.O., K. Dalgarno, and J. Munguia, Process control testing for fused filament fabrication. Rapid Prototyping Journal, 2017. 23(2): p. 246-256.
10. Hernandez, R., et al. Analyzing the tensile, compressive, and flexural properties of 3D printed ABS P430 plastic based on printing orientation using fused deposition modeling. in 27th Annual International Solid Freeform Fabrication Symposium, Austin, TX. 2016.
11. Rankouhi, B., et al., Failure Analysis and Mechanical Characterization of 3D Printed ABS With Respect to Layer Thickness and Orientation. Journal of Failure Analysis and Prevention, 2016. 16(3): p. 467-481.
12. Farzadi, A., et al., Effect of layer thickness and printing orientation on mechanical properties and dimensional accuracy of 3D printed porous samples for bone tissue engineering. PLoS One, 2014. 9(9): p. e108252.

13. Abdelrhman, A.M., W.W. Gan, and D. Kurniawan. Effect of part orientation on dimensional accuracy, part strength, and surface quality of three dimensional printed part. in IOP Conference Series: Materials Science and Engineering. 2019. IOP Publishing.
14. Patton, M.V., et al., Manipulating magnetic anisotropy in fused filament fabricated parts via macroscopic shape, mesoscopic infill orientation, and infill percentage. Additive Manufacturing, 2019. 27: p. 482-488.
15. Nomani, J., et al., Effect of layer thickness and cross-section geometry on the tensile and compression properties of 3D printed ABS. Materials Today Communications, 2020. 22.
16. Tymrak, B., M. Kreiger, and J.M. Pearce, Mechanical properties of components fabricated with open-source 3-D printers under realistic environmental conditions. Materials & Design, 2014. 58: p. 242-246.
17. Jerez-Mesa, R., et al., Fatigue lifespan study of PLA parts obtained by additive manufacturing. Procedia Manufacturing, 2017. 13: p. 872-879.
18. Akhoundi, B., A.H. Behravesh, and A. Bagheri Saed, Improving mechanical properties of continuous fiber-reinforced thermoplastic composites produced by FDM 3D printer. Journal of Reinforced Plastics and Composites, 2019. 38(3): p. 99-116.
19. Gomez-Gras, G., et al., Fatigue performance of fused filament fabrication PLA specimens. Materials & Design, 2018. 140: p. 278-285.
20. Bakrani Balani, S., et al., Influence of printing parameters on the stability of deposited beads in fused filament fabrication of poly(lactic) acid. Additive Manufacturing, 2019. 25: p. 112-121.
21. Vicente, C.M.S., et al., Influence of fused deposition modeling parameters on the mechanical properties of ABS parts. Polymers for Advanced Technologies, 2019. 31(3): p. 501-507.
22. Terekhina, S., et al., Effects of the Infill Density on the Mechanical Properties of Nylon Specimens Made by Filament Fused Fabrication. Technologies, 2019. 7(3).
23. Tanveer, M.Q., A. Haleem, and M. Suhaib, Effect of variable infill density on mechanical behaviour of 3-D printed PLA specimen: an experimental investigation. SN Applied Sciences, 2019. 1(12).
24. Abdullah Aloyaydi, B., S. Sivasankaran, and H. Rizk Ammar, Influence of infill density on microstructure and flexural behavior of 3D printed PLA thermoplastic parts processed by fusion deposition modeling. AIMS Materials Science, 2019. 6(6): p. 1033-1048.
25. Mahmood, S., et al., Tensile strength of partially filled FFF printed parts: experimental results. Rapid Prototyping Journal, 2017. 23(1): p. 122-128.

26. Tsouknidas, A., et al., Impact absorption capacity of 3D-printed components fabricated by fused deposition modelling. Materials & Design, 2016. 102: p. 41-44.
27. Akhoundi, B. and A.H. Behravesh, Effect of Filling Pattern on the Tensile and Flexural Mechanical Properties of FDM 3D Printed Products. Experimental Mechanics, 2019. 59(6): p. 883-897.
28. Agarwal, K., et al. Process–property relationships in additive manufacturing of nylon-fiberglass composites using taguchi design of experiments. in Proceedings of solid freeform fabrication symposium. 2017.
29. Ertay, D.S., A. Yuen, and Y. Altintas, Synchronized material deposition rate control with path velocity on fused filament fabrication machines. Additive Manufacturing, 2018. 19: p. 205-213.
30. Jiao, Y. and J. Fish, Is an additive decomposition of a rate of deformation and objective stress rates passé? Computer Methods in Applied Mechanics and Engineering, 2017. 327: p. 196-225.
31. Xiao, H., O.T. Bruhns, and A. Meyers, Elastoplasticity beyond small deformations. Acta Mechanica, 2006. 182(1-2): p. 31-111.
32. Ward, I.M. and D.W. Hadley, An introduction to the mechanical properties of solid polymers. 1993.
33. Bourell, D.L., M. Leu, and D. Rosen, Roadmap for additive manufacturing-Identifying the future of freeform processing. The University of Texas at Austin, Laboratory for Freeform Fabrication. Advanced Manufacturing Center, 2009. 32.
34. Hemanth, R., M. Sekar, and B. Suresha, Effects of fibers and fillers on mechanical properties of thermoplastic composites. Indian Journal of Advances in Chemical Science, 2014. 2: p. 28-35.
35. Makes, A. and A.A.M.S. Collaborative, Standardization roadmap for additive manufacturing. February), Public Draft, 2017.
36. Handbook-MIL-HDBK, M., 17-3F: Composite Materials Handbook, Volume 3-Polymer Matrix Composites Materials Usage, Design, and Analysis. US Department of Defense, 2002.
37. Es-Said, O.S., et al., Effect of Layer Orientation on Mechanical Properties of Rapid Prototyped Samples. Materials and Manufacturing Processes, 2000. 15(1): p. 107-122.
38. Galantucci, L.M., F. Lavecchia, and G. Percoco, Quantitative analysis of a chemical treatment to reduce roughness of parts fabricated using fused deposition modeling. CIRP Annals, 2010. 59(1): p. 247-250.

39. Tymrak, B.M., M. Kreiger, and J.M. Pearce, Mechanical properties of components fabricated with open-source 3-D printers under realistic environmental conditions. Materials & Design, 2014. 58: p. 242-246.
40. Casavola, C., et al., Orthotropic mechanical properties of fused deposition modelling parts described by classical laminate theory. Materials & Design, 2016. 90: p. 453-458.
41. Wu, W., et al., Influence of Layer Thickness and Raster Angle on the Mechanical Properties of 3D-Printed PEEK and a Comparative Mechanical Study between PEEK and ABS. Materials (Basel), 2015. 8(9): p. 5834-5846.
42. Travieso-Rodriguez, J.A., et al., Mechanical Properties of 3D-Printing Polylactic Acid Parts subjected to Bending Stress and Fatigue Testing. Materials (Basel), 2019. 12(23).
43. Domingo-Espin, M., et al., Fatigue Performance of ABS Specimens Obtained by Fused Filament Fabrication. Materials (Basel), 2018. 11(12).
44. Swainson, W.K., Method, medium and apparatus for producing three-dimensional figure product. 1977, Google Patents.
45. Yokohara, T. and M. Yamaguchi, Structure and properties for biomass-based polyester blends of PLA and PBS. European Polymer Journal, 2008. 44(3): p. 677-685.
46. Rout, J., et al., Novel eco-friendly biodegradable coir-polyester amide biocomposites: Fabrication and properties evaluation. Polymer composites, 2001. 22(6): p. 770-778.
47. Mohanty, A., et al. Eco-friendly composite materials from biodegradable polymers: Biocomposites to nanocomposites. in ABSTRACTS OF PAPERS OF THE AMERICAN CHEMICAL SOCIETY. 2001. AMER CHEMICAL SOC 1155 16TH ST, NW, WASHINGTON, DC 20036 USA.
48. Tripathy, S., G. Levita, and L. Di Landro, Interfacial adhesion in jute-polyolefin composites. Polymer composites, 2001. 22(6): p. 815-822.
49. Jang, M., et al., Characteristics of preparation and thermal properties of PLA stereocomplex. Appl. Chem., 2010. 14: p. 1-4.
50. Cho, D., et al., Eco-friendly biocomposite materials using biofibers. Polym Sci Technol, 2002. 13(4): p. 460-76.
51. David, S., et al., Biodegradation and Composting Studies of Polymeric Materials. Biodegradable Plastics and Polymers, Y. Doi and K. Fukuda, Editors, Elsevier, Osaka, 1993. 601.
52. Vink, E.T., et al., Applications of life cycle assessment to NatureWorks™ polylactide (PLA) production. Polymer Degradation and stability, 2003. 80(3): p. 403-419.

53. Jo, M.Y., et al., Effects of compatibilizers on the mechanical properties of ABS/PLA composites. Journal of Applied Polymer Science, 2012. 125(S2): p. E231-E238.
54. Bassett, K., R. Carriveau, and D.S.K. Ting, 3D printed wind turbines part 1: Design considerations and rapid manufacture potential. Sustainable Energy Technologies and Assessments, 2015. 11: p. 186-193.
55. Wittbrodt, B. and J.M. Pearce, The effects of PLA color on material properties of 3-D printed components. Additive Manufacturing, 2015. 8: p. 110-116.
56. Le Duigou, A., et al., 3D printing of wood fibre biocomposites: From mechanical to actuation functionality. Materials & Design, 2016. 96: p. 106-114.
57. Yang, T.C., Effect of Extrusion Temperature on the Physico-Mechanical Properties of Unidirectional Wood Fiber-Reinforced Polylactic Acid Composite (WFRPC) Components Using Fused Deposition Modeling. Polymers (Basel), 2018. 10(9).
58. Guessasma, S., S. Belhabib, and H. Nouri, Microstructure and Mechanical Performance of 3D Printed Wood-PLA/PHA Using Fused Deposition Modelling: Effect of Printing Temperature. Polymers (Basel), 2019. 11(11).
59. Kariz, M., et al., Effect of wood content in FDM filament on properties of 3D printed parts. Materials Today Communications, 2018. 14: p. 135-140.
60. Rahimizadeh, A., et al., Recycled Glass Fiber Composites from Wind Turbine Waste for 3D Printing Feedstock: Effects of Fiber Content and Interface on Mechanical Performance. Materials (Basel), 2019. 12(23).
61. Mazzanti, V., L. Malagutti, and F. Mollica, FDM 3D Printing of Polymers Containing Natural Fillers: A Review of their Mechanical Properties. Polymers (Basel), 2019. 11(7).
62. Migneault, S., et al., Effects of processing method and fiber size on the structure and properties of wood–plastic composites. Composites Part A: Applied Science and Manufacturing, 2009. 40(1): p. 80-85.
63. Hung, K.C., et al., Characterization of Wood-Plastic Composites Made with Different Lignocellulosic Materials that Vary in Their Morphology, Chemical Composition and Thermal Stability. Polymers (Basel), 2017. 9(12).
64. Ozcelik, B., A. Ozbay, and E. Demirbas, Influence of injection parameters and mold materials on mechanical properties of ABS in plastic injection molding. International Communications in Heat and Mass Transfer, 2010. 37(9): p. 1359-1365.
65. Maidin, S., et al., Feasibility study of vacuum technology integrated fused deposition modeling to reduce staircase effect. Journal of Fundamental and Applied Sciences, 2018. 10(1S): p. 633-645.

Bibliography of Chapter 3

1. Jerez-Mesa, R.; Travieso-Rodriguez, J. A.; Llumà-Fuentes, J.; Gomez-Gras, G.; Puig, D. (2017) Fatigue Lifespan Study of PLA Parts Obtained by Additive Manufacturing. Procedia Manuf 13, 872-879.
2. Domingo-Espin, M.; Travieso-Rodriguez, J. A.; Jerez-Mesa, R.; Lluma-Fuentes, J. (2018) Fatigue Performance of ABS Specimens Obtained by Fused Filament Fabrication. Materials. 11, 2521.
3. Fayazbakhsh, K.; Movahedi, M.; Kalman, J. (2019) The Impact of Defects on Tensile Properties of 3D Printed Parts Manufactured by Fused Filament Fabrication. Mater. Today Commun. 18, 140-148.
4. Morales-Planas, S.; Minguella-Canela, J.; Lluma-Fuentes, J.; Travieso-Rodriguez, J. A.; García-Granada, A. A. (2018) Multi Jet Fusion PA12 Manufacturing Marameters for Watertightness, Strength and Tolerances. Materials. 11, 1472.
5. Es-Said, O. S.; Foyos, J.; Noorani, R.; Mel Mendelson.; Marloth, R.; Pregger, B. A. (2000) Effect of Layer Orientation on Mechanical Properties of Rapid Prototyped Samples. Mater Manuf Processes. 1, 107-122.
6. Sood, A. K.; Ohdar, R. K.; & Mahapatra, S. S. (2010) Parametric Appraisal of Mechanical Property of Fused Deposition Modelling Processed Parts. Mater. Des. 31, 287-295.
7. Fernandez-Vicente, M.; Calle, W.; Ferrandiz, S.; Conejero, A. (2006) Effect of Infill Parameters on Tensile Mechanical Behavior in Desktop 3D Printing. 3D Print Addit Manuf. 3, 183-192.
8. Laureto, J. J.; Pearce, J. M. (2018) Anisotropic Mechanical Property Variance Between ASTM D638-14 Type I and Type IV Fused Filament Fabricated Specimens. Polym. Test. 68, 294-301.
9. Cwikla, G.; Grabowik, C.; Kalinowski, K.; Paprocka, I.; Ociepka, P. (2017) The Influence of Printing Parameters on Selected Mechanical Properties of FDM/FFF 3D-Printed Parts. IOP Conf. Ser.: Mater. Sci. Eng. 227, No. 1, 012033.
10. Marat-Mendes.; Rosa, M.; Guedes, M.; Leite, Baptista, R. (2018) Effect of Fused Filament Fabrication Processing Parameters on The Mechanical Properties of PLA Components. XVI PCF.
11. El Magri, A.; El Mabrouk, K.; Vaudreuil, S.; Ebn Touhami, M. (2019) Mechanical properties of CF-Reinforced PLA Parts Manufactured by Fused Deposition Modeling. J. Thermoplast Compos Mater. 0892705719847244.

12. Tymrak, B, M.; Kreiger, M.; Pearce, J, M. (2014) Mechanical Properties of Components Fabricated with Open-source 3-D Printers Under Realistic Environmental Conditions. Mater Des. 58, 242-246.
13. Mazzanti, V.; Pariante, R.; Bonanno, A.; de Ballesteros, O. R.; Mollica, F.; Filippone, G. (2019) Reinforcing Mechanisms of Natural Fibers in Green Composites: Role of Fibers Morphology in a PLA/hemp Model System. Compos Sci Technol. 180:51-9.
14. Ochi, S. (2008) Mechanical properties of kenaf fibers and kenaf/PLA composites. Mech. Mater. 40, 446-52.
15. Oksman, K.; Skrifvars, M.; Selin, J. F. (2003) Natural Fibres as Reinforcement in Polylactic Acid (PLA) Composites. Compos Sci Technol. 63, 1317-24.
16. Huber, T.; Müssig, J. (2008) Fibre matrix adhesion of natural fibres cotton, flax and hemp in polymeric matrices analyzed with the single fibre fragmentation test. Compos Interfaces. 15, 335-49.
17. Tisserat, B.; Liu, Z.; Finkenstadt, V.; Lewandowski, B.; Ott, S.; Reifschneider, L. (2015) 3D Printing Biocomposites. J. Plast. Res. [Online early access]. Feb 23.
18. Zhao, D, X.; Cai, X.; Shou, G, Z.; Gu, Y, Q.; Wang, P, X. (2016) Study on the Preparation of Bamboo Plastic Composite Intend for Additive Manufacturing. Key Eng. Mater. 667, 250-258.
19. Daver, F.; Lee, K, P.; Brandt, M.; Shanks, R. (2018) Cork–PLA Composite Filaments for Fused Deposition Modelling. Compos Sci Technol. 168, 230-7.
20. Tao, Y.; Wang, H.; Li, Z.; Li, P.; Shi, S, Q. (2017) Development and Application of Wood Flour-Filled Polylactic Acid Composite Filament for 3D Printing. Materials. 10, 339.
21. Xie, G.; Zhang, Y.; Lin, W. (2017) Plasticizer Combinations and Performance of Wood Flour–Poly (Lactic Acid) 3D Printing Filaments. BioResources. 12, 6736-48.
22. Gkartzou, E.; Koumoulos, E, P.; Charitidis, C, A. (2017) Production and 3D Printing Processing of Bio-Based Thermoplastic Filament. Manuf. Rev. 4, 1.
23. Filgueira, D.; Holmen, S.; Melbø, J. K;. Moldes, D.; Echtermeyer, A. T.; Chinga-Carrasco, G. (2017) Enzymatic-Assisted Modification of Thermomechanical Pulp Fibers to Improve the Interfacial Adhesion with Poly (lactic acid) for 3D Printing. ACS Sustain. Chem. Eng. 5, 9338-46.
24. Stoof, D.; Pickering, K.; Zhang, Y. (2017) Fused Deposition Modelling of Natural Fibre/Polylactic Acid Composites. J. Compos. Sci. 1, 8.
25. Kariz, M.; Sernek, M.; Obućina, M.; Kuzman, M. K. (2017) Effect of Wood Content in FDM Filament on Properties of 3D Printed Parts. Mater. Today Commun. 14, 135-40.

26. Guo, R.; Ren, Z.; Bi, H.; Song, Y.; Xu, M. (2018) Effect of Toughening Agents on The Properties of Poplar Wood Flour/Poly (lactic acid) Composites Fabricated with Fused Deposition Modeling. Eur. Polym. J. 107, 34-45.
27. Depuydt, D.; Balthazar, M.; Hendrickx, K.; Six, W.; Ferraris, E.; Desplentere, F.; Ivens, J.; Van Vuure, A. W. (2019) Production and Characterization of Bamboo and Flax Fiber Reinforced Polylactic Acid Filaments for Fused Deposition Modeling (FDM). Polym Compos. 2019, 40, 1951-63.
28. Ozcelik, B.; Ozbay, A.; Demirbas, E. (2010) Influence of Injection Parameters and Mold Materials on Mechanical Properties of ABS in Plastic Injection Molding. Int. Commun. Heat Mass Transf. 37, 1359-1365.
29. Casavola, C.; Cazzato, A.; Moramarco, V.; Pappalettere, C. (2016) Orthotropic Mechanical Properties of Fused Deposition Modelling Parts Described by Classical Laminate Theory. Mater Des. 90, 453-458.
30. Quintana, R.; Choi, J. W.; Puebla, K.; Wicker, R. (2010) Effects of Build Orientation on Tensile Strength for Stereolithography-Manufactured ASTM D-638 type I Specimens. Int. J. Adv Manuf Tech. 46, 201-215.
31. Galantucci, L. M.; Lavecchia, F.; Percoco, G. (2010) Quantitative Analysis of a Chemical Treatment to Reduce Roughness of Parts Fabricated Using Fused Deposition Modeling. CIRP Ann. 59, 247-250.
32. Maidin, S.; Mohamed, A. S.; Akmal, S.; Mohamed, S. B.; Wong, J. H. U. (2018) Feasibility Study of Vacuum Technology Integrated Fused Deposition Modeling to Reduce Staircase Effect. Jouranl of Fundamental Applied Science. 10, 633-645.
33. Lederle, F.; Meyer, F.; Brunotte, G. P.; Kaldun, C.; Hübner, E. G. (2016) Improved Mechanical Properties of 3D-Printed Parts by Fused Deposition Modeling Processed Under the Exclusion of Oxygen. Addit. Manuf. 1, 3-7.
34. Malinauskas, M.; Rekštytė, S.; Lukoševičius, L.; Butkus, S.; Balčiūnas, E.; Pečiukaitytė, M.; Baltriukienė, D.; Bukelskienė, V.; Butkevičius, A.; Kucevičius, P.; Rutkūnas, V. (2014) 3D Microporous Scaffolds Manufactured via Combination of Fused Filament Fabrication and Direct Laser Writing Ablation. Micromachines. 5, 839-858.
35. Mazzanti, V.; Malagutti, L.; Mollica, F. (2019) FDM 3D Printing of Polymers Containing Natural Fillers: a Review of Their Mechanical Properties. Polymers. 11, 1094.
36. Mohamed, O. A.; Masood, S. H.; Bhowmik, J. L. (2015) Optimization of Fused Deposition Modeling Process Parameters: a Review of Current Research and Future Prospects. Adv Manuf. 3, 42-53.

37. Zandi, M. D.; Jerez-Mesa, R.; Lluma-Fuentes, J.; Roa, J. J.; Travieso-Rodriguez, J. A. (2020) Experimental Analysis of Manufacturing Parameters' Effect on The Flexural Properties of Wood-PLA Composite Parts Built Through FFF. Int. J. Adv Manuf Tech. 10, 1-4.
38. Endruweit, A.; Gommer, F.; Long, A, C. (2013) Stochastic Analysis of Fibre Volume Fraction and Permeability in Fibre Bundles with Random Filament Arrangement. Compos. Part A: Appl. Sci Manuf. 49, 109-18.

Bibliography of Chapter 4

1. Chia HN, Wu BM (2015) Recent advances in 3D printing of biomaterials. Journal of biological engineering 9(1) 4
2. Brenken B, Barocio E, Favaloro A, Kunc V, Pipes RB (2018) Fused filament fabrication of fiber-reinforced polymers. A review. Additive Manufacturing 21:1-16
3. Cuan-Urquizo E, Barocio E, Tejada-Ortigoza V, Pipes RB, Rodriguez CA, Roman-Flores A (2019) Characterization of the Mechanical Properties of FFF Structures and Materials. A Review on the Experimental, Computational and Theoretical Approaches. Materials (Basel) 12(6)
4. Jerez-Mesa R, Travieso-Rodriguez JA, Lluma-Fuentes J, Gomez-Gras G, Puig D (2017) Fatigue lifespan study of PLA parts obtained by additive manufacturing. Procedia Manufacturing 13:872-879
5. Afrose MF, Masood SH, Lovenitt P, Nikzad M, Sbarski I (2015) Effects of part build orientations on fatigue behaviour of FDM-processed PLA material. Progress in Additive Manufacturing 1(1-2): 21-28
6. Gomez-Gras G, Jerez-Mesa R, Travieso-Rodriguez JA, Lluma-Fuentes J (2018) Fatigue performance of fused filament fabrication PLA specimens. Materials & Design 140: 278-285
7. Es-Said OS, Foyos J, Noorani R, Mendelson M, Marloth R, Pregger BA (2000) Effect of Layer Orientation on Mechanical Properties of Rapid Prototyped Samples. Materials and Manufacturing Processes 15: 107-122
8. Wu W, Geng P, Li G, Zhao D, Zhang H, Zhao J (2015) Influence of Layer Thickness and Raster Angle on the Mechanical Properties of 3D-Printed PEEK and a Comparative Mechanical Study between PEEK and ABS. Materials (Basel) 8(9): 5834-5846

9. Shabat D, Rosenthal Y, Ashkenazi D, Stern A (2017) Mechanical and structural characteristics of fused deposition modeling ABS material. Annals of “Dunarea de Jos” University, Fascicle XII, Welding Equipment and Technology 28: 16-24
10. Sood AK, Ohdar RK, Mahapatra SS (2010) Parametric appraisal of mechanical property of fused deposition modelling processed parts. Materials & Design 31: 287-295
11. Araya-Calvo M, López-Gómez I, Chamberlain-Simon N, León-Salazar JL, Guillén-Girón T, Corrales-Cordero JS (2018) Evaluation of compressive and flexural properties of continuous fiber fabrication additive manufacturing technology. Additive Manufacturing 22: 157-164
12. El Margi A, El Mabrouk k, Vaudreui S, Ebn (2019) Touhami M Mechanical properties of CF-reinforced PLA parts manufactured by fused deposition modeling. Journal of Thermoplastic Composite Materials p. 0892705719847244
13. Jo MY, Ryu YJ, Ko JH, Yoon JS (2012) Effects of compatibilizers on the mechanical properties of ABS/PLA composites. Journal of Applied Polymer Science 125(S2): E231-E238
14. Rosenzweig DH, Carelli E, Steffen T, Jarzem P, Haglund L (2015) 3D-Printed ABS and PLA Scaffolds for Cartilage and Nucleus Pulposus Tissue Regeneration. Int J Mol Sci 16(7): 15118-35
15. Cantrell JT, Rohde S, Damiani D, Gurnani R, DiSandro L, Anton J, Young A, Jerez A, Steinbach D, Kroese C, Ifju PG (2017) Experimental characterization of the mechanical properties of 3D-printed ABS and polycarbonate parts. Rapid Prototyping Journal 23(4): 811-824
16. Tymrak BM, Kreiger M, Pearce JM (2014) Mechanical properties of components fabricated with open-source 3-D printers under realistic environmental conditions. Materials & Design 58: 242-246
17. Ozcelik B, Ozbay A, Demirbas E (2010) Influence of injection parameters and mold materials on mechanical propertie s of ABS in plastic injection molding. International Communications in Heat and Mass Transfer 37(9): 1359-1365
18. Casavola C, Cazzato A, Moramarco V, Pappalettere C (2016) Orthotropic mechanical properties of fused deposition modelling parts described by classical laminate theory. Materials & Design 90: 453-458
19. Quintana R, Choi JW, Puebla K, Wicker R (2009) Effects of build orientation on tensile strength for stereolithography-manufactured ASTM D-638 type I specimens. The International Journal of Advanced Manufacturing Technology 46(1-4): 201-215

20. Galantucci LM, Lavecchia F, Percoco G (2010) Quantitative analysis of a chemical treatment to reduce roughness of parts fabricated using fused deposition modeling. CIRP Annals 59: 247-250
21. Maidin S, Mohamed AS, Akmal S, Mohamed SB, Wong JHU (2018) Feasibility study of vacuum technology integrated fused deposition modeling to reduce staircase effect. Journal of Fundamental and Applied Sciences 10(1S): p.p 633-645
22. Lederle F, Meyer F, Brunotte GP, Kaldun C, Hübner EG (2016) Improved mechanical properties of 3D-printed parts by fused deposition modeling processed under the exclusion of oxygen. Progress in Additive Manufacturing 1(1-2): p.p 3-7
23. Malinauskas M, Rekštytė S, Lukoševičius L, Butkus S, Balčiūnas E, Pečiukaitytė M, Baltriukienė B, Bukelskienė V, Butkevičius A, Kucevičius P, Rutkūnas V, Juodkazis S (2014) 3D Microporous Scaffolds Manufactured via Combination of Fused Filament Fabrication and Direct Laser Writing Ablation. Micromachines 5(4): 839-858
24. De Ciurana J, Serenóa L, Vallès È (2013) Selecting Process Parameters in RepRap Additive Manufacturing System for PLA Scaffolds Manufacture. Procedia CIRP 5: 152-157
25. Testing A.S.f. and Materials, Standard Test Method for Flexural Properties of Unreinforced and Reinforced Plastics and Electrical Insulating Materials by Four-point Bending. (2002): ASTM International.
26. Mohamed OA, Masood SH, Bhowmik JL (2015) Optimization of fused deposition modeling process parameters a review of current research and future prospects. Advances in Manufacturing 3: 42-53
27. Travieso-Rodriguez JA, Jerez-Mesa R, Llumà J, Traver-Ramos O, Gomez-Gras G, Roa Rovira JJ (2019) Mechanical Properties of 3D-Printing Polylactic Acid Parts Subjected to Bending Stress and Fatigue Testing. Preprints 2019100293 doi: 10.20944/preprints201910.0293.v1

Bibliography of Chapter 5

1. Jerez-Mesa R, Travieso-Rodriguez JA, Corbella X, Busqué R, Gomez-Gras G. Finite element analysis of the thermal behavior of a RepRap 3D printer liquefier. Mechatronics. 2016; 36;119-126.

2. Jerez-Mesa R, Gomez-Gras G, Travieso-Rodriguez JA, Garcia-Plana V. A comparative study of the thermal behavior of three different 3D printer liquefiers. Mechatronics. 2018;56;297-305.
3. Gomez-Gras G, Jerez-Mesa R, Travieso-Rodriguez JA, Lluma-Fuentes J. Fatigue performance of fused filament fabrication PLA specimens. Materials and Design. 2018;140;278-285.
4. Pringle AM, Rudnicki M, Pearce JM. Wood Furniture Waste–Based Recycled 3-D Printing Filament. Forest Products Journal. 2018;68(1);86-95.
5. Zhao DX, Cai X, Shou GZ, Gu YQ, Wang PX. Study on the Preparation of Bamboo Plastic Composite Intend for Additive Manufacturing. Key Engineering Materials. 2015;667;250-258.
6. Ochi S. Mechanical properties of kenaf fibers and kenaf/PLA composites. Mechanic of Materials. 2008;40;446-52.
7. Oksman K, Skrifvars M, Selin JF. Natural Fibres as Reinforcement in Polylactic Acid (PLA) Composites. Composite Science Technology. 2002;3;1317-24.
8. Huber T, Müssig J. Fibre matrix adhesion of natural fibres cotton, flax and hemp in polymeric matrices analyzed with the single fiber fragmentation test. Composite Interfaces. 2008;15;335-49
9. Tao Y, Wang H, Li Z, Li P, Shi SQ. Development and Application of Wood Flour-Filled Polylactic Acid Composite Filament for 3D Printing. Materials. 2017;10;339.
10. Kariz M, Sernek M, Obućina M, Kuzman MK. Effect of Wood Content in FDM Filament on Properties of 3D Printed Parts. Materials Today Communication. 2017;14;135-40.
11. Lin W, Xie G, Qiu Z. Effects of Aging on Properties of Wood Flour–Poly (Lactic Acid) 3D Printing Filaments. BioResources. 2019;18;14(4):8689-700.
12. Daver F; Lee KP; Brandt M; Shanks R. Cork–PLA Composite Filaments for Fused Deposition Modelling. Composite Science Technology. 2018;168;230-7.
13. Gkartzou E, Koumoulos EP, Charitidis CA. Production and 3D Printing Processing of Bio-Based Thermoplastic Filament. Manuf. Rev. 2017;4;1.
14. Depuydt D, Balthazar M, Hendrickx K, Six W, Ferraris E, Desplentere F, Ivens J, Van Vuure AW. Production and Characterization of Bamboo and Flax Fiber Reinforced Polylactic Acid Filaments for Fused Deposition Modeling (FDM). Polymer Composite. 2019;40;1951-63.

15. Tisserat, B, Joshee, N, Mahapatra, AK, Selling, GW, Finkenstadt, VL. Physical and mechanical properties of extruded poly (lactic acid)-based Paulownia elongata biocomposites. Industrial crops and products. 2013;44;88-96.
16. Guo R, Ren Z, Bi H, Song Y, Xu M. Effect of Toughening Agents on The Properties of Poplar Wood Flour/Poly (lactic acid) Composites Fabricated with Fused Deposition Modeling. European Polymers Journal. 2018;107;34-45.
17. Filgueira D, Holmen S, Melbø JK, Moldes D, Echtermeyer AT, Chinga-Carrasco G. Enzymatic-Assisted Modification of Thermomechanical Pulp Fibers to Improve the Interfacial Adhesion with Poly (lactic acid) for 3D Printing. ACS Sustain. Chem. Eng. 2017;5;9338-46.
18. Yang, TC. Effect of extrusion temperature on the physico-mechanical properties of unidirectional wood fiber-reinforced polylactic acid composite (WFRPC) components using fused deposition modeling. Polymers.2018;10(9);976.
19. Xie G, Zhang Y, Lin W. Plasticizer Combinations and Performance of Wood Flour–Poly (Lactic Acid) 3D Printing Filaments. BioResources. 2017;12;6736-48.
20. Stoof D, Pickering K, Zhang Y. Fused Deposition Modelling of Natural Fibre/Polylactic Acid Composites. Journal of Composite Science. 2017;1;8.
21. Sood AK, Ohdar RK, Mahapatra SS. Parametric appraisal of mechanical property of fused deposition modelling processed parts. Materials and Design. 2010;31(1);287-295.
22. Domingo-Espin M, Puigoriol-Forcada JM, Garcia-Granada AA, Llumà J, Borros S, Reyes G. Mechanical property characterization and simulation of fused deposition modeling polycarbonate parts. Materials and Design. 2015;83;670-677.
23. Domingo-Espin M, Travieso-Rodriguez JA, Jerez-Mesa R, Lluma-Fuentes J. Fatigue performance of ABS specimens obtained by fused filament fabrication. Materials. 2018;11(12);2521-2536.
24. Tymrak BM, Kreiger M, Pearce JM. Mechanical properties of components fabricated with open-source 3-D printers under realistic environmental conditions. Materials and Design. 2014;58;242-246.
25. Singh R. Some investigations for small-sized product fabrication with FDM for plastic components. Rapid Prototyping Journal. 2013;19(1);58-63.
26. Durgun I, Ertan R. Experimental investigation of FDM process for improvement of mechanical properties and production cost. Rapid Prototyping Journal. 2014;20(3);228-235.

27. Jerez-Mesa R, Travieso-Rodriguez JA, Lluma-Fuentes J, Puig D. Fatigue lifespan study of PLA parts obtained by additive manufacturing. Procedia Manufacturing. 2017;13;872-879.
28. Singh R. Process capability analysis of fused deposition modelling for plastic components. Rapid Prototyping Journal. 2013;20(1);69-76.
29. Wahl L, Maas S, Waldmann D, Zurbes A, Freres P. Shear stresses in honeycomb sandwich plates: Analytical solution, finite element method and experimental verification. Journal of Sandwich Structures and Materials. 2012;14(4);449-468.
30. Spierings AB. Fatigue performance of additive manufactured metallic parts. Rapid Prototyping Journal. 2013;19(2);88-94.
31. Edwards P, Ramulu M. Fatigue performance evaluation of selective laser melted Ti-6Al-4V. Materials Science and Engineering: A.2014;598;327-337.
32. Riemer A, Leuders S, Thöne M, Richard HA, Tröster T, Niendorf T. On the fatigue crack growth behavior in 316L stainless steel manufactured by selective laser melting. Engineering Fracture Mechanics. 2014;120;15-25.
33. Afrose MF, Masood SH, Iovenitti P, Nikzad M, Sbarski I. Effects of part build orientations on fatigue behaviour of FDM-processed PLA material. Progress in Additive Manufacturing. 2016;1(1);21-28.
34. Taguchi G, Chowdhury S, Wu Y. Taguchi's Quality Engineering Handbook. Hoboken:John Wiley & Sons;2005.
35. ASTM. D7774-12 Standard Test method for flexural fatigue properties of plastics. West Conshohocken:ASTM International;2013.
36. Wirsching PH, Light MC. Fatigue under wide band random stresses, Journal of the Structural Division. 1980;106(7);1593–1607.
37. Burhan I, Kim HS. S-N Curve Models for Composite Materials Characterisation: An Evaluative Review. Journal of Composite Science. 2018; 2;38.